Annual Report 2006

Center for Microtechnologies (ZfM)

(in cooperation with the Branchlab Chemnitz of the Fraunhofer IZM)

Editors:
Prof. Thomas Gessner
Dr. Wolfgang Seckel

Postal address: Reichenhainer Str. 70
D – 09107 Chemnitz

Contents Page

1 Preface

As in preceding years, the Center for Microtechnologies in close cooperation with the Branchlab Chemnitz of the Fraunhofer Institute for Microintegration and Reliability (FhG IZM, headquarter Berlin) has further consolidated its position as a Center of Excellence in the fields of Nano- and Microelectronics and MEMS technologies.

The key to our success was an interdisciplinary cooperation of several chairs within the ZfM. Based on this idea, ZfM's primary mission is to provide an intellectual and working environment that makes possible student education and research in areas that require or may benefit from advanced ULSI-interconnect technologies, Si-nanotechnology and new developments and ideas in the field of MEMS by using microfabrication technologies. ZfM's technology laboratories provide a complex of modern microelectronics laboratories, clean rooms and microfabrication facilities.

The location Chemnitz was selected for a new institute part of the Fraunhofer IZM having sole responsibility at the end of 2005. It is a pleasure to announce that the ZfM with the Branchlab Chemnitz of the Fraunhofer IZM has established new research focus areas in the year 2006. The research groups in Chemnitz in cooperation with other locations of the Fraunhofer IZM will push the **Smart Systems Integration** of sensors,actuators, different kinds of MEMS with nano- and microelectronics components. Multi devices will be integrated by using several materials as well as technologies.

The Branchlab Chemnitz of the FhG-IZM was very active in term of the establishment of the new European Plattform on Smart Systems Integration (EPOSS) in the year 2006.

The Collaborative Research Center No. 379 (Sonderforschungsbereich) could be finished at the end of 2006 after 12 years of very promising and successful research work.
We can announce that in April 2006 an International Research Training Group with the FUDAN University, Jia Tong University (Shanghai) and the TU Berlin as well as the TU Chemnitz and FhG-IZM has been started. Furthermore the international relationship to China (areas Shanghai, Chongqing, Xian) and Japan has been intensified in the year 2006.

We spent a lot of effort in the year 2006 regarding the organisation and design of a new **Systems Research Park** nearby our already existing buildings. Starting in the year 2006 the construction of **new buildings** for
- cleanroom facilities of the ZfM together with the Institute of Physics of the TU Chemnitz
- the Branchlab Chemnitz of the FhG-IZM
- facilities for start up companies

is carried out and will be finished at the end of 2008. Some information concerning the Systems Research Park you will find after the preface within the annual report 2006.

The 2006 Annual Report of the Center for Microtechnologies provides an overview of the facilities, staff, faculty and students associated with the ZfM, as well as a description of many of the ongoing research projects which make use of the ZfM facilities.

These developments, which are based on close links with industry and cooperation with German as well as international institutes, contribute to an advanced education for our students. We kindly

acknowledge the support of the Federal Ministry of Research, the German Research Foundation, the Saxon Ministry of Science and the European Commission.

As always, we are driven by our triple aims of excellence in education, scientific and technological research and by providing a comprehensive range of research and development services to industry.

I would like to thank all my colleagues, the scientific fellows and technicians for all their dedicated work.

I look forward to participating in the promising development of new devices and concepts through the use of silicon technology.

Thomas Gessner
President of the Center for Microtechnologies
Director of the FhG-IZM Branchlab Chemnitz
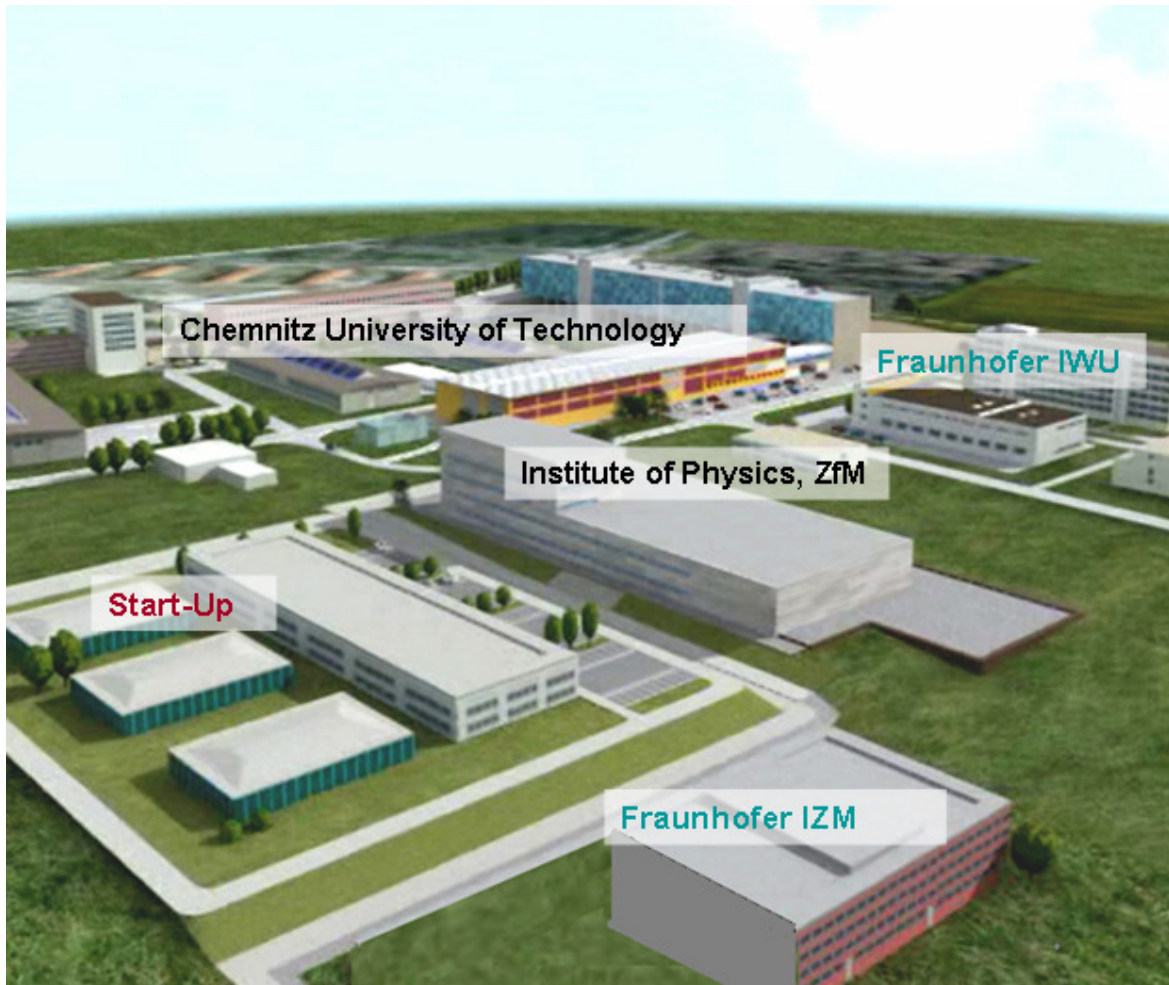
Systems Research Park Chemnitz – will be finished end of 2008

New cleanroom facilities are under construction for the Center for Microtechnologies within the new building of the Institute of Physics.
The foundation stone was laid on September 13th 2006. The building will be finished end of 2007.

The Branchlab Chemnitz of the Fraunhofer IZM will get an own building located at the Systems Research Park Chemnitz. Currently it is in the planning phase. It will be finished end of 2008.

International Research Training Group

Materials and Concepts for Advanced Interconnects

Internationales Graduiertenkolleg

At a Glance

On 1 April 2006, the International Research Training Group (Internationales Graduiertenkolleg 1215) "Materials and Concepts for Advanced Interconnects", jointly sponsored by the German Research Foundation (DFG) and the Chinese Ministry of Education, was established for the next 4.5 years between the following institutions:

- Chemnitz University of Technology
    - Institute of Physics
    - Institute of Chemistry
    - Center for Microtechnologies
- Fraunhofer Institute for Reliability and Microintegration
- Technische Universität Berlin
- Fudan University, Shanghai
- Shanghai Jiao Tong University

This International Research Training Group (IRTG) is the first of its kind at Chemnitz University of Technology. It is lead by Prof. Ran Liu of Fudan University as the coordinator on the Chinese side and Prof. Thomas Gessner on the German side. A graduate school like this offers brilliant young PhD students the unique opportunity to complete their PhD work within 2.5 to 3 years in a multidisciplinary environment. Up to 14 PhD students of the German and 20 of the Chinese partner institutions, as well as a post-doctoral researcher at the Center for Microtechnologies are involved in the current program. The different individual backgrounds of the project partners bring together electrical and microelectronics engineers, materials scientists, physicists, and chemists. In particular, the IRTG is working to develop novel materials and processes as well as new concepts for connecting the devices within integrated microelectronic circuits. Smaller contributions are being made in the field of device packaging and silicides for device fabrication. In this sense, the IRTG project is helping to solve problems currently encountered on the way to nanoelectronics.

Therefore, the research program of the IRTG concentrates on both applied and fundamental aspects, and treats the mid- and long-term issues of microelectronics metallization. Atomic layer deposition (ALD) of metals, new precursors for metal-organic chemical vapor deposition (MOCVD), ultra low-k dielectrics and their mechanical and optical characterization together with inspection techniques on the nanoscale are considered. New and innovative concepts for future microelectronics such as carbon nanotube interconnects or molecular electronics along with silicides to form links to front-end of line processes are of interest, as well as the evaluation of manufacturing-worthy advanced materials. Moreover, the research program addresses reliability and packaging issues of micro devices. Highlighting links between fundamental materials properties, their characteristics on the nanoscale, technological aspects of materials and their applications to microelectronic devices is the main objective of the program.

Nevertheless, the principal idea of the IRTG is four-fold: The research program defines the framework of the activities and the topics of the PhD theses. This is accompanied by a specially tailored study program including lectures, seminars and laboratory courses to provide comprehensive special knowledge in the field of the IRTG. The third part of the program comprises annual schools

held either in China or Germany, bringing together all participants of the IRTG and leading to vivid discussions during the presentation of the research results. Moreover, an exchange period of 3 to 6 months for every PhD student at one of the foreign partner institutions is another essential component. Besides special knowledge in the scientific field, these activities will provide intercultural competencies that cannot easily be gained otherwise.

Current Activities

Official Opening
The IRTG was officially opened in Chemnitz on 5 July 2006 with the ceremonial admission of the PhD students working at TU Berlin (TUB), Fraunhofer IZM and Chemnitz University of Technology (TUC). Currently 11 PhD students and one Postdoc are involved:

Name	Origin	Working field	Supervisor	Institute
Chenping JIA (Postdoc)	China	Advanced packaging technologies for microsystems	Prof. Thomas Gessner (TUC)	Center for Microtechnologies
Nicole AHNER	Germany	Methods for cleaning sub-100 nm structures	Prof. Thomas Gessner (TUC)	Center for Microtechnologies
Olena CHUKHRAI	Ukraine	Mechanical characterization of thin films	Prof. Frank Richter (TUC)	Institute of Physics
Ines EIDNER	Germany	Elastic under-bump structures for wafer-level packaging	Prof. Herbert Reichl (TUB)	Fraunhofer IZM Berlin
Benjamin GRAFFEL	Germany	SPM investigations of semiconductor-metal interfaces	Prof. Michael Hietschold (TUC)	Solid Surfaces Analysis Group
Sascha HERMANN	Germany	Carbon nanotube interconnects	Prof. Thomas Gessner (TUC)	Center for Microtechnologies
Anastasia MOSKVINOVA	Russia	Charactization of nano-scaled interconnect systems by TEM and SEM	Prof. Michael Hietschold (TUC)	Institute of Physics
Nina ROTH	Germany	Transition metal complexes as precursors for CVD, Spin-On and ALD processes	Prof. Heinrich Lang (TUC)	Institute of Chemistry
Sukumar RUDRA	India	Optical spectroscopy of ultra thin films	Prof. Dietrich R.T. Zahn (TUC)	Institute of Physics
Uwe SIEGERT	Germany	Metal formiates and carboxylates as precursors for CVD, Spin-On and ALD	Prof. Heinrich Lang (TUC)	Institute of Chemistry
Teodor TOADER	Romania	Electron spectroscopy studies of advanced interconnects	Prof. Dietrich R.T. Zahn (TUC)	Institute of Physics
Thomas WÄCHTLER	Germany	ALD of copper thin films	Prof. Thomas Gessner (TUC)	Center for Microtechnologies

The official opening of the IRTG in Shanghai took place on 18 September 2006 at Fudan University. Due to the high importance of the project for the Chinese and European semiconductor business, representatives of major microelectronics companies such as AMD, Qimonda or Grace Semiconductor as well as scientists from outstanding institutes such as the Research Center Jülich attended the opening ceremonies and gave invited talks. Moreover, representatives of several political institutions such as the Chinese embassy in Germany and the German Consulate in Shanghai were among the guests.

Autumn School

The first Autumn School of the IRTG was held in Chemnitz from 20 to 24 November 2006. During the technical program, the PhD students of the collaborating Chinese and German institutions presented the topics of their work, discussed recent results and had to defend themselves against the critical questions of their supervising professors. Six invited talks broadened the view of the entire IRTG research field: Dr. Mikhail Baklanov (IMEC, Leuven) talked about the characterization of porous low-k dielectrics while Dr. Lucile Arnaud (CEA-Leti, Grenoble) gave a lecture on reliability issues of interconnect systems. Prof. Margit Zacharias (University of Paderborn) and Dr. Albrecht Leonhardt (Leibniz Institute IFW, Dresden) took a look on very advanced technologies in their talks about nanowires and carbon nanotubes. Moreover, Dr. Naoufal Bahlawane (University of Bielefeld) presented results on precursor analysis for silver CVD, while Knut Schulze (Center for Microtechnologies, Chemnitz) talked about his work on airgap structures for nanoscaled interconnect systems.

Dr. Mikhail Baklanov answering questions after his talk.

To complement the technical program, several social activities were organized during the week of the Autumn School. Among these, the IRTG participants visited the Castle of Rochsburg and the Museum of Industry in Chemnitz. In conjunction with a visit to Fraunhofer IZM in Berlin a bus tour through the German capital provided fascinating views of the formerly divided city.

Lab tour through the cleanrooms of the Center for Microtechnologies.

Visiting the Museum of Industry in Chemnitz.

Study Program and Exchange of PhD Students

In October 2006, the IRTG study program started with an "Introduction to Microelectronics Fabrication" and a course on "Deposition Processes for Back-End of Line in Microelectronics". The study program will be continued with lectures on analytical techniques and spectroscopic methods for thin-film characterization, as well as a course on metal-organic chemistry for metallization processes. In addition to the lectures, laboratory courses are planned that will be organized by the PhD students themselves.

Xiangmeng JING presenting his work at the Autumn School.

Immediately after the Autumn School, the first PhD student from Shanghai Jiao Tong University started his exchange period in Germany. From November 2006 to February 2007, Mr. Xiangmeng JING is working at Fraunhofer IZM Berlin in the group of Prof. Herbert Reichl and Oswin Ehrmann on advanced technologies for wafer-level packaging.

Further information about the IRTG is available at http://www.zfm.tu-chemnitz.de/irtg .

2 Organization

Center for Microtechnologies

Prof. Dr. Wolfram Dötzel
Prof. Dr. Gunter Ebest
Prof. Dr. Joachim Frühauf
Prof. Dr. Thomas Gessner
Prof. Dr. Ulrich Heinkel
Prof. Dr. Josef Lutz
Prof. Dr. Christian Radehaus

Our scientific research focuses on microsystem technology, microelectronics, as well as opto-electronics and integrated optics. In these fields, the Chemnitz University of Technology has had a tradition and experience for more than 30 years.

The research comprises ULSI metallization technologies, fabrication and application of micromechanical components, modeling, simulation and design of processes, devices, components, circuits and test structures down to the nanometer range, as well as single electron tunneling technologies, nonlinear photonic materials and fiber optics.

In education, the specified and related topics are taught in the basic and main courses. The institute offers the specializations Electronics/Microelectronics, Microsystem/Device Technology and Mechatronics.

The equipment is provided for the institute in combination with the Center for Microtechnologies and comprises a complete silicon wafer line, mask making equipment, commercial software and hardware for simulation and design, as well as extensive analysis and semiconductor measurement technology.

The Center for Microtechnologies facilities include 1000 m² of clean rooms (about 30 % of it class 10 to 100) with equipment for mask and wafer processes.

Visit our homepage: **http://www.zfm.tu-chemnitz.de**

Chair Microsystems and Precision Engineering
Professur Mikrosystem- und Gerätetechnik
Prof. Dr.-Ing. Wolfram Dötzel
phone   (+49 371) 531 33264
fax   (+49 371) 531 24439
e-mail: wolfram.doetzel@etit.tu-chemnitz.de
www.infotech.tu-chemnitz.de/ ~microsys/index.html

Chair Electronic Devices
Professur Elektronische Bauelemente
Prof. Dr.-Ing. Gunter Ebest
phone   (+49 371) 531 33125
fax   (+49 371) 531 24419
e-mail: ebest@etit.tu-chemnitz.de
www.tu-chemnitz.de/etit/leb/

Chair Microtechnology
Professur Mikrotechnologie
Prof. Dr. Dr. Prof. h.c. mult. Thomas Gessner
phone   (+49 371) 531 24060
fax   (+49 371) 531 24069
e-mail: Thomas.Gessner@zfm.tu-chemnitz.de
www.zfm.tu-chemnitz.de

Chair Circuit and System Design
Professur Schaltungs- und Systementwurf
Prof. Dr.-Ing. Ulrich Heinkel
phone   (+49 371) 531 24310
fax   (+49 371) 531 24319
e-mail: ulrich.heinkel@etit.tu-chemnitz.de
www.tu-chemnitz.de/etit/sse/

Chair Power Electronics and Electromagnetic Compatibility
Professur für Leistungselektronik und elektromagnetische Verträglichkeit
Prof. Dr.-Ing. Josef Lutz
phone   (+49 371) 531 33342
fax   (+49 371) 531 800 127
e-mail: Josef.Lutz@etit.tu-chemnitz.de
www.tu-chemnitz.de/etit/le

Chair Opto- and Solid-State Electronics
Professur Opto- und Festkörperelektronik
Prof. Dr. rer. nat. Christian Radehaus
phone   (+49 371) 531 33086
fax   (+49 371) 531 24419
e-mail: cvr@zfm.tu-chemnitz.de
www.tu-chemnitz.de/etit/opto/

Group for Material Science
Arbeitsgruppe „Werkstoffe der Elektrotechnik / Elektronik"
Prof. Dr. rer. nat. habil. Joachim Frühauf
phone   (+49 371) 531 33178
fax   (+49 371) 531 24439
e-mail: joachim.fruehauf@e-technik.tu-chemnitz.de
www.infotech.tu-chemnitz.de/~wetel/wetel-home.html

Center for Microtechnologies (Scientific Institution)
Zentrum für Mikrotechnologien (ZfM)
President: Prof. Dr. Dr. Prof. h.c. mult. Thomas Gessner
phone   (+49 371) 531 24060
fax   (+49 371) 531 24069
e-mail: Thomas.Gessner@zfm.tu-chemnitz.de
www.zfm.tu-chemnitz.de

3 Memberships

Prof. Wolfram Dötzel

Vice President for Research of Chemnitz University of Technology, October 2003 – Sept. 2006
Member of the Academy of Science of Saxony, Leipzig / Germany
Member of acatech (Council of Technical Sciences of the Union of German Academies of Sciences and Humanities)
Gesellschaft für Mikroelektronik und Mikrotechnik (VDI/VDE-GMM)
ESPRIT III – Network „NEXUS"

Prof. Gunter Ebest

Vertrauensdozent „Studienstiftung des Deutschen Volkes"

Prof. Thomas Gessner

Member of the Academy of Science of Saxony, Leipzig / Germany
Member of acatech (Council of Technical Sciences of the Union of German Academies of Sciences and Humanities)
Member of "Senatsausschuss Evaluierung der Wissenschaftsgemeinschaft Gottfried Wilhelm Leibnitz" (WGL)
Member of the Board of „KoWi", Service Partner for European R&D funding, Bruessel
The Institute of Electrical and Electronics Engineers, Inc. (IEEE) , USA
The Electrochemical Society, USA
„Advisory Professor" of FUDAN University: honorary professor, 1st June 1999
„Advisory Professor" of Chongqing University: honorary professor, 1st July 2003
Referee of the German Science Foundation (DFG-Fachgutachter) „Systemtechnik"
Dean of the Faculty of Electrical Engineering and Information Technology at TU Chemnitz since March 2006

Prof. Josef Lutz

International Steering Committee of the European Power Electronics and Drives Association (EPE), Brussels
Member of the Advisory Board of the Power Conversion Intelligent Motion Conference (PCIM), Nuremberg
International programme committee of the International Seminar on Power Semiconductors (ISPS), Prague
Honourable professor at the North Caucasus State Technical University, Stavropol, Russia

Prof. Christian Radehaus

Optical Society of America (OSA)
The Institute of Electrical and Electronics Engineers, Inc. (IEEE), USA
The American Physical Society (APS)
Deutsche Physikalische Gesellschaft (DPG)

Fraunhofer Institute for Reliability and Microintegration IZM
Branch Lab Chemnitz
Dept. Multi Device Integration

Director: Prof. Thomas Gessner   **Management: Dr. Thomas Otto**

Since 1998 a strong co-operation exists between the Fraunhofer Institute for Reliability and Microintegration (Fraunhofer IZM, Berlin, Munich & Chemnitz) and the Center for Microtechnologies. Consequently the department was founded to combine the packaging know-how of the Fraunhofer IZM with the MEMS devices of the Center for Microtechnologies. Now, the main focus of the branch lab Chemnitz is the smart systems integration.

The main research activities of the IZM branch lab Chemnitz are divided in the following topics:

- *Multi Device Integration* contains the development of MEMS, the Integration of such devices together with microelectronic components to systems and the use of different test engineering technologies. Examples are micro mirror spectrometer or micro projection systems.

- *Development of advanced technologies* like CMP (chemical mechanical polishing) and 3D-patterning by deep silicon etching as well as increasing the core competence in *MEMS packaging* (chip and wafer bonding including combinations of new materials and bonding at low temperatures)

- *Back end of Line (BEOL)* group assist the microelectronic industries in the field of advanced metallization systems for the leading edge technology. The goal is the reduction of parasitic effects like signal delay, electro migration or overheating by using of new materials (cupper, low k materials) for the interconnection system.

- *Reliability of Micro and Nano Systems,* the primary research field is thermo-mechanical reliability of microcomponents in high tech systems. Special competence is thermo-mechanical simulation combined with advanced experimental methods. Internationally recognized results have been obtained in the following fields, for example: reliability of automotive electronics, quality assurance and life-time estimation of Microsystems, crack and fracture avoidance and evaluation in microelectronics applications

- *Printed Electronics* deals with the fabrication of polymer based microelectronic circuits by mass printing processes. Main activities in this field are the technology development and an adapted measurement technique.

In near future microsystems will be quite more intelligent and multifunctional e. g. the integration of electronics for signal and information processing with sensors and actuators in silicon and nonsilicon technologies. The so called multi device integration to smaller and smarter systems is our vision. Therefore further research fields are back-end-of-line technologies for micro and nano electronics, printed electronic systems or ubiquitous low-cost applications and investigation of micro and nano reliability for smart systems.

To derive benefits from the potential of Asian markets, the Fraunhofer IZM Chemnitz established a representative office in Shanghai (PR China) in July 2002, which is managed from Chemnitz. The aim of these activities is to evaluate the microelectronics and microsystems markets in the science and economic areas in Shanghai, Chongqing, and whole China. Furthermore we would like to use this knowledge for common R & D projects and for getting in contact with industry in China.

In general the strategic alliance between the Fraunhofer Institute for Reliability and Microintegration and the Center for Microtechnologies as described ensures strong synergies in the technology and device development.

Nanotechnology Center of Excellence "Ultrathin Functional Films"

The Center of Excellence "Ultrathin Functional Films" (UFF), distinguished by the Federal Ministry of Research (BMBF) as a nation-wide center, is coordinated by Fraunhofer-IWS Dresden. It joins 51 enterprises, 10 university institutes, 22 research institutes, and 5 corporations into a common network. Nanotechnology is one of the key technologies of the 21st century. In order to channel the research results already available at institutes and universities as well as the growing demand from industry, the Nanotechnology Centers of Excellence (CE) had been established in 1998. The Center for Microtechnologies is an active member within this center, especially in the field of microelectronics related topics.

Contact: Office of Center of Excellence "Ultrathin Functional Films"
             at Fraunhofer-IWS Dresden
             Dr. Ralf Jaeckel
             Phone +49 (0) 351 / 25 83 444, Fax +49 (0) 351 / 25 83 300
             www.nanotechnology.de

Activities within the frame of Nano-CE-UFF are subdivided into 6 Working Groups (WG), every one of which is administered and coordinated by one member:

WG 1: Advanced CMOS
WG 2: Novel components
WG 3: Biomolecular films for medical and technological purposes
WG 4: Mechanical and protective film applications
WG 5: Ultrathin films for optics and photonics
WG 6: Nano-size actorics and sensorics

The Working Groups, in which the Center for Microtechnologies is mainly involved, are described briefly in the following:

Advanced CMOS
Structural widths of about 100nm are state-of-the-art in CMOS technology. A reduction down to below 50nm within 10 years, for further miniaturization, is envisaged by the International Technology Roadmap for Semiconductors ITRS (by Semiconductor Industry Association (SIA) and SEMATECH). Along with this trend, higher frequency and reliability are required. This implies novel developments in materials and processes for both the active elements and the interconnect system, including advanced equipment for larger Si-wafer production. High k dielectrics will be applied to ensure further scaling of effective gate oxide thickness. Most present-day interconnect systems are made of contacts (e.g. titanium or cobalt silicide), barrier layers (TiN, TiW), isolating interlayers (SiO$_2$ and low-k dielectrics like FSG, OSG), interlayer connections and conducting paths (Al-alloys and Copper). Copper with its high conductivity and stability with respect to electromigration has been introduced as conductor material leading to higher frequency and reliability. This requires the availability of suitable barrier layers suppressing interdiffusion and reactions. The barrier layers must not affect the conductivity of the paths remarkably, which requires ultra-thin films. Interfaces and nanometer scale effects become increasingly important.
Head of the Working Group: Prof. Dr. Thomas Gessner
                               Chemnitz University of Technology

Novel components

The continuing trend towards miniaturization of integrated circuits has given rise to increasing efforts to supplement and gradually replace conventional CMOS-technologies by nanotechnologies and nanoelectronics in near future. The latter include magneto-electronics, and single electron devices, nanocluster storage elements, and resonant tunneling elements, among others.

Magnetoelectronics is based on the concept of replacing semiconductor magnetic field sensors (Hall sensors) in multi-layer systems by Giant Magneto Resistance (GMR) sensors, and CMOS memories by persistent magnetic memories (M-RAMS). For this purpose it is necessary to deposit stacks of extremely thin metallic and insulating films of about 1nm thickness with well defined interfaces.

There is a new generation of novel components based on the transfer of individual electrons in nano-scale structures. Work centers on memory elements based on the transfer of individual electrons between metal electrodes and on the memory effect of semiconductor nano-clusters in SiO_2 films.

Head of the Working Group: Prof. Dr. Christian Radehaus
                                        Chemnitz University of Technology

4 Research activities of ZfM in cooperation with the FhG-IZM, Branch Lab Chemnitz

Fields of research

- Smart Systems Integration of MEMS, MOEMS and electronics components
- Design and fabrication of microelectronic and micromechanical elements and arrays
- ULSI metallization
- High temperature stable metallization
- Analysis of micromechanical systems
- Development and application of design tools and methods for micromechanical components and systems & coupled field analysis
- Coupling of microsystems and instrumentation (mechanical, electrical, thermal and substantial interfaces)
- Function, principles and modelling of electronic devices (test structures, parameter extraction, model building)
- Microelectronic circuit design (read out- and controlling circuits for sensors and actuators)
- Electronics for micro-electromechanical systems (MEMS)
- Development of infrared measurement systems
- Nanoelectronics
- Integrated Optics
- Colour measurement

Subjects of research

- Microfabricated scanner arrays
- Acceleration sensors
- Electostatically driven torsion actuators with one or two DOF
- Air gap insulated microstructures (AIM) technology
- High temperature applications of MEMS, e.g. gas sensor for exhaust measurement
- Vibration monitoring based on Si-sensor arrays
- Sensor / actuator systems for high precision scanning with a large vertical range
- Gyroscopes
- Wafer bond techniques / SOI – substrat fabrication / MEMS wafer level packaging
- Simulation of micromechanical and microelectronical components, materials databases

- Design tools for microsystems and microelectronics
- Macromodels for simulation of micromechanical components using PSpice
- Design and fabrication of integrated optical waveguides on silicon
- Fiber-optical communication systems
- Single Electron Tunnelling Technologies
- Infrared measurement and sensors
- Orientation dependent etching of silicon: Development of etchants and determination of etch rates, design of etch masks and simulation of etch process, development of new structures by multi-step etch processes
- Geometrical measurement on microstructures
- Plastic deformation of silicon-microstructures
- Copper metallization / Diffusion barriers / CMP
- Low k dielectrics / Air gap structures for ultra low-k values
- Equipment and process simulation for microelectronics
- Development of probing equipment for 1/f measurements
- Microwave Device and Circuit Design and Simulation
- Reliability analyses

4.1 Current research projects

DFG Internationales Graduiertenkolleg – International Research Training Group (IRTG) "Materials and Concepts for Advanced Interconnects"

Coordinators:	Prof. T. Gessner (TU Chemnitz), Prof. Ran Liu (Fudan University, Shanghai, China)
Partners:	TU Chemnitz, TU Berlin, Fraunhofer IZM, Fudan University Shanghai, Shanghai Jiao Tong University
Project duration:	01.04.2006 – 30.09.2010
Project goal:	The IRTG is working to develop novel materials and processes as well as new concepts for connecting the devices within integrated microelectronic circuits. Smaller contributions are being made in the field of device packaging and silicides for device fabrication.

BMBF Project "InnoRegio – InnoSachs: Joint Project – Formation of a regional network for the fabrication of silicon MEMS (MIKROFE); Part: Sensor development and fabrication"

Project leader:	Dr. T. Otto, FhG IZM Chemnitz
Partners:	GEMAC mbH Chemnitz; Turck Beierfeld GmbH
Project duration:	01.09.2004 - 31.03.2006
Project goal:	Development and integration of a *low* g sensor for a regional fabricated system

BMBF Project "Active Smart ID-Label for transportation monitoring (ASIL)"

Project leader:	Dr. F. Kriebel, KSW Microtec AG, Dresden
Partners:	KSW Microtec AG Dresden, ELMOS Semiconductor AG Dortmund, Schenker Deutschland AG Dresden, ZfM TU Chemnitz
Project duration:	01.09.2005 - 31.08.2008
Project goal:	Development, adaptation and integration of sensors for shock and tilt sensing within an active rf ID label

BMBF Project „Modular Optical Analyser System (MOPAL)"

Project manager:	Prof. T. Gessner
Partners:	Endress+Hauser Conducta GmbH & Co. KG, COLOUR CONTROL Farbmesstechnik GmbH, SENTECH GmbH, Micro System Research Center of Chongqing University (VR China)
Project duration:	01.08.2004 - 31.07.2007
Project goal:	Development and realization of an economical, efficient and universally applicable modular optical miniature analysis system for the spectral range from 300 nm – 10 µm.

BMBF Project "Visualisierung mit halbleiter-basierten RGB Lasern im Automobil- und Consumerbereich - VISULASE"

Project leader:	OSRAM Opto Semiconcuctors GmbH
Partners:	FhG IZM Chemnitz, ZfM TU Chemnitz, FhG-IOF Jena, Robert Bosch GmbH, ELOVIS GmbH
Project duration:	01.10.2004 - 30.09.2007
Project goal:	The goal of the project is the development of a complex micromechanical system for a head-up display in a car.

BMBF Project „Isolation schemes for ultra high RF-circuits" (Isosurf)

Project manager:	Dr. H. Höhnemann, Atmel Germany GmbH
Partners:	Atmel Germany GmbH, IMS chips Stuttgart, FZ ISG Jülich, FhG IZM Department Chemnitz, TU Ilmenau, TU Ulm
Project duration:	04/2003 – 04/2006
Project goal:	Fabrication of new transistor structures based on SOI-substrates with buried silicides layers

BMBF Project „Design und Technologie für SOI-CMOS Bauelemente mit Gatelängen kleiner 50nm (MOSTEDE)"

Project manager:	Prof. C. Radehaus
Partners:	AMD Saxony, HTW Dresden
Project duration:	01.04.2004 – 31.03.2007
Project goal:	Atomic scale modelling of new dielectrics for CMOS technologies

BMBF-Project : "Advanced Supercaps based on nanostructured materials (Nanocap®II)"

Project manager:	Mr. P. Malcher, Brandenburgische Kondensatoren GmbH
Partners:	FhG ISC Würzburg, Bosch Group, BMW Group, TU Chemnitz – Prof. Lutz
Project duration:	01.09.2005 – 31.08.2008
Project goal:	Development of a new generation of supercaps with improved technical features

BMBF Project "NMR Metabolic Profiling of the Stem Cell Niche (METASTEM)"

Project manager:	Dr. Michael Cross, Universität Leipzig
Partners:	Zentrum für Mikrotechnologien Chemnitz, Universität Leipzig, Max-Planck-Institut für molekulare Genetik Berlin, NMR Service Erfurt
Project duration:	01.10.2006-30.09.2009
Project goal:	Development of MEMS tunable capacitors for tuning and matching of highly sensitive dual channel NMR micro resonators.

DFG Project „Polymere als low-k Dielektrika für Metallisierungssysteme in der Mikroelektronik" – Polymers as low-k dielectrics for microelectronic metallization schemes

Project manager:	Prof. T. Gessner
Partners:	Prof. M. Bauer, BTU Cottbus
Project duration:	01.02.2002 – 31.01.2004
	01.12.2004 – 30.11.2006

Project goal: Development and characterization of organic ultra low k material with reduced density; Patterning process development and compatibility with copper interconnect processing.

DFG Project „Bestimmung und Optimierung des mechanischen Verhaltens von Schichtstapeln mit porösen low-k-Dielektrika" – Evaluation and Optimization of mechanical behavior of film stacks containing porous low-k dielectrics

Project manager: Prof. T. Gessner

Partners: Prof. F. Richter, Chair Solid-State Physics, Chemnitz University of Technology

Project duration: 01.11.2004 - 31.10.2006

Project goal: Development of fundamental models and software for mechanical characterization technique based on nanoindentation of porous low-k dielectrics. Correlation with CMP loads on porous materials.

Integrated Project (IST) "NANOCMOS": CMOS backbone for 2010 e- Europe. From the 45 nm node down to the limits

Project leader: ST Microelectronics SA (F)

Project manager: Prof. T. Gessner / Dr. S. E. Schulz

Partners: Infineon Technologies AG (D), Philips Electronics Nederland B.V. (NL), Philips Semiconductors R&D France (F), Philips Innovative Technology Solutions NV (B), IMEC Leuven (B), ST Microelectronics Srl. (I), CNRS (F), CEA-LETI Grenoble (F), Fraunhofer (D), isiltec GmbH (D), Ion Beam Services (F), Magwell (B), ACIES Europe (F)

Project duration: 01.03.2004 – 30.06.2006

Project goal: NANOCMOS is a project focussing on the RTD activities necessary to develop the 45nm, 32nm and below CMOS technologies. From these technology nodes it will be mandatory to introduce revolutionary changes in the materials, process modules, device and metallization architectures and all related characterization, test, modelling and simulation technologies, to keep the scaling trends viable and make all future IST applications possible. NANOCMOS covers all these aspects. The first objective of the project is the demonstration of feasibility of Front-End and Back-End process modules of the 45nm node CMOS logic technology. The project intents to process as demonstrator a very aggressive SRAM chip displaying worldwide best characteristics. The second objective of the project is to realize exploratory research on critical issues of the materials, devices, interconnect and related characterization and modelling to start preparing the 32/22 nodes considered to be within the limits of the CMOS technologies. The third objective of the project is to prepare the take up of results described in the Objective I and implement a 45nm Full Logic CMOS Process Integration in 300 mm wafers by the end of 2007. This integration will be part of a separate MEDEA+ project.

Website: www.nanocmos-eu.com

Integrated Project (IST) "PULLNANO": PULLing the limits of NANOcmos electronics

Project leader: ST Microelectronics SA (F)

Project manager: Prof. T. Gessner / Dr. S. E. Schulz

Partners: 35 partners involving main European IC manufacturers, research institutes, universities and SME's, e.g. Freescale Semiconductor (F), Infineon Technologies AG (D), NXP founded by Philips (NL, F), ST Microelectronics (F, I), IMEC Leuven (B), CNRS (F), CEA-LETI Grenoble (F), Fraunhofer (D), ACIES Europe (F)

Project duration: 01.06.2006 – 30.11.2008

Project goal: PULLNANO is a 30-month Integrated Project (IP) proposal for a powerful project focused on advanced RTD activities to push forward the limits of CMOS technologies. PULLNANO focuses on the development of 32 and 22nm CMOS technology nodes opening the way to the long term future of these technologies. The 1st objective of the project is the feasibility demonstration of 32nm node Front-End and Back-End process modules through a very aggressive SRAM chip and a multilevel metal stack structure. The 2nd objective is to realize research on the materials, devices, architectures, interconnects modelling and characterization to prepare the future 22nm node. The 3rd objective is to establish a common action between technology and design people in order to assess the technologies in terms of performances and power consumption. The 4th objective is to define, through a forum of European equipment suppliers, the specifications of future advanced process, characterization and metrology equipments. PULLNANO starts from the very successful NANOCMOS project focused on the 45nm technology.

BMBF Project „Verdrahtungstechniken für besondere Geschwindigkeitsanforderungen in flüchtigen Speichern und Mikroprozessoren – High speed interconnects for volatile memories and microprocessors" - VERBINDEN

Project coordinator: AMD Fab36 LLC & Co. KG
Project manager: FhG-IZM: Dr. Stefan E. Schulz
Partners: AMD Fab36 LLC & Co. KG, Qimonda AG, Fraunhofer CNT
Subcontractors: Fraunhofer IZM Chemnitz / TU Chemnitz, TU Dresden, TU Berlin
Project duration: 01.04.2006 – 31.03.2009
Project goal: Subproject KUWANO (low resistivity copper interconnects): Development of processes and technology for fabrication of low resistivity Cu interconnect embedded in SiO_2 and dense low-k dielectrics for microprocessors in 45 and 32 nm technology node.

BMBF Project „Poröse Ultra-low-k Dielektrika: Abscheidung, Ausheilung, Strukturierung, Planarisierung und Integration – Porous ULK Dielectrics: Deposition, Patterning, Planarization and Integration" - PULSAR

Project coordinator: AMD Fab36 LLC & Co. KG
Project manager: FhG-IZM: Dr. Stefan E. Schulz
Subcontractors: Fraunhofer IZM Chemnitz, TU Dresden
Project duration: 01.07.2006 – 30.06.2009
Project goal: Development of processes and technology for integration of porous ultra-low-k dielectrics into Cu interconnect systems for microprocessors in 45 and 32 nm technology node.

BMBF-Projekt „Mx Mobile „Multi-Standard Mobile Platform" Phase 1"

Project manager: Prof. U. Heinkel
Partners: Alcatel-Lucent Technologies GmbH, Nürnberg
Project duration: 1.3.2006 – 28.2.2009
Project goal: Development of a multi-standard mobile platform (mobile communication), modeling and verification of the system function, generation of program code, methods and platform of simulation

BMBF-Projekt   Netz der Zukunft - Mx Mobile „Multi-Standard Mobile Platform" (Teilvorhaben: Kostenmodellierung zur verbesserten Design Space Exploration)

Project manager: Prof. U. Heinkel
Partners: Alcatel SEL AG, Stuttgart; AMD DDC, Dresden; FhG-HHI Berlin; IHP, Frankfurt/Oder; IMST; Infineon, München; Alcatel-Lucent; Nokia; Philips Semiconductors Dresden; Siemens AG, München; Signalion GmbH ; TU Dresden

Project duration: 1.3.2006 – 28.2.2009
Project goal: Cost modeling for improving design space exploration

BMBF-Project Innoprofile „Generalisierte Plattform zur Sensordaten-Verarbeitung GPS"
Project manager: Prof. U. Heinkel
Partners: Agilion GmbH; Gesellschaft für Mikroelektronik Anwendung Chemnitz mbH;
                       Intelligente Sensorsysteme Dresden GmbH; Neumann Elektrotechnik GmbH;
                       PANTA GmbH; Peppercon AG; PRETTL Elektronik Radeberg GmbH;
                       Unicontrol Systemtechnik GmbH
Project duration: 1.3.2006 – 28.2.2011
Project goal: Development of a central universal control platform with standardized
                       interfaces for sensor data processing, flexible solution for connecting sensors
                       to the platform

**BMBF-Project URANOS „Analysemethoden für den Entwurf anwendungs-robuster
                       nanoelektronischer Systeme"**
Project manager: Prof. U. Heinkel
Partners: AMD Saxony LLC&Co.KG, Dresden (Unterauftraggeber)
Project Duration: 1.7.2005 – 30.6.2008
Project Goal: Development of methods for analysing application-robust nanoelectronical
                       systems

BMBF-Project Herkules „Hardwareentwurfstechnik für Null-Fehler-Designs"
Project manager: Prof. U. Heinkel
Partners: Lucent Technologies GmbH, Nürnberg (Unterauftraggeber)
Project duration: 1.12.2006 – 31.11.2009
Project goal: R & D work in the field of zero defect designs

**SMWA Project "Development of an ICP-cluster-tool for high aspect ratio dry etching of silicon
dioxide (C2T/SiO2)"**
Project leader: Dr. R. Fendler, Mr. W. Hentsch, FHR Anlagenbau GmbH
Partner: FHR Anlagenbau GmbH
Project duration: 01.06.2004 - 30.11.2006
Project goal: Development of process and system for deep dry etching of silicon oxide and
                       silicon oxide based glasses.

**DFG-Project "Hotpressing of multifunctional standards for image processing microscopes for
measurements on microsystems and nanostructures" (SPP 1159/1)**
Project manager: Prof. J. Frühauf
Partner: Prof. E. Reithmeier, University of Hannover
Project duration: 01.04.2005 - 31.03.2007
Project goal: Development of pressing tools made out of silicon

EU Project "Surface Enhanced Micro Optical Fluidic Systems – SEMOFS"
Project manager: Dr. K. Hiller
Partners: CSEM (Switzerland), CEA (France), Cardiff University (UK), Bayer
                       (Schweiz) AG (Switzerland), Eurogentec (Belgium), CHR Citadelle
                       (Belgium), ALMA Consulting (France)
Project duration: 01.09.2005 – 31.08.2008
Project goal: Development of polymer based integrated probecards (including microfluidic
                       and micro optical parts) for health diagnoses

SAB compound project GEMO, part "Silicon basic components for instruments for the measurement of mechanical surface properties in the micro-nano region"

Project manager:	Prof. J. Frühauf
Partners:	Institut für Physik, Prof. F. Richter, TU Chemnitz
	ASMEC Advanced Surface Mechanics GmbH Radeberg
	Anfatec Instruments AG Oelsnitz
	IMA Materialforschung und Anwendungstechnik GmbH
Project duration:	01.08.2005 - 31.07.2007
Project goal:	Development of systems of springs and tips made by the silicon microtechnologies

EFRE Project „NMR-Mikroresonatoren zur Erstellung von Metabolit-Profilen hämatopoetischer Stammzellen"

Project manager:	Dr. T. Riemer, Interdisziplinäres Zentrum für Klinische Forschung Leipzig
Partners:	Zentrum für Mikrotechnologien Chemnitz, Universität Leipzig
Project duration:	01.07.2005 - 31.06.2007
Project goal:	The goal of the project is the development of a nuclear magnetic resonance detector with very high sensitivity, suitable for analyzing small amounts of biological sample material.

AIF Project "Entwicklung von Siliziumaktoren mit lasertrimmbaren Feder-Masse-Strukturen"

Project manager:	Prof. T. Gessner
Partner:	3D-Micromac AG
Projekt duration:	01.05.2004 - 31.10.2006
Projekt goal:	Aim of the collaboration is to investigate achievable accuracy and efficiency as well as developing new laser systems and equipment for in-line laser treatment of MEMS.

Industrial research contract „Wafer level packaging for micro scanners"

Project manager:	Prof. T. Gessner
Partner:	Ricoh Company, Ltd., Japan
Projekt duration:	01.10.2004 – 30.06.2006
Project goal:	Development of a new packaging technology for micro scanners on wafer level by wafer bonding.

Industrial research contract „Charakterisierung der dielektrischen Isolation eines Hoch-voltprozesses"

Project managers:	Prof. G. Ebest
Partner:	X-Fab Erfurt
Projekt duration:	01.09.2005 – 05.03.2007
Project goal:	Research of trench isolation

Industrial research cooperation "Development of micromachined gyroscopes"

Project manager:	Prof. T. Gessner
Partner:	Gyrooptics company limited, St. Petersburg, Russia
Project duration:	1.1. 2006 –
Project goal:	Development of technology and fabrication of prototypes of high precision angular rate sensors

Industrial research contract "Fabrication of tunable Fabry-Perot filters"

Project manager:	Prof. T. Gessner
Partner:	InfraTec GmbH Dresden
Project duration:	01.05.2006 –
Project goal:	Fabrication of prototypes for a micromachined Fabry-Perot-Interferometer

Industrial research contract "Development of multi-use acceleration sensors"

Project manager:	Prof. T. Gessner
Partners:	Fara New Technologies, Xi´an, China, Memsfab GmbH, Chemnitz
Project duration:	01.09.2006 – 31.08.2008
Project goal:	Support for development of a high precision acceleration sensor

DFG-Project "Development of X-ray optics from elements made by silicon microtechnology"

Project manager:	Prof. J. Frühauf
Partner:	Prof. B. Michel, FhG IZM Berlin
Project duration:	01.04.2006 - 31.03.2008
Project goal:	Development of collimation slit systems made out of silicon

Project "Ab initio Berechnung von Defektbildungsenergien und Gleichgewichtskonzentrationen in GaAs"

Project manager:	Prof. C. Radehaus
Partner:	GWT-TUD GmbH, Dresden
Project duration:	1. 9. 2006 – 31. 12. 2006
Project goal:	Calculation of Energies of Defect Formation and Defect Equilibrium Concentrations in GaAs

Robo Tool „Entwicklung einer funkbasierten Kontroll- und Steuereinheit von Robotern zur Fernwartung"

Project manager:	Prof. U. Heinkel
Partner:	Agilion GmbH, Chemnitz
Project duration:	1.6.2006 – 30.4.2008
Project goal:	Development and evaluation of mobile and stationary RF-communication modules

Project „ASIC-Baustein"

Project manager:	Prof. U. Heinkel
Partner:	Bosch GmbH, ZfM
Project duration:	1.10.2006 – 28.2.2007
Project goal:	Chip analysis

SAB-Project „Entwicklung eines integrierten digitalen Sensors zur berührungslosen Längen- und Geschwindigkeitsmessung an bewegten nichtleitenden Materialien", Teilthema „Entwicklung einer digitalen Sensorsignalverarbeitung"

Project manager:	Prof. U. Heinkel
Partner:	Neumann Elektrotechnik GmbH, Chemnitz
Project duration:	1.6.2006 – 30.9.2007
Project goal:	Development of a digital sensor signal processing

4.2   Collaborative Research Center No. 379 :
(Sonderforschungsbereich SFB Nr. 379)
01. 01. 1995 – 31. 12. 2006

„Arrays of micromechanical sensors and actuators"

The MEMS research field covers several provinces using different microtechnology methods for the fabrication.
The subject of the SFB deals with the well-defined part of the microsystems research:
"The realization of sensor and actuator arrays consisting of a number of single components".
Thus, results concerning the behaviour and new application fields of the devices would be expected.
As a vision of the future it is aimed toward a system which combines the arrays with the electronics by microtechnology integration.

Within the focus of interest are the following topics:
- Micromechanical scanning devices (actuators fabricated in bulk and surface micromachining)
- Use of micromechanical basic components, e.g. for ultrasonic arrays and positioning systems, including the application of new materials
- Optimization of the AIM process flow

The following institutions are working together

Faculty of Electrical Engineering and Information Technology
Chair Microsystems and Precision Engineering, Prof. Dr. Wolfram Dötzel
Chair Electronic Devices, Prof. Dr. Gunter Ebest
Group Material Science, Prof. Dr. Joachim Frühauf
Chair Microtechnology, Prof. Dr. Thomas Gessner
Chair Circuit and System Design, Prof. Dr. Ulrich Heinkel
Chair Opto- & Solid-State Electronics, Prof. Dr. Christian Radehaus

Faculty of Natural Science
Chair Semiconductor Physics, Prof. Dr. Dietrich R. T. Zahn
Chair Solid Surfaces Analysis, Prof. Dr. Michael Hietschold

Faculty of Mechanical Engineering
Institute for Print and Media Technology, Prof. Dr. Arved C. Hübler

Fraunhofer Institute for Reliability and Microintegration, Branch Lab Chemnitz
Micro Materials Center Chemnitz, Prof. Dr. Bernd Michel

Institut für Mechatronik e.V. Chemnitz, Prof. Dr. Peter Maißer

Subproject A1: Design of Micromechanical Components Development of Accelerometer Arrays for Drift Compensation

M. Dienel[1], W. Dötzel[1]
[1]Chemnitz University of Technology, Faculty of Electrical Engineering and Information Technology

1 Introduction

Main research topics of Subproject A1 are the methods for MEMS development and the development of several silicon components in micrometer scale.

This article describes the development and the optimization of an array of accelerometers, which will be used in an inertial measurement unit (IMS). The purpose of the array is the reduction of drift in the sensor signals.

Two strategies are implemented. Firstly, the design of the chips was optimized, with respect to the influence on temperature and packaging stress on the sensor array. Secondly, a redundancy of the sensor signals is provided. Either, this could be used for fault tolerance or for increasing the performance. In this research the later is in the centre of interest.

Ideally, two noncollinear acceleration sensors fulfill the requirements to measuring motion in plane. The magnitude and the angle of the acting acceleration can be calculated. Practically, the measured sensor signal is superimposed by the real acceleration and a term caused by drift and mechanical and electrical noise. Eq. (1) illustrates this issue.

$$a_{measure} = a + a_{offset}(t,T) + a_{offset,fixed} + \varepsilon \qquad (1)$$

Assuming that a similar temperature dependency of each sensor element exists, the offset in Eq. (1) can be eliminated. Therefore a special sensor design is used.

To reduce the noise redundant sensor signals are used. If more then two acceleration signals are measured for an in-plane movement, the signals can be simply averaged. But, here are ways for optimization available. For a given number of single sensors in [1] the way for finding the best sensor orientation for increasing performance is described. This approach was transposed to an in-plane acceleration sensor array. The measured signals can be easily averaged with a least squares estimate (Eq. (2)).

$$\begin{pmatrix} a_x \\ a_y \end{pmatrix} = (W^T W)^{-1} W^T \left(\vec{a}_{diff} - \vec{a}_{offset,fixed} \right) \qquad (2)$$

2 The Sensorarray

The sensor array consists of six sensor elements. All sensor elements are placed on one silicon chip. Every sensor element provides another sensitive direction. For equal impact of external influences (temperature, packaging stress) the sensor elements basically have got the similar structure. The sensor element is concentrically anchored. The seismic mass and the comb segments are suspended by three springs, which were aligned equally in the mono crystalline silicon for every sensor element. The different
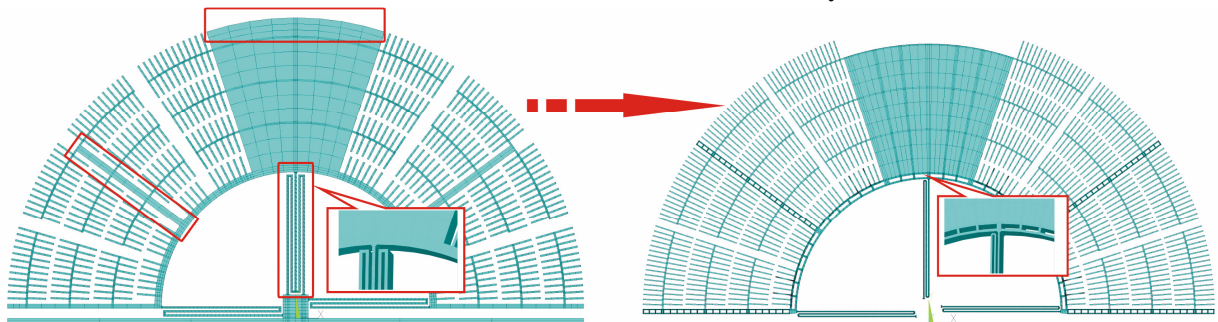

Figure 1: Details of the optimized sensor parts in the FE-model

Freq. in Hz	Element 1		Element 2		Element 3	
	Simulation	Meas.	Simulation	Meas.	Simulation	Meas.
Mode 1	870 (745)	744	851 (729)	743	788 (675)	648
Mode 2	5280 (4893)	4578	5056 (4739)	4625	4802 (4529)	4416
Mode 3	8206 (7757)	7706	7888 (7395)	7334	7566 (7020)	6971

Figure 3: Simulation of Eigen frequencies with expected and estimated spring widths compared to measurement results

sensitive directions are obtained by changing the centre of gravity. Three defined seismic mass setups (Figure 2) are possible. [2]
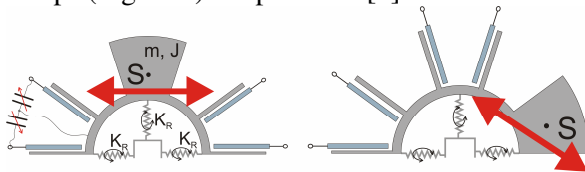
Figure 2: Changing the centre of gravity varies the detection axis in the sensor design

The sensor arrays were fabricated using the BDRIE Technology [3]. They were characterized with respect to mechanical and electrical properties [4].

The results obtained, lead to a reengineered sensor design. The aims can be summarized as follows: increasing and equalizing sensitivity, reducing and equalizing parallel capacitances, optimizing the measurement directions.

During optimization of sensitivity two points were in focus: decreasing the spring constant using 3.5 µm thick bending beams and increasing the number of capacitances using thinner fingers (2.9 µm). Equalizing the sensitivity means that every sensor element provides the same deflection in its measurement direction with a given acceleration. This is achieved by different mass sizes (Figure 4). Finally, the measurement directions were stronger separated. All details of the optimization are shown in Figure 1. The redesigned sensors were fabricated and the mechanical properties were analyzed. The sensor elements provide a higher mechanical sensitivity than expected. Varying the spring properties in the simulation model and comparing the Eigen frequency of the measurements the average spring width was estimated (the cross section is only destructive measurable).

The reengineered sensor and the signal processing PCB which was developed in cooperation with subproject A2 is shown in Figure 5.

4 References

[1] Harrision, J.v.; Gai, E.G.: *Evaluating Sensor Orientations for Navigation Performance and Failure Detection*. IEEE Transaction on Aerospace and Electronic Systems, Vol. AES-13 No. 6, 1977

[2] Billep, D.; Dienel, M.: *Beschleunigungssensor*, Patent DE 10 2004 046 411.4, Germany, 2004.

[3] Hiller, K.; et al. : *Bonding and Deep RIE – a powerful combination for high aspect ratio sensors and actuators.* In proceedings of SPIE Photonics West [5715-08], San Jose, 2005.

[4] Dienel, M.: *Komponentenentwurf.* 7. Chemnitzer Fachtagung Mikromechanik & Mikroelektronik 26./27.10.05, Chemnitz, 2005.

Figure 4: Simulation of sensor rotation in the field of gravity
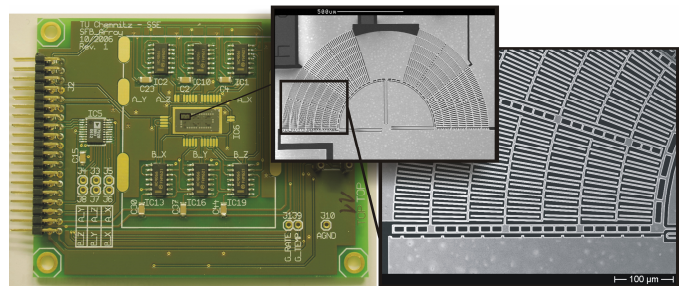

Figure 5: PCB (left) with analogue signal processing and SEM of a sensor element and sensor details (right)

Subproject A2: Overview of an inertial navigation system based on acceleration sensor arrays

Markert, Erik; Hermann, Göran; Heinkel, Ulrich
TU Chemnitz, Fakultät für Elektrotechnik & Informationstechnik, Professur Schaltkreis- und Systementwurf

1 Introduction

Today navigation systems based on the Global Positioning System (GPS) are state of the art. But due to limited precision and difficult satellite connection inside buildings also navigation based only on onboard sensors is necessary. These so called inertial navigation systems determine their position usually on motion data like acceleration and rotation.

A new sensor structure [3] is used to measure accelerations by detecting changes of the capacity. The sensor array [3] consists of six single sensors as shown in figure 1. Their detection axes differ resulting in measuring two acceleration directions with the possibility to compensate offsets.
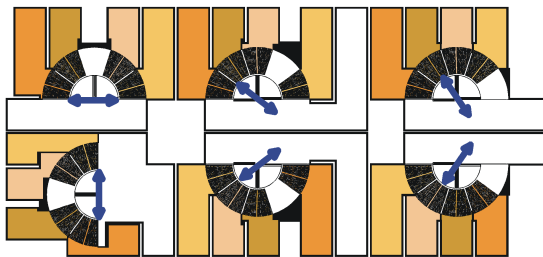
Figure 1: Structure of the 2D sensor array [3]

2 System overview

2.1 General overview
The inertial navigation system consists of three main parts: the analog sensors with analog-digital conversion, a digital coordinate transformation with supporting point inclusion and a PC-based software part. Figure 2 gives an overview of the system structure.

The sensors measure the acceleration and the angular velocity. The digitalized signals are provided to the digital part. Here acceleration and rotation values are converted into position values and corrected by information from other signal sources (camera, map, compass). This position data is sent to a PC using a USB interface. The PC is used for graphical output and provides the initialization data. After initialization the system is able to proceed independently from PC, showing the position information on a small onboard LCD display.

2.2 Analog part
The analog part consists of sensors for acceleration and rotation and the related converter circuits. The acceleration sensor arrays and the DeltaC-U converters were developed at the Chemnitz University of Technology while the sensors for rotation and the ADCs are provided by external suppliers. The acceleration is detected by two acceleration sensor arrays. Each of these arrays is able to measure two directions of acceleration. The array structure is drawn in figure 1. It includes six single acceleration sensors. Each acceleration sensor consists of five segments. Its model was presented in [2].
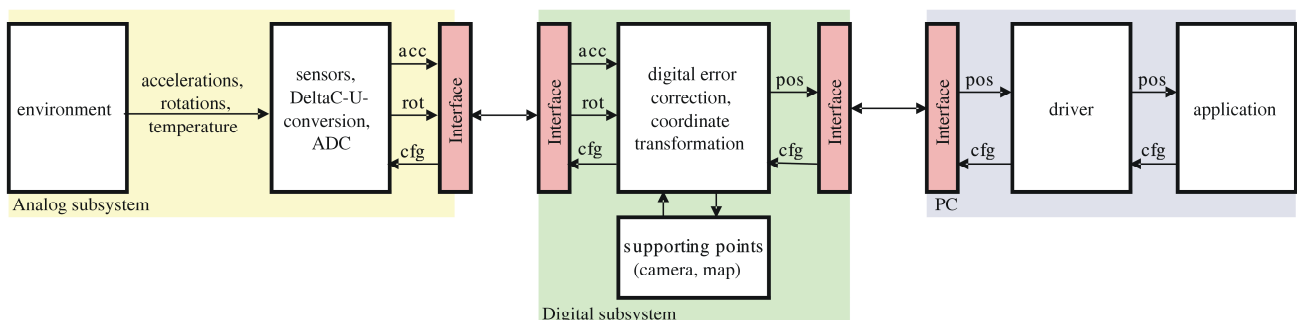

Figure 2: System overview of inertial navigation system

Two capacitive segments form a differential capacitor. So the current flow caused by an acceleration is doubled. This current flow needs to be converted to a voltage for further signal processing. For this reason a DeltaC-U converter is used. The converter generates a triangle voltage for the capacitive segments which causes a continuous loading and unloading of the capacitor at a higher frequency than the measurements. A switch at the input of the DeltaC-U converter rectifies the current flow. Then this flow is converted into a voltage using a two-stage operation amplifier circuit with changeable amplification values.

2.3 Digital and software part

The digital hardware subsystem includes all calculations needed for the inertial navigation system. So the system is able to work without PC connection after receiving initialization data. All digital components are integrated into a Xilinx SpartanIII FPGA. The belonging board has an onboard text display to visualize the position data. The analog data is converted to 12 bit digital values. But for error minimization the digital fixed point algorithms use an internal data width of up to 44 bits especially for integration and coordinate transformation.

A quaternion-based coordinate transformation [4] is necessary for conversion of the sensor measurements from the sensor coordinate system (SCS) to the environment reference system (ERS). This enables the proper function of gravitation compensation in all positions of the system as well as inclusion of map data.

Every integration step as presented in the last section causes a small error. The three steps of integration leads to a significant difference of the position data compared to the reality. So additional algorithms are necessary for position correction. This is done by referencing position data to a map.

The map contains the immobile objects in the system's environment like walls and furniture. Each object is represented by a sum of cuboids. Each cuboid can uniquely be described by two fixed corner points and the angles to the axes of the ERS. The position of the system is compared to the cuboids. If the current system position conflicts to a cuboid a position correction is necessary.

The PC-based software supports the inertial navigation system with initialization data and plots the covered way. This software is based on Tcl/Tk to get maximum platform independence.

3 Results

The inertial navigation system is not yet finally assembled. The system parts are tested individually. The presented realizations for coordinate transformation and map data inclusion work properly with a test sensor equipment. But this test sensor is too heavy and too large for final integration. The uncorrected position after quaternion transformation shows a significant random walk due to the three steps of integration. The map data inclusion reduces this random walk on a tolerable level on z axis. For xy-plane other correction algorithms based on classification and optical state recognition are currently under development. There the special movement conditions of the carrier vehicle will be taken into consideration.

Figure 3 shows the result of a system-level simulation using SystemC-AMS [1] for a circular path. The differences from the ideal path mainly result from the ADC bitwidth.
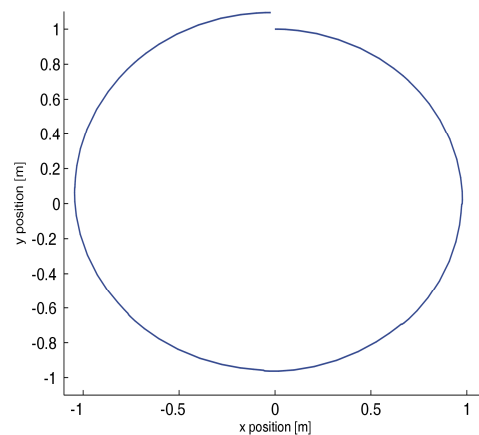

Figure 3: Simulation result of a circular path

References
[1]   http://www.systemc-ams.org
[2]   Markert, E. et. al.: *Acceleration sensor modeling.* Center for Microtechnologies Annual Report 2005, Chemnitz 2006
[3]   Dienel, M. et. al.: *Development of a drift compensated acceleration sensor array.* 50. IWK Ilmenau, Germany, September 19th-23rd 2005
[4]   J. C. Hart et. al.: *Visualizing quaternion rotation.* ACM Transactions on Graphics, vol. 13, pp. 256-276, July 1994.

Subproject A4: Adaptive Resonant Low Frequency Vibration Detection Based on a Micromachined Force Coupled Sensor-Actuator System

Forke, Roman[1]; Scheibner, Dirk[2]; Mehner, Jan[3]; Gessner, Thomas[3]; Dötzel, Wolfram[1]
[1]Chemnitz University of Technology, Department of Microsystems and Precision Engineering,
D-09107 Chemnitz, Germany,
[2]Siemens Automation and Drives, Advanced Technologies and Standards, D-90475 Nuremburg, Germany
[3]Fraunhofer IZM, Dept. MDI, Reichenhainer Str. 88, D-09126 Chemnitz, Germany

1 Introduction

Vibration monitoring is the primary method of machine health diagnostics and process control, e.g. at gears, bearings, drives, engines and other highly stressed machine components [1]. Common sensor elements for vibration diagnostics are piezoelectric wideband transducers or piezoresistive micro-electro-mechanical (MEM) wideband sensors. For evaluation of the time series sophisticated signal analyzing electronics are used. Because of the high costs, permanent monitoring is only reasonable at expensive equipment or in safety related applications.

In most applications it is sufficient to observe only a few spectral lines for extracting the relevant information about the wear state and process conditions. Combining the frequency selectivity and the expected low manufacturing costs, micro-mechanical frequency selective vibration sensors are powerful means for this type of application and have been investigated earlier [2]. The main drawback of these resonant sensors is that monitoring of the low frequencies requires excessively large chip area or a weak suspension to lower the stiffness to mass ratio for applications well below 1 kHz.

To bypass this restriction and extend the frequency range down to a few Hertz, we developed a novel sensor system. Following the superheterodyne principle, well known from radio receivers, the mechanical signal of low frequency is transformed to a higher intermediate frequency. This approach allows a mechanical filtering of low frequency vibrations in a spectral range where MEMS oscillators typically have their eigenfrequencies. The spectral information can directly be observed by capacitive pick-up without subsequent Fast Fourier Transformation (FFT) leading to fewer costs for wear state monitoring.

2 Principle of Operation

The force coupled oscillator system (FCOS) consists of two separated but electrostatically coupled spring-mass-damper systems as shown in Fig. 1. The left oscillator operates as an optimally damped wideband vibration sensor. Its eigenfrequency is set to about 2.5 kHz. The right oscillator is a high Q narrowband resonator with its eigenfrequency set to approx. one decade above the latter. In terms of the superheterodyne principle this resonator can also be described as the amplifying filter.
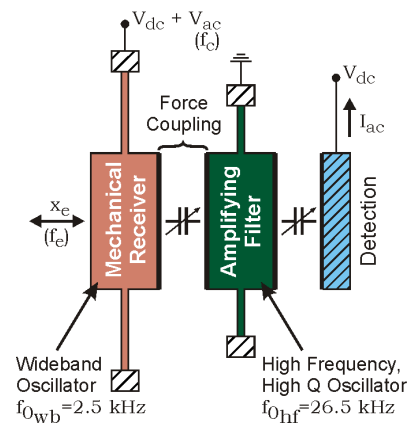

Fig. 1: Basic structure of the force coupled oscillator system

In case of mechanical vibration, the wideband oscillator couples electrostatic forces to the high Q resonator, which is additionally stimulated by a carrier signal. Amplitude modulation occurs in the same way as in the mixer stage of the superheterodyne receiver. Consequently one obtains the lower and upper sidebands which carry all the information of the vibration stimulus.

By variation of the carrier frequency f_c the lower (or upper) sideband can be adjusted exactly to the resonance frequency of the high Q oscillator. Thanks to the high Q-Factor the signal is amplified in a very small band and with a high signal-to-noise ratio as shown in Fig. 2. Moreover, the sense frequency can simply be tuned by variation of the carrier frequency in order to set or sweep the desired spectral line.
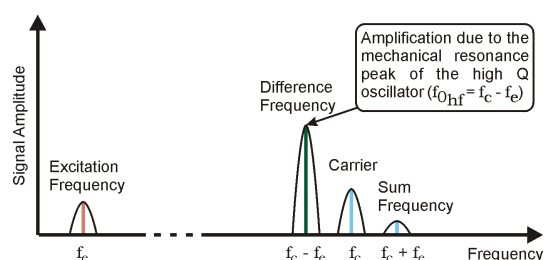

Fig. 2: Principle of operation

3 Fabricated Silicon Structure

The sensor is fabricated with the BDRIE (Bonding and Deep Reactive Ion Etching) silicon technology which allows a maximum aspect ratio of 30:1 [3]. The following figure shows a scanning electron microscopy (SEM) image of the fabricated silicon structure. The smallest gaps are $2\,\mu m$ and the height of the structure is $50\,\mu m$. The seismic masses are $40\,\mu g$ for the wideband oscillator and $60\,\mu g$ for the high Q resonator respectively.
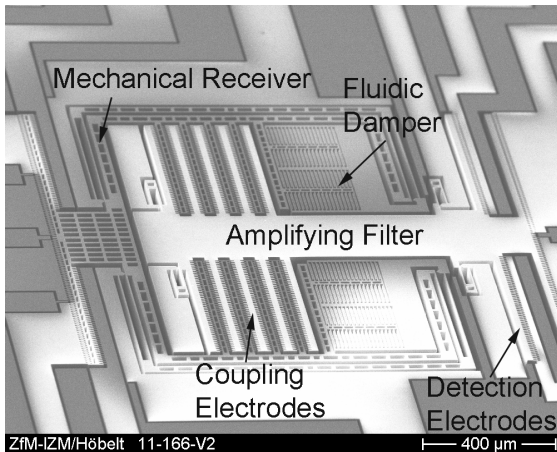
Fig. 3: SEM view of the force coupled oscillator system

4 Results

The oscillators are equipped with self test electrodes allowing an electrostatic actuation and sensing to record the transfer functions of each oscillator and also test the whole system. Hence the mechanical characteristics of the oscillators could be measured.

The high frequency oscillator shows a resonance frequency of 26.54 kHz and a quality factor of $Q = 140$ at ambient pressure. The low frequency wideband oscillator shows a damping factor of approx. $\upsilon = 0.82$.
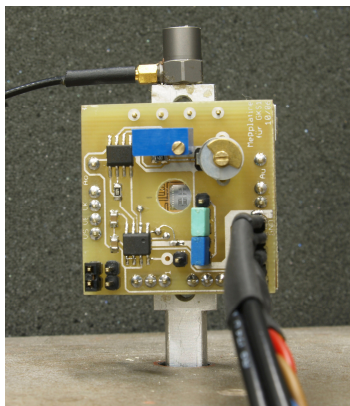
Fig. 4: Sensor mounted on shaker with lab-electronics

The micro system was stimulated on a shaker with frequencies between 40 Hz and 1 kHz (Fig. 4). The low frequency vibration signals have been transformed by the superheterodyne principle up to 26.5 kHz, where the mechanical resonance was observed. Signal detection is achieved by an ordinary I/V converter. Fig. 5 shows the spectrum of the output signal.
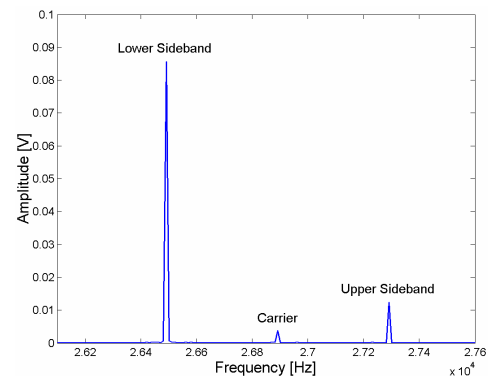
Fig. 5: Frequency domain with mechanical excitation of 2 g at 400 Hz

5 Conclusion

The presented micromachined force coupled oscillator system shows a novel mechanism of action to detect mechanical vibration of low frequency (< 1 kHz) without a subsequent Fourier transformation. The principle of operation is based on amplitude modulation and selective filtering at one specific frequency as known from the superheterodyne principle. The sense frequency is acquired by a simple frequency tuning mechanism. Further work will focus on a characterization of the micromechanical system with regard to warping and damping effects. We are also working on a plain electronic for providing the carrier signal as well as picking up the detection current and self test of the two coupled oscillators.

Acknowledgements

References

[1] V. Wowk, Machinery Vibration: *Measurement and Analysis*, McGraw-Hill, New York, 1991

[2] D. Scheibner, J. Mehner et al: *A spectral vibration detection system based on tunable micromechanical resonators*, Sensors and Actuators A 123-124 (2005), pp. 63-72

[3] K. Hiller, M. Küchler et al: *Bonding and Deep RIE – a powerful combination for high aspect ratio sensors and actuators*, Progress in Biomedical Optics and Imaging - Proceedings of SPIE, vol. 5715 2005, pp. 80-91

Subproject B2: Experimental characterization, model adaption – reliability

Doetzel, Wolfram[1], Michel, Bernd[2]

[1]TU Chemnitz, Faculty of Electrical Engineering and Information Technology, Department for Micro Systems and Precision Engineering

[2] FhG-IZM Berlin, Department MR & MM

Characterization technique for quality control of MEMS

Hanf, Marian[1], Shaporin, Alexey[1]

1 Introduction

In the last ZfM annual report in 2005 we introduced a novel characterization method for micro electro mechanical systems (MEMS). It is based on a comprehensive theoretical analysis in terms of a sensitivity analysis and a multi parametric modal variational analysis. The sensitivity analysis is performed to determine

i) those parameters that are responsible for the MEMS performance and

ii) those the method is able to determine.

l_f	- flexure length:	300 µm
l_s	- support length:	360 µm
l_m	- mirror length:	900 µm
w_f	- flexure width:	5 µm
w_m	- mirror width:	80 µm
th_s	- structure thickness:	5 µm
w_{slit}	- slit width:	30 µm
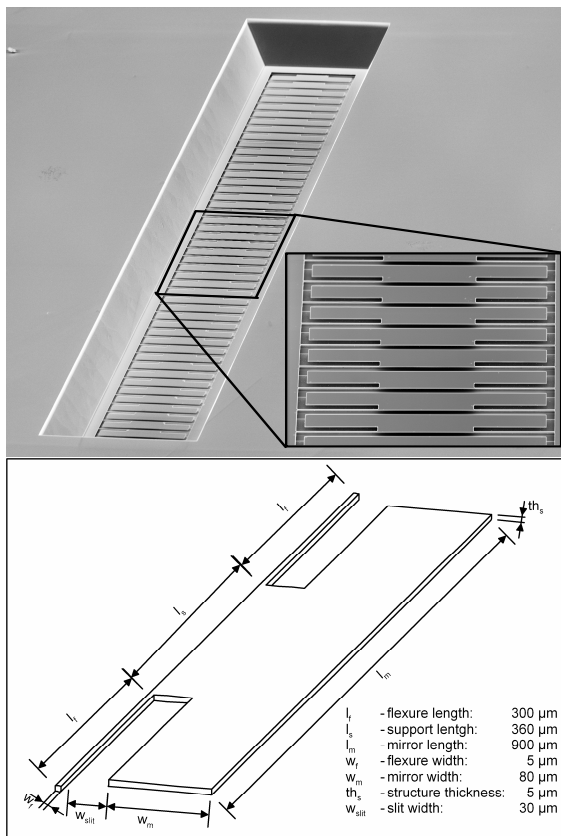
Fig. 1: SEM view of the micro mirror array (upper), sketch of a mirror with design parameters

The investigated structure is a micro mirror array (Fig. 1 upper) with the significant parameters flexure's width, structure's thickness and intrinsic mechanical stress in the flexures (Fig. 1 lower).

The multi parametric modal variational analysis calculates the first 10 Eigen-frequencies of a mirror model. It provides a matrix that contains three parameters varying in a certain range and the according Eigenfrequencies. In a second step these data are approximated by an appropriate polynomial to obtain an analytical expression for the dependency of the Eigenfrequencies on the three parameters.

The practical characterization merely is the determination of the Eigenfrequencies. This is performed by electrostatically exciting the mirrors with a pseudorandom noise sequence and measuring their response with a Laser-Doppler-inter-ferometer. A signal analyzer records the excitation signal and the response signal and calculates the frequency response function that shows the Eigenfrequencies as peaks in the imaginary part (Fig. 2).
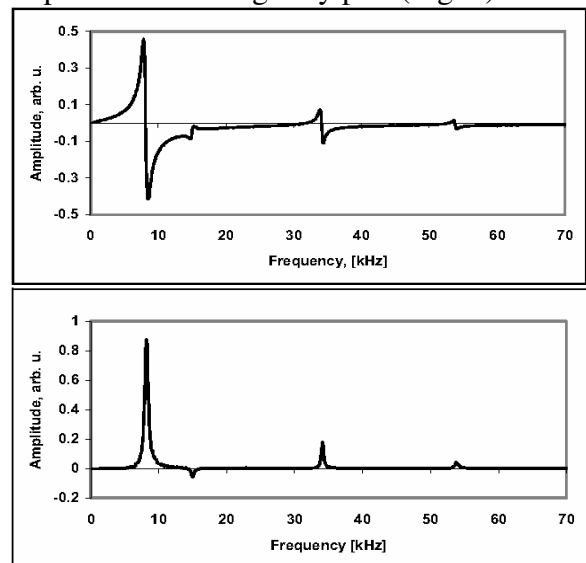

Fig. 2: Measured frequency response function of a mirror as real and imaginary part (upper and lower)

Applying a Lorentian fit to each peak provides a very accurate estimation of the Eigenfrequencies.

2 Results

In terms of a validation of the method two mirrors were investigated at six different temperatures while heating them from room temperature to 120°C. As expected the mechanical stress changes significant while the geometrical parameters remain almost constant with a standard deviation of 1.8% for the width and <0.09% for the thickness.

Several arrays of a wafer were characterized. As already shown in the last ZfM annual report the results identify the thickness and the mechanical stress as those parameters that deteriorate the mirrors performance. That's why the mirror layout is redesigned and the technology is changed. The new design in Fig. 3 shows stress reducing corners in the flexure and larger mirror plates for an increased fill-factor of the array.
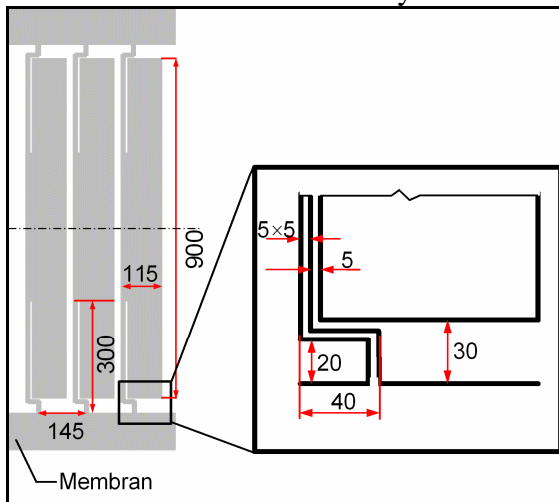
Fig. 3: New mirror layout with larger mirror plates and stress reducing flexure design

The technological process is changed to that effect that now commercially available SOI-wafers (silicon on insulator) are used with a thickness of the functional silicon of 5 µm and a guaranteed total thickness variation of ±0.5 µm. To realize the gap between the mirror plates and the driving electrodes the second wafer (electrode wafer) contains grooves with the electrodes therein. That implies the possibility to use SU8-wafer bonding that enables to easily vary the gap width.
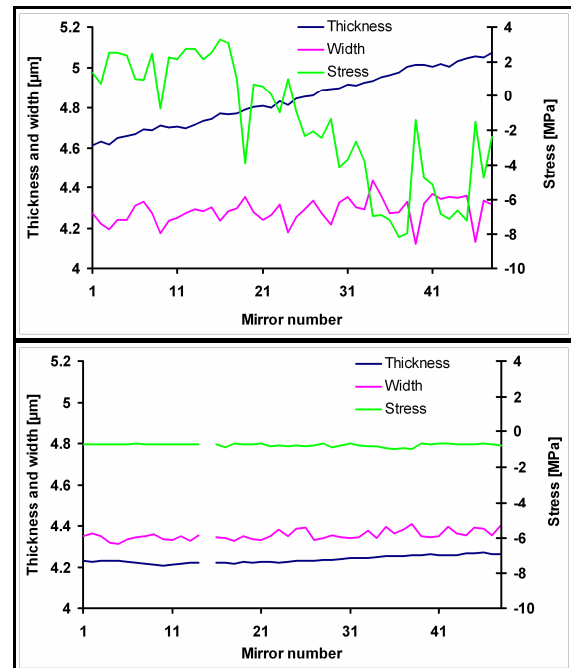
Fig. 4: Results for flexure's width, thickness and mechanical stress of an old (upper) and a new array (lower)

The characterization method is applied to the new arrays. For better comparison the upper diagram in Fig. 4 shows results of an old array. The lower diagram uses the same scale to demonstrate the improved performance of the new arrays. The absolute value of the mechanical stress is reduced to <1 MPa. The width and the thickness vary ca. 100 nm over the whole array. These results prove in an impressive way the success of the redesign and the changes in the technological process.

3 Summary

The presented characterization method was developed for the determination of geometrical and material parameters of MEMS. The method bases on the fusion of numerical and experimental data, in particular the Eigenfrequencies. Once the numerical data are calculated the method is very efficient, due to the comparatively simple and few measurements. The characterization of the mirror arrays shows very good results according the resolution of the method. The revision of the array was very successful so that the new performance matches the requirements.

Subproject B5: Development of a Spectral Imaging Technology Based on Microactuators with a Diffraction Grating

Flaspöhler, Martin[1]; Hübler, Arved Carl[1]; Bonitz, Jens[2]; Hahn, Ramon[2]; Kaufmann, Christian[2]
[1]TU Chemnitz, Faculty of Mechanical Engineering, Institute for Print and Media Technology
[2]TU Chemnitz, Center for Microtechnologies

1 Introduction

The accurate colour reproduction of an arbitrary original is a common problem in pre-press and the following printing process. The first important part in this workflow is the digitising of the original. The use of state-of-the-art RGB-based image capturing systems, however, is not sufficient for every application. Due to the known theoretical limitations of RGB-techniques, multispectral and spectral methods of image capturing using more than three colour channels have been introduced in the last years. Chemnitz University of Technology has presented one of these spectral imaging systems using an oscillating micro mirror with a diffraction grating [1, 2], where each pixel of an original image is recorded in a spectroscopic way. Because of the high oscillation frequency of the micro mirror, very high light intensities are needed. The aluminium layer of the mirror absorbs about 10 % of the incoming light intensity leading to a heating of the mirror surface. To solve this problem, the reflective grating will be replaced by a transmission grating. Therewith absorption losses should not occur, allowing the use of higher light intensities compared to a reflective mirror.

2 The Microactuator with a transmission grating

The actuator is a silicon micro mirror with a transmission grating (Figure 1). The mirror is fabricated with silicon bulk technology by anisotropic Si etching, DRIE and wafer bonding processes. The grating is implemented in a 2 µm thin, optical transparent membrane and has a height of 500 nm. The grating constant and other important properties of the actuator are shown in Table 1.
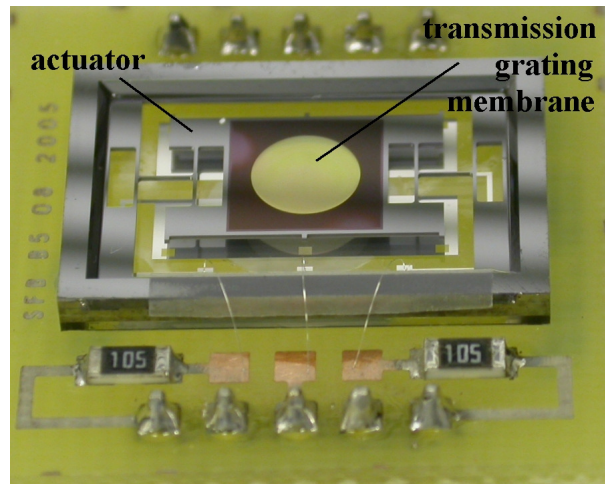

Figure 1: Actuator on conductor board

Table 1: Properties of the actuator

Resonant Frequency	500 Hz
Optical deflection angle	25° (±12.5°)
Membrane warping	<100 nm (<$\lambda/4$… $\lambda/8$)
Grating period	1.6 / 2.0 µm
Membrane diameter	4.2 mm

3 Colorimetric and optical characterisation

The realised microactuators are mounted in a spectral image capture device (ICD). The principle of this system is shown in Figure 2. The diffracted light of the transmission grating illuminates the original. Because of the exit slit only a small wavelength interval of the light can pass the original. A total of 35 spectral intervals in a range between 400 nm and 740 nm are recorded. The complete spectral ICD has to be examined with regard to the optical and the resulting colorimetric properties. The most important parameter is the achievable spectral reproduction accuracy and the resulting colour accuracy. The results are presented below.
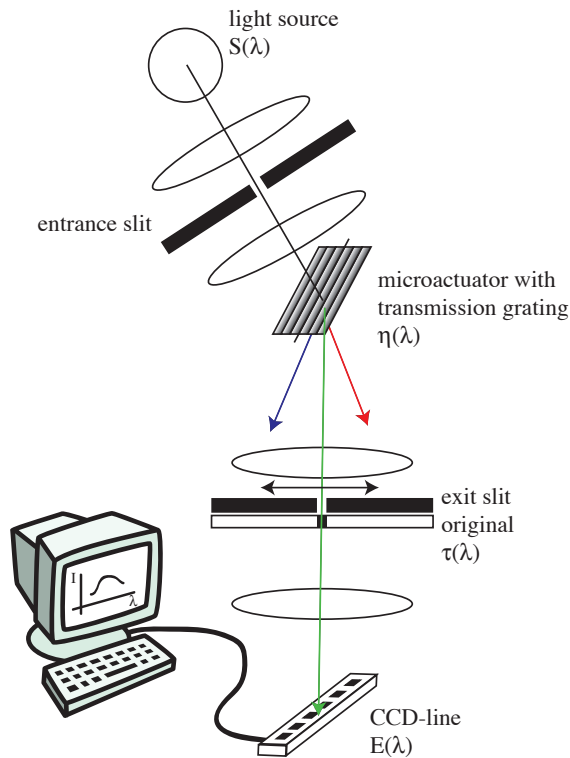
Figure 2: Principle of the spectral ICD

3.1 Spectral and colorimetric reproduction accuracy

The spectral reproduction accuracy is tested using a transparent Kodak Q-60 IT8/7.1 colour test chart (Figure 3). The spectral transmission properties of the 240 colour patches are measured using the spectral ICD. For reference purposes the spectral transmission properties are also measured using a two-beam spectrometer. Calculating the root mean square error between the measured spectra of the ICD and the spectrometer allows determining the spectral reproduction accuracy for each colour patch.
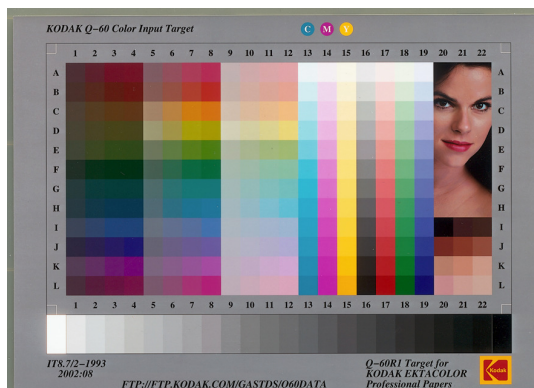
Figure 3: Kodak Q-60 IT8/7.1 colour test chart

An example for the colour patch K19 of the IT8/7.1 test chart is shown in Figure 4. The solid line represents the spectral properties measured by the spectrometer. The squares are the measuring points of the spectral ICD. In this case the root mean square error between these two measurements is 0.009.

To evaluate the influence of the deviations between the two spectral distributions on the colour accuracy, the corresponding colour values regarding light source D65 are estimated. To quantify the colour accuracy, the colour difference ΔE_{ab} between the two measured spectra is calculated. In this example, ΔE_{ab} is 3.2. With regard to the complete colour test chart, the values of the measured ΔE_{ab} are in a range between 3.1 and 7.9. This is a slightly better colour accuracy compared to the former reflection gratings.
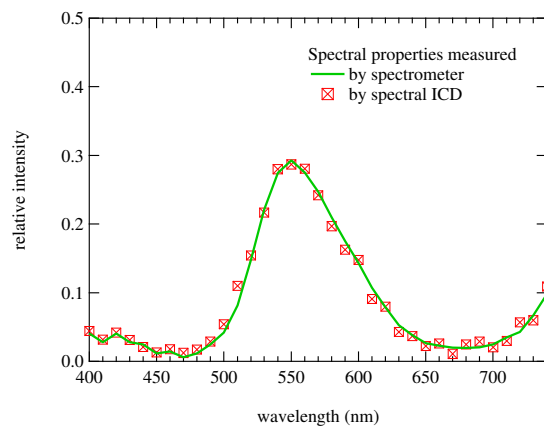
Figure 4: Measured spectral transmission properties of the IT8/7.1 K19 colour patch using a two-beam spectrometer and the spectral ICD with a 1.6 μm grating.

References

[1]   Hübler, A.; Guessous, F.; Reuter, S.: *New Approach for a Spectral Image Capture Device Based on a Micro Mirror System.* Proc. of SPIE, Vol. 4300, pp. 18 – 24, January 2001, ISBN: 0-8194-3978-9

[2]   Flaspöhler, M.; Buschnakowski S.; Kuhn, M.; Kaufmann, C.; Frühauf, J.; Gessner, T.; Ebest, G.; Hübler, A.: *Multispectral Image Capturing System Based on a Micro Mirror Device with a Diffraction Grating.* Proc. of IS&T's 2003 PICS Conference, pp. 183 – 187, May 2003, ISBN: 0-89208-245-3

Subproject C2: A Novel High Aspect Ratio Technology for MEMS Fabrication Using Standard Silicon Wafers

Bertz, Andreas[1]; Reuter, Danny[1]; Lohmann, Christian[1*]; Heinz, Steffen[2]; Ebest, Gunther[2]; Gessner, Thomas[1,3]

[1]TU Chemnitz, Fakultät für Elektrotechnik und Informationstechnik, Zentrum für Mikrotechnologien

[2] [1]TU Chemnitz, Fakultät für Elektrotechnik und Informationstechnik, Professur für Elektronische Bauelemente

[3] FhG-IZM Chemnitz, Abteilung MDI

* now with Phillips Semiconductor GmbH

1 Introduction

During the last few years the subproject C2 was focused on the development of a powerful and versatile technology for the fabrication of high aspect ratio microstructures (HARMs). Several demonstrators of *"Air gap insulated Microstructures (AIM)"* have been manufactured and characterized [1, 2]. As will be shown further decisive benefits of the AIM-technology are proven. On the other hand the structure design and the process flow (including individual steps) had to be optimized in order to meet the requirements of high-yield fabrication.

2 Anchor Design

While having real advantages in the fabrication process as well as e.g. in the thermal performance of the AIM devices a special anchor structure is required for isolation. As shown by FEM calculations care should be taken for this structure with respect to the device lifetime but even for the manufacturing process. Electrostatic charging during plasma processing is a critical issue - especially in combination with the very high quality factor of the movable structures due to low chamber pressure. Therefore the anchor structure has been modified in order to get a more uniform force distribution compared to the previous structure. This is illustrated by Fig.1 (FEM model and SEM of fabricated anchor.
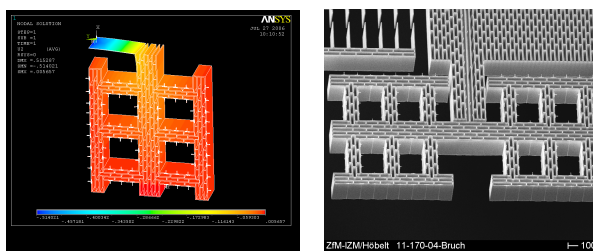

Fig.1: The modified anchor structure as FEM model (left, half of structure shown) and SEM after fabrication (right)

But not only the layout of this structure has to be considered because the reliability of the carrier structures depends on the material properties too. Therefore it was decided to replace the simple Al based carrier by an Al/ dielectrics stack. Extensive investigations have been carried out in order to ensure the required film stability, adhesion as well as significant tensile stress even under high temperature influence. Additionally the carrier beam cross section has been reworked so that any pinch within the Al film is avoided (Fig. 2). This is required for a good long-term stability of the devices.
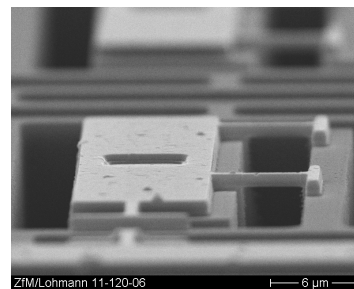

Fig.2: SEM photograph of the reworked carrier illustrating fully flat interconnect lines in order to avoid any migration effects caused by pinches

3 Sensor Performance

In general, high aspect ratio devices based on crystalline silicon have strong benefits compared to thin film structures: large signal to area ratio, mechanical overdamping possibility and others. A special advantage of the AIM principle compared to e.g. SOI technology was expected to be the thermal behavior however. That is because an additional interface, potentially generating mechanical stress is avoided. Therefore a variety of measurements have been carried out: capacitance change vs. temperature on wafer level by parametric testing, capacitance change vs. temperature on single sensors by a capacitance meter as well as voltage drift vs. temperature by using a hybrid integrated CV converter. The latter one offers the most reproducible results. As indicated by Fig. 3 the "zero g level shift" of the *low g-*sensors measured is lower than +/- 0.06 mg/K.
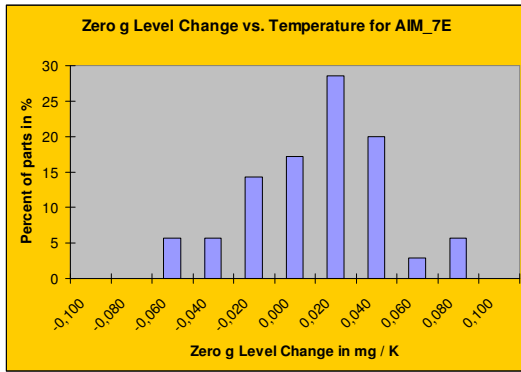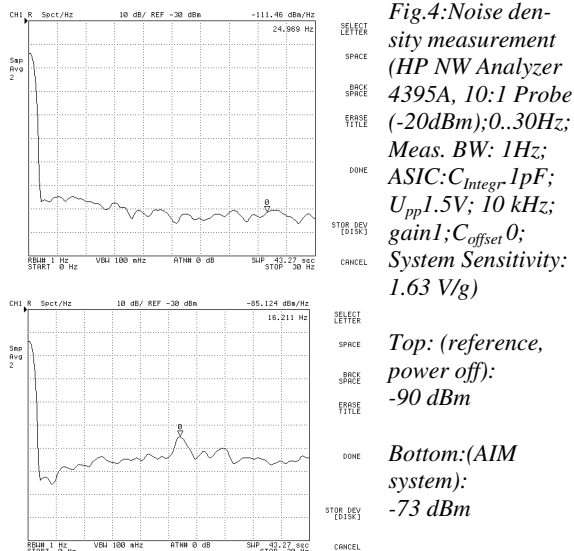
Fig.3: Histogram of "zero g level shift" vs. temperature of AIM low g sensors

Taking into consideration that there is an additional temperature influence of the CV converter these are really encouraging data.

Furthermore, noise measurements have been done (sensor and analogue ASIC) by using an HP Network Analyzer 4395A (Fig. 4).

Fig.4: Noise density measurement (HP NW Analyzer 4395A, 10:1 Probe (-20dBm);0..30Hz; Meas. BW: 1Hz; ASIC:C_{Integr} 1pF; U_{pp}1.5V; 10 kHz; gain1;C_{offset} 0; System Sensitivity: 1.63 V/g)

Top: (reference, power off): -90 dBm

Bottom:(AIM system): -73 dBm

Using these data a noise floor of 30.7 µg/Hz^{-1} is obtained. Considering the ratio of capacitive sensitivity (600 fF/g) with respect to the noise floor (nearly 20) this is an excellent value compared to the overview in [3]. Moreover, there are chances to increase this ratio because the ultimate limit of the noise density for the sensor itself (calculated thermal noise) is as low as 6.84 µg/Hz^{-1}.

4 Readout Circuit

The concept for signal processing of the differential capacitance measurement is based on the Delta-Sigma Modulation technique as shown in Fig. 5.
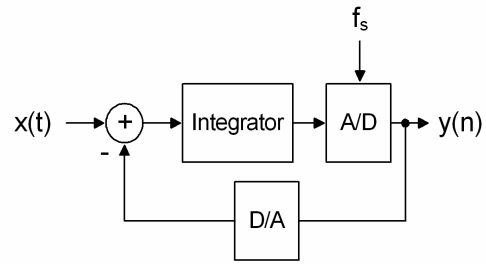
Fig.5: Principle of Delta-Sigma Modulation as used

The modulator consists of an integrator and an A/D converter only. Compared to other methods the output signal represents a digital bit stream which is proportional to the input signal. Thus the requirements for the A/D converter and input filters are reduced. Due to the oversampling technique only a 1st order low pass input filtering is required. The circuitry is based on the Switched-Capacitor technique and includes the modulator and blocks for signal conditioning as well as sensor driving [4]. A 2nd order modulator with a clock frequency of 200 kHz is used. An overview of the circuit layout is shown in Fig. 6.
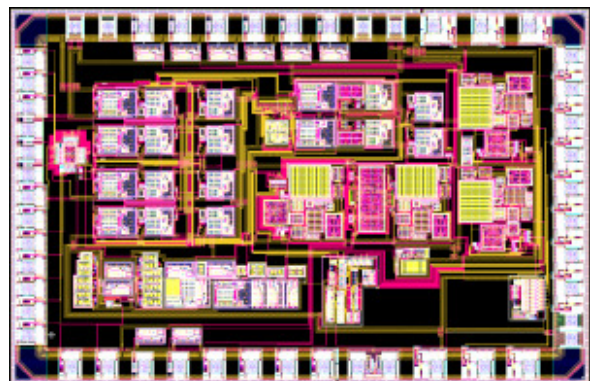

Fig.6: Circuit layout of the Delta-Sigma converter

References

[1]   Lohmann, C. et al.: *High Aspect Ratio Micromachining using AIM Technology*. World of Electronic Packaging and System Integration, pp 544-548

[2]   Bertz, A. et al.: *Efficient and Flexible High Aspect Ratio Micromachining for the Fabrication of low-g-Sensors*. Microcar 2005; Vol. 04 (2005) p 79

[3]   Chae, J. et al.: *A CMOS-compatible high aspect ratio silicon-on-glass in-plane micro-accelerometer*. JMM 15 (2005), pp. 336-345

[4]   Luf, Alexander: *Eine integrierte Sensoraus-werteschaltung nach dem Prinzip der Delta-Sigma-Modulation*. DA, TU-Chemnitz, 2006

Subproject C4: Resonator arrays with adjustable stiffness and investigations of low temperature bonded wafers

Hiller, K.[1]; Seifert, M.[2]; Shaporin, A.[3]; Hanf, M.[3]; Louis, S. J[4].; Friedrich, M[4].; Frühauf, J.[2]; Gessner, T.[1]; Dötzel, W.[3]; Zahn, D.R.T.[4]

TU Chemnitz, Faculty for Electrical Engineering and Information Technology, [1]Center for Microtechnologies, [2]Workgroup Materials in Electrical Engineering and Electronics, [3]Professorship Microsystems and Precision Engineering, [4] Faculty for Natural Sciences, Professorship Physics of Semiconductors

1 Resonator arrays with variable stiffness

During the 4th period of SFB 379, resonators with adjustment of spring stiffness controlled by electrostatic forces have been investigated. The approach presented here is based on a bulk technology. Two wafers with an array of parallel springs are bonded together, whereby a gap of 2 µm between the springs is created (Fig. 1). Electrostatic forces will pull together the springs. Hereby, the stiffness of the spring suspension is changed by a factor of 4. The concept and the design process are described in detail in [1], [2].
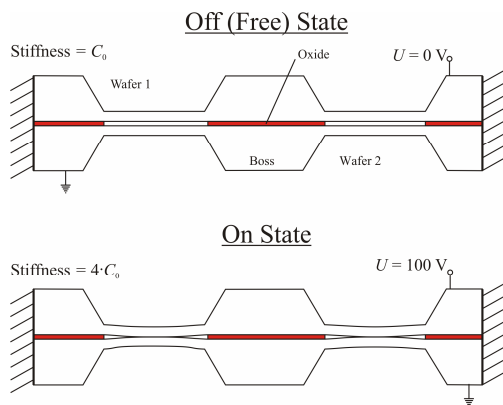
Fig. 1: Adjustment of spring stiffness by change in topology, controlled by electrostatic force
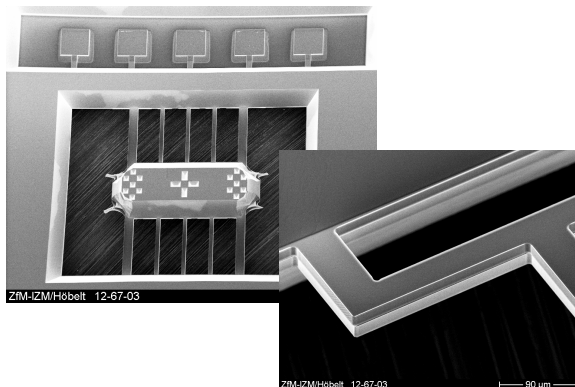

Fig. 2: SEM pictures of the resonator structure: whole bonded resonator and detail of two parallel springs with stress compensation beams

First demonstrators have been fabricated successfully. Fig. 2 shows the resonator and some details of springs. The spring dimensions are thickness 20 µm, width 50…100 µm and length varying from 750 µm to 1500 µm. In order to enable the gap opening when the voltage is switched off, the roughness of the spring surface has been increased by means of plasma etching. R_q values of 1.7 nm and 2.3 nm have been measured by AFM. Using special test structures, corresponding adhesion energies of 0.023 J/m² and 0.00024 J/m² have been determined [2]. For comparison, the polished surface shows a R_q of 0.3 nm and an adhesion energy of 0.1 J/m².

The switch characteristics as well as the dynamic behaviour of the resonators have been investigated. Table 1 gives the switching voltages for the four different variants. The simulated and measured values are in very good agreement. However, successful closing and opening of the gaps between the springs was only possible with AC voltage and up to 1250 µm spring length. It is assumed that charging effects influence the switching behaviour additionally to adhesion.

Table 1: Switching voltages

Spring length [µm]	Switching voltage [V] FEM simulation	Switching voltage [V] measurement
750	153	130
1000	88	61
1250	57	48
1500	40	31 (not reversible)

Fig. 3 shows the shift of the resonant frequency with respect to the 8 different switch modes for a typical resonator (upper wafer fabricated from a Si wafer). It is clearly visible that the dynamic behaviour can be controlled by the proposed method. There is still a deviation between

simulated and measured frequencies especially for modes 5 to 8, that is when the outer springs come into action. These deviations are due to etch tolerances, which can be minimized by use of SOI wafers both for the lower and the upper wafer. As indicated in Fig. 4, hereby a much better linearity can be obtained. Further details and results are given in [2].
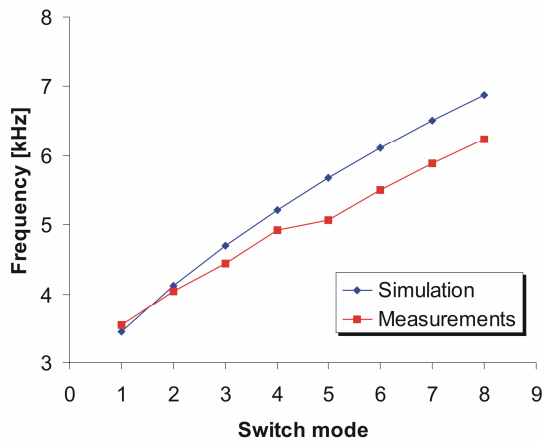

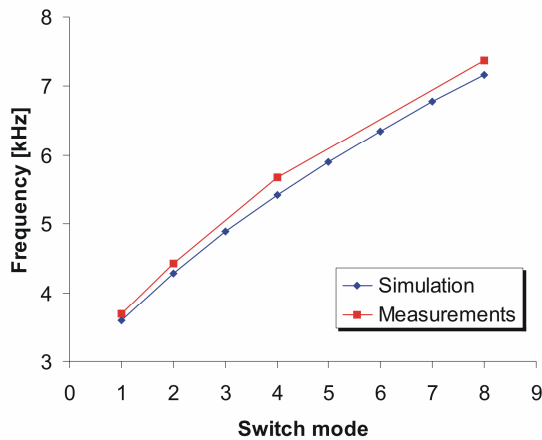*Fig. 3: Simulated and measured shift of the resonant frequency with respect to switch modes – upper wafer Si*

Fig. 4: Simulated and measured shift of the resonant frequency with respect to switch modes – upper wafer SOI

2 Infrared spectroscopy

Multiple internal transmission (MIT) IR spectra of directly bonded Si wafers with different treatments before bonding (RCA cleaning, O_2 barrel reactor plasma and O_2 RIE reactor plasma) are recorded during annealing at different temperatures ranging from 25-325° C [2]. At room temperature there is a broad absorption band in the spectral region between 3000 cm^{-1} and 3600cm^{-1}, due to the stretching vibration of

hydroxyl groups in water. On heating the samples, a reduction in the intensity of the band at 3400 cm^{-1} occurs which indicate the loss of water at the interface (see Fig. 5). The same trend is observed for all samples till 225°C. It is evident that even at high temperatures the RIE treated samples contain more water in their interface.
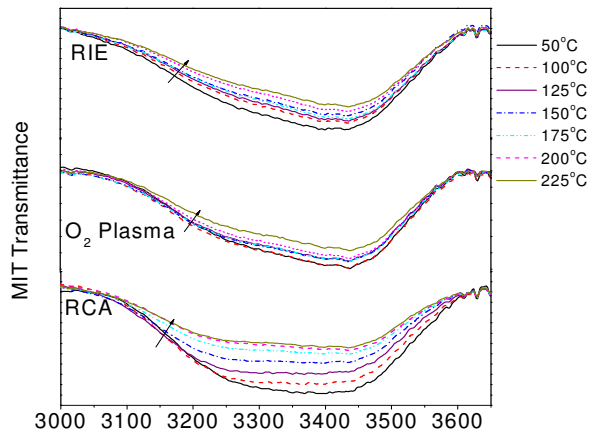

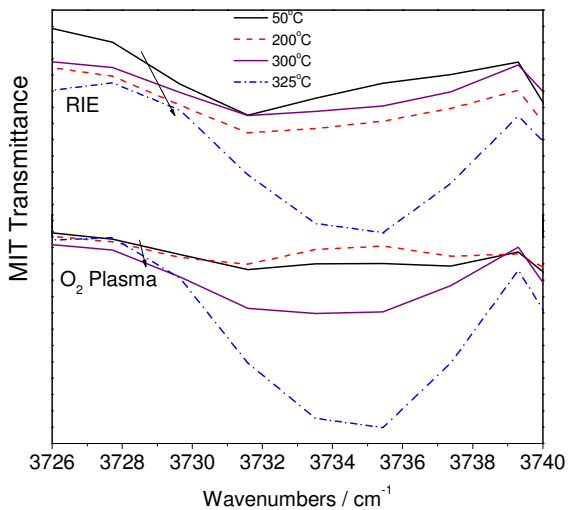*Fig. 5: In situ MIT IR spectra in the region of water and SiO-H absorption*

Fig. 6: In situ MIT IR spectra in the region of H stretching vibration

As temperature is increased above 150°C, for the O_2 plasma and RIE treated samples a shoulder appears at 3735 cm^{-1} to develop to a short band during the higher temperatures above 250°C (see Fig. 6). This indicates the formation of O - SiOH species. Further increase above 250°C, results in the formation of siloxane bridges (Si-O-Si), which contribute to the strong bonding of the wafers.

3   Raman spectroscopy

Micro-Raman spectroscopy has proven to be a valuable tool to measure mechanical stress in silicon device structures [3]. Raman spectroscopy probes lattice vibrations which are sensitive to internal and external perturbations. The important aspect of Raman spectroscopy for micro system devices is its ability to determine local temperature and strain in the lattice. Micro-Raman spectroscopy allows investigation with μm spatial resolution.

Micro-Raman spectra have been taken at different points across a silicon wafer covered with few nm of native oxide and across another silicon wafer covered on front side with PECVD Si_3N_4 (thickness 500 nm) and treated at 600°C. The spectra taken as such are presented in Fig. 7. It can be seen, that the Si peak for the wafer with native oxide is present at 519.8 cm^{-1}. Even at a casual glance one can detect the shift in the peak position for the wafer covered with Si_3N_4 with respect to the bare wafer peak position.

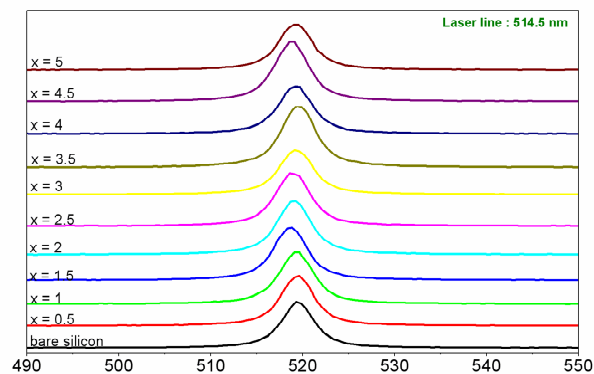*Fig. 7: Raman spectra of the Si_3N_4 covered wafer in comparison to the Si wafer*

The shift $\Delta\omega$ of this line from the spectral position indicates mechanical stress. A positive shift means compressive stress while a negative shift means tensile stress. In order to determine the Raman peak for the strain measurements, the measured Raman peaks are fitted with Lorentz function. The shift measured as a function of position on the wafer to obtain the stress pattern is shown in Fig 8. The main observation is that mainly the stress observed is compressive stress. Under the assumption that these are uniaxial stresses the stress values are calculated using the simple relation [4]

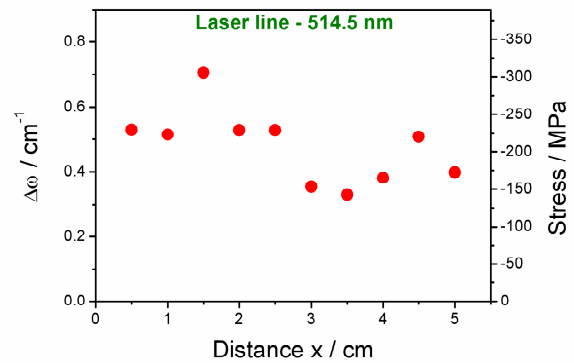$$\sigma / MPa = -434\Delta\omega / cm^{-1}.$$

Fig. 8: Difference in peak position across the wafer and corresponding stress values with respect to unstrained wafer
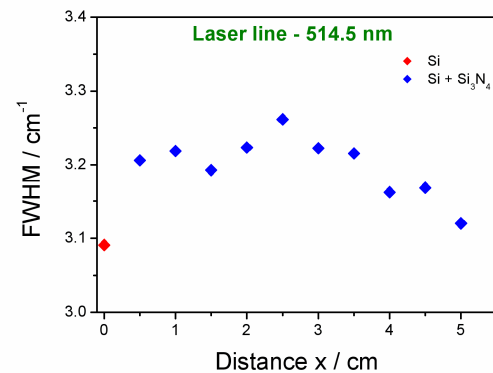

Fig. 9: Variation in the FWHM of the Raman peak

Furthermore, the Full Width at Half Maximum (FWHM) of the peaks has been investigated. In a perfect crystal without strain the FWHM is about 3 cm^{-1}. Imperfections and impurities as well as stress enhance the dispersion of phonon energy and therefore increase the FWHM. This effect is observed in our measurements, too (see Fig. 9). From the above results information about the stress in the probed Si wafer volume can be derived. Further investigations are planned in order to compare Raman results with other measurement methods.

4 References

[1] Seifert, M. et al.: *Niedertemperaturbonden für rekonfigurierbare Resonatorarrays*. Chemn. Tagung MST 2005, pp. 172-180

[2] Hiller, K. et al.: SFB 379, *Arbeits- und Ergebnisbericht TP C4*, 2006, to be publ.

[3] Ogura A et al: *UV-Raman Spectroscopy System for Local and Global Strain Measurements in Si*. Jap. Journ. of Appl. Phys. Vol. 45 (2006), No. 4B, 3007-3011

[4] Ingrid de Wolf: *Stress measurements in Si microelectronics devices using Raman spectroscopy*. J. Raman Spectroscopy, 30 (1999), 877-883

Evaluation of the gap-fill properties of dense low-k and porous ultralow-k spin-on dielectrics

N. Ahner [1]; S. Frühauf [1]; S. E. Schulz [1,2]

[1]Chemnitz University of Technology, Center for Microtechnologies, 09107 Chemnitz, Germany
[2]Fraunhofer IZM, Department Micro Devices and Equipment, 09126 Chemnitz, Germany

1 Introduction

Shrinking feature sizes and thus higher parasitic capacitances lead to rising RC delay of the interconnect system. Within BEOL low-k and ultralow-k dielectrics, either deposited by CVD or spin-coating, are used for isolation to lower delay times and crosstalk. Looking onto application of those materials within FEOL, e.g. as premetal dielectrics to decrease word and bitline coupling in DRAM circuits or on usage within BEOL as isolator materials within Aluminium technology, defect free filling of partly high aspect ratio features is one of the major challenges. Filling those structures by CVD is limited because of non-conformal film growth and so spin-on materials are considered for application.

Spin-on precursors for low-k and ultralow-k dielectrics are liquids, mainly consisting of a solvent, solid parts which finally form the low-k film, and additives, e.g. porogens for fabricating porous ultralow-k dielectrics.

Filling high aspect ratio gaps, defects like film cracks, mainly caused by shrinking, and formation of voids due to air inclusion can occur. The thicker the film the stronger it shrinks and so this defect can be overcome e.g. by variation of the spin-on parameters like spin-speed. Void formation is mainly caused by poor wettability of the surface to be coated and wetting behaviour of the used precursor. Wetting behaviour strongly depends on the surface energies of the solid as well as of the liquid and therefore has to be evaluated to make any predictions if the gap-fill will be without defects.

In this work the gap-fill properties of 3 spin-on low-k and ultralow-k materials on different surfaces have been tested. The wetting behaviour of the precursors has been evaluated by contact angle measurement on several surfaces and structures with different aspect ratios have been filled.

2 Experimental

PE-CVD SiO_2 with a film thickness of 500 nm and 900 nm has been deposited on 150mm p-doped (100) Si substrates. The film was patterned and the structures were refilled with LP-CVD SiO_2 to produce aspect ratios from around 1 to 10. In addition some patterned samples have been coated with a 30 nm Aluminium film, produced by sputter deposition. Aerogel[1], developed by the Center for Microtechnolgies, Rohm and Haas Zirkon® LK2000, both porous ultralow-k dielectrics, and Honeywell ACCUGLASS ™ T-512B, a dense low-k spin-on glass, were deposited onto the patterned samples by spin-coating. The wetting behaviour of the SiO_2 and Aluminium surface has been evaluated by contact angle measurement using several testing liquids and the precursor liquids, used for the gap-fill. The surface energy of the films was calculated using the method of Owens and Wendt by creating a Kaelble-plot [2].

3 Results and Discussion

Fig. 1 shows the contacts angles of the testing liquids on SiO_2 and Aluminium, arranged by the surface energy of the liquids, both with a similar wetting behaviour.
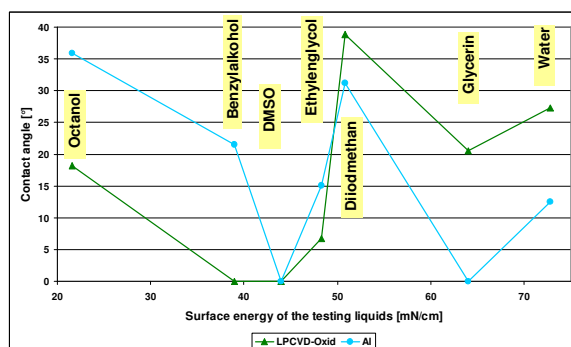

Fig. 1: Contact angles of several testing liquids on LP-CVD SiO_2 and Aluminium

The calculation of the surface energy also led to comparable results with 65.1 mN/m for the Aluminium surface and 64.9 mN/m for the LP-CVD SiO_2 surface. From the contact angle measurements of the spin-on precursors, which showed angles between 0 and 10°, no gap-fill defects resulting from poor wetting behaviour are expected.

Gap-fill experiments on structures with an aspect ratio of 1 and below with aerogel led to cracked films for low spin-speeds because of the high film thickness (Fig. 2a). Increasing spin-speed and therefore thinner films showed no cracking (Fig. 2b), but no feature with an aspect ratio higher than 1 could be filled defect free.
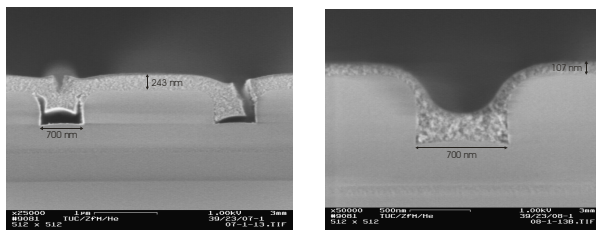

Fig. 2: a) Cracked aerogel film spun on with 1500 rpm;
b) Structure with the same aspect ratio and aerogel spun on with 3000 rpm)

LK2000 and Accuglass™ showed very good gap-fill properties, filling structures with an aspect ratio of 5 (LK2000) or 10 (Accuglass) without visible defects (Fig. 3a, 3b).
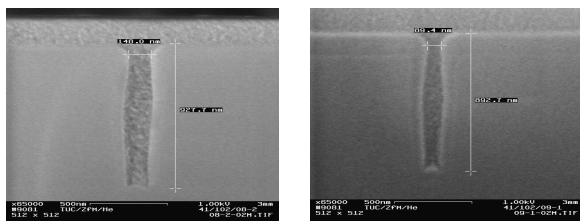

Fig. 3: a) Structure with AR=5 filled with LK2000 and
b) with AR=10 filled with Accuglass

Experiments on filling gaps covered with Aluminium (AR=1,5) with LK2000 also didn't show any defects resulting from incomplete wetting or film shrinkage (Fig. 4a, 4b).
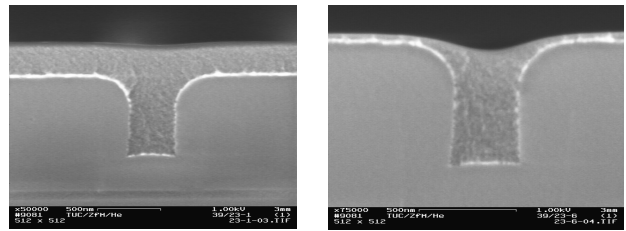

Fig. 4: LK2000 filling gaps covered with Aluminium;
a) spin speed: 1500 rpm, b) spin speed: 3000 rpm

4 Conclusions

Defect free gap-fill with Aerogel was possible only by usage of higher spin-speeds leading to thinner films and on structures with aspect ratios below 1. LK2000 and Accuglass™ showed a very good gap-fill behaviour, both filling structures with high aspect ratios without any visible defects.

The evaluation of the surface energy of LP-CVD SiO_2 and Aluminium showed similar values, which could be due to the oxidized aluminium surface. From this results no problems due to poor wettability of this surface were expected and the gap-fill with LK2000 of Aluminium covered structures actually was free from defects.

References

[1] Winkler, T.; Schulz, S.E.: Fabrication of SiO_2 based nanoporous aerogel thin films for advanced IC metallization; Advanced Metallization and Interconnect Systems for ULSI Applications in 1997; San Diego, CA; USA; 30 Sept.-2 Oct. 1997. pp. 347-351. 1998

[2] Preusser, W, Gierl, C., Rainer, A.: Oberflächenspannung - Messmethoden im Vergleich, JOT 10, S. 106-108, 2002

Thermal stability of spin-on MSQ low-k and ultralow-k dielectrics

N. Ahner [1]; S. E. Schulz [1,2] ; F. Blaschta [1]; M. Rennau [1]

[1] Chemnitz University of Technology, Center for Microtechnologies, 09107 Chemnitz, Germany
[2] Fraunhofer IZM, Department Micro Devices and Equipment, 09126 Chemnitz, Germany

1 Introduction

As device dimensions are further scaled down, RC delay of the interconnect system becomes more significant. Using low dielectric constant (k) materials for isolation within the interconnect system, parasitic capacitances and thus signal delay and crosstalk can be reduced. Within BEOL processing temperature load is limited to values of about 400°C to 450°C and so e.g. spin-on dielectrics are designed to achieve their desired electrical, optical and mechanical characteristics at curing temperatures within this range. Looking onto spin-on and low-k material application in the FEOL, higher processing temperatures are one of the major integration challenges. Possible applications for spin-on dielectrics range from STI to low-k integration as premetal dielectrics, e.g. to decrease word and bitline coupling in DRAM circuits. In this work the thermal stability of the electrical and optical parameters of two spin-on MSQ materials has been evaluated.

2 Experimental

Rohm and Haas Zirkon® LK2000, a porous ultralow-k dielectric (k ≈ 2,1), and Honeywell ACCUGLASS ™, a dense low-k spin-on glass (k ≈ 3,2), have been deposited by spin-coating on 150mm p-doped Si (100) substrates. The film was dried using hotplates and cured in N_2

ambient for 1h each, applying temperatures from standard value (450°C for LK2000 and 425°C for Accuglass™) up to 850°C and 900°C, respectively, in steps of 100°C.

Film thickness and refractive index have been measured by spectral ellipsometry, k-value and leakage current density were determined using a mercury-probe measurement. To detect changes within the chemical structure of the materials caused by applying high temperatures, a FTIR analysis has been performed.

3 Results and Discussion

Fig. 1 shows the change in film thickness and refractive index of LK2000 at different curing temperatures as an example. Accuglass™ showed a comparable behaviour. At temperatures up to 650°C (LK2000) and 700°C (Accuglass™) the film thickness is only slightly changing and the refractive index is almost constant. For higher temperatures the material is heavily shrinking and the refractive index is strongly increasing. Leakage current density and permittivity of LK2000 and Accuglass™ (Fig. 2 e.g. for LK2000) are showing the same behaviour, both rapidly increasing at temperatures higher than 650°C and 700°C, respectively.

For temperatures above 650°C (LK2000, Fig. 3) and 700°C (Accuglass™, Fig. 4) FTIR spectra show a shift of the Si-O-Si peaks at wave numbers from 1000/cm to 1200/cm.
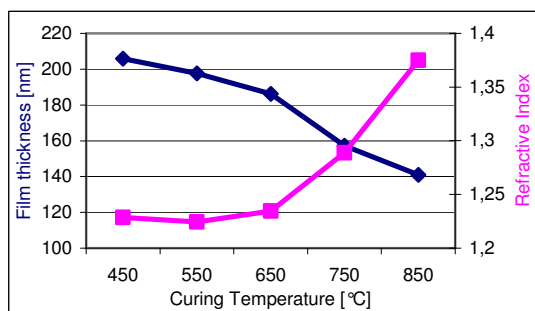

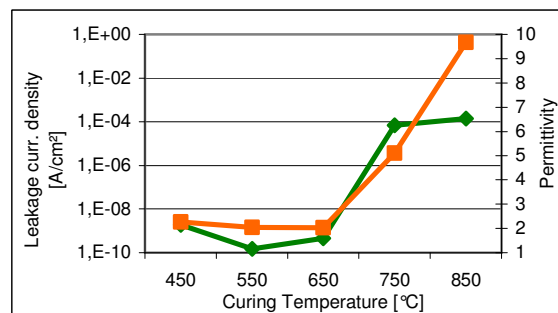Fig. 1: Film thickness and refractive index of LK2000

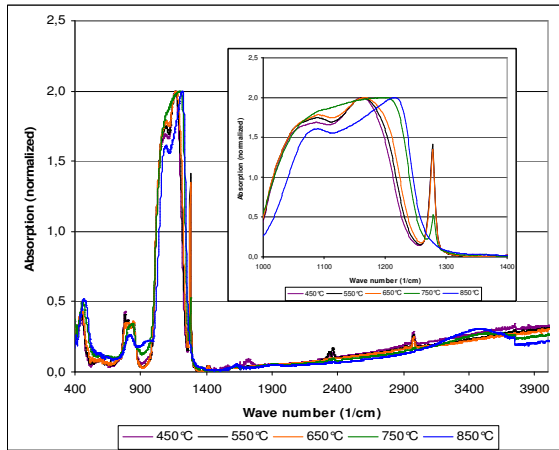Fig. 2: Leakage current density and permittivity of LK2000

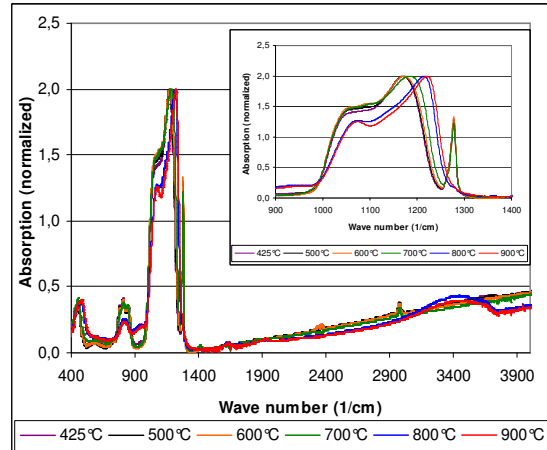*Fig. 3: FTIR spectra for LK2000 at different temperatures*

Fig. 4: FTIR spectra for Accuglass at different temperatures

The Si-CH$_3$ peak at 1275/cm and the CH$_3$ peak at 2975/cm vanish, but therefore OH peaks appear at wave numbers around 3400/cm.

The CH$_3$ within the MSQ materials is not stable at higher temperatures and so the increase of the k-value, refractive index and leakage current density is caused by the destruction of these groups. The materials become denser and so the film thickness is decreasing. The appearance of OH groups indicates a hydrophilization of the materials, which also causes higher k-value and leakage currents.

4 Conclusions

The MSQ based dielectrics Zirkon® LK2000 and ACCUGLASS™ T-512B show thermal stability and therefore potential for usage within processes applying temperatures up to 650°C and 700°C, respectively. For higher temperatures a degradation of the materials caused by the destruction of CH$_3$ groups occurs.

Evaluation of Air Gap structures produced by wet etch of sacrificial dielectrics:

Extraction of k_{eff} for different technology nodes and film permittivity

Schulze, Knut; Schulz, Stefan E.; Gessner, T.
Chemnitz University for Technology, Center for Microtechnologies, Chemnitz

1 Introduction

Air gaps are considered a promising alternative to achieve ultra low k-values in metallization systems of high performance integrated circuits. As for porous ultra low-k dielectrics, the ultimate low k value of vacuum or gas of ~ 1 is exploited to lower the effective dielectric constant in the respective metal level. Different approaches exist to realize air gap structures as cavities between interconnect line pairs: (1) Formation by deposition (non-conformal or selective CVD) and (2) Formation using sacrificial layers (by decomposition or by etching). On the other hand porous materials are under investigation as ultra-low-k (ULK) dielectrics. A number of challenges exist for integration into Cu damascene metallization systems due to the properties of these materials including poor adhesion, porosity, weaker mechanical strength, decreased chemical stability, and lower thermal conductivity compared to dense dielectrics. By using air gaps the potential of sufficiently low effective k-values is provided by circumventing the known integration issues of porous ULK materials at the same time. Especially selective air gap formation within densely packed areas and on the other hand the remaining of dense dielectric within relaxed structures is a main contribution to achieve a sufficient mechanical stability for reliable CMP processing and packaging and thus a successful multi-level fabrication.

This contribution is dealing with the electrical characterization of two sacrificial layer air gap approaches, called "mask" and "spacer", developed at TU Chemnitz by simulation using the Finite Element Method (FEM). Schematics of processing and showcase SEMs are given in [1]. "Air Gap formation using wet etch of sacrificial PECVD SiO_2". The objective is the extraction of k_{eff} and of the main factors to control the k_{eff} for both approaches in future node geometries (for ITRS requirements see Tab. 1). Main characteristics of the two air gap technologies are:

- Application of PECVD SiO_2 for inter metal dielectric (IMD)
- Local and selective removal of IMD by buffered HF impact
- Wet etch process alignment by the copper interconnect lines, distinct PECVD SiC:H films on top and beneath the lines.

Tab. 1: ITRS 2005 MPU interconnect technology requirements for the 65 nm and 45 nm node

Year of Production	2007	2010
DRAM ½ Pitch [nm]	65	45
k_{eff} required	2.7-3.0	2.5-2.8

2 Extraction of k_{eff}

Extraction is done in the following way [2]:
- Simulation of the capacity C_{Model} between two electrodes using a schematical copy of the real structures
- Merging of all functional films needed for integration (hard mask films, stop layers, IMD, …) between the lines into one homogeneous area "A" with a fixed k_{eff} value
- Simulation of the shaped capacitance C_{eff} using "A" between the lines – and subsequently following iterative fitting of k_{eff} until C_{eff} is equal to C_{Model} (application of a binary search algorithm)

3 Modeling

2d models of schematic cross sections of both approaches, see Fig. 1 and Fig. 2, have been used for simulation. Left part of each illustration shows SiO_2 filled line spaces, right parts are

representative for air gap structures after wet etch treatment. The used geometries for these models are according to the intended values of the ITRS 2005 for 65 nm and 45 nm nodes (see Tab. 2). On top and beneath of the structures bulky SiO_2 layers were arranged. Only static analyses were performed.
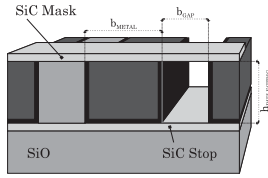

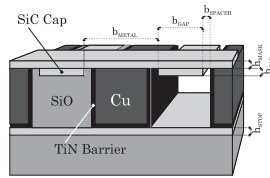Fig 1: Schematic simulation model of the "mask" approach

Fig 2: Schematic simulation model of the "spacer" approach

4 Simulation results

The effective k values extracted from the geometries of the 65 nm and 45 nm node are given in Fig. 3 and Fig. 4. A constant thickness of all functional SiC:H films of 10 nm was used. The highest values can be observed for the densely packed metal level "Metal 1" of the 45 nm node for both approaches (k_{eff} MASK = 1.96; k_{eff} SPACER = 2.07). k_{eff} shows a distinct dependence on node geometries. The reason is quite clear, relaxed structures include a lower ratio of SiC:H areas in comparison to the etched regions which finally results in a lower effective permittivity. The additional SiC:H (IMD capping) film between the metal lines "spacer" approach causes slightly higher k_{eff}-values versus the "mask" approach. Comparing the two the k_{eff} of the "spacer" approach is a minimum of 0.04 higher for relaxed structures (65 nm node, global level) up to a maximum of 0.11 for the densely packed architectures (45 nm, metal 1 level). The specified values of the ITRS 2005 (minimum required k_{eff} of 2.5, Tab. 1) for both nodes have been achieved in all examined cases. Nevertheless a further reduction of the SiC:H film thickness would be beneficial regarding to the electrical properties. In Fig. 5 a scaling of 0.7 (equivalent to 7 nm) was used for SiC:H film thickness for the 45 nm node. A significant decrease of 0.15 occurs in all cases. The resulting values are comparable to the 65 nm node simulations of Fig. 3. This appears logical, because changing the thickness in this way, the model in Fig. 5 is the same as in Fig. 3, only scaled by a factor of approximately 0.7. Fig. 6 up to Fig. 9 focus on a film thickness depending impact of permittivity of these functional films

on k_{eff}. Impact of both parameters on electrical performance is definitely strong. Pushing one parameter offers the possibility of the relaxation of the other one. The k_{eff} level lines of 1.8, 2.0,
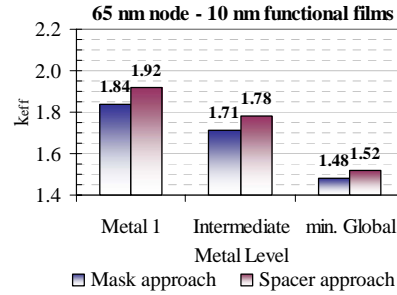

Fig 3: k_{eff} of "mask" and "spacer" approaches using 10nm thickness for all functional films and 65 nm node geometries
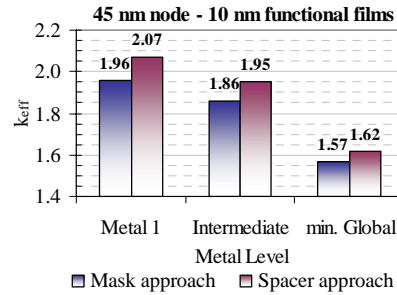

Fig 4: k_{eff} of "mask" and "spacer" approaches using 10 nm thickness for all functional films and 45 nm node geometries

Fig 5: k_{eff} of "mask" and "spacer" approaches using 7 nm thickness for all functional films and 45 nm node geometries

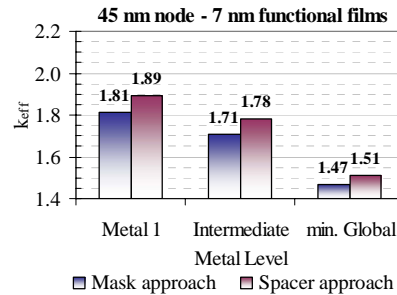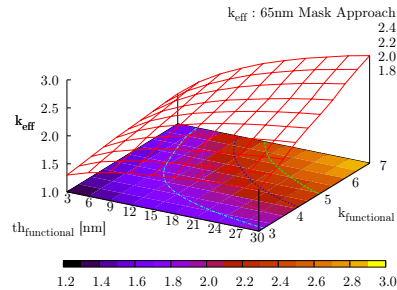Fig 6: k_{eff} of "mask" approach using 65 nm node "metal 1" geometries depending on thickness and k-value of all functional films

Fig 7: k_{eff} of "spacer" approach using 65 nm node "metal 1" geometries depending on thickness and k-value of all functional films

Fig 8: k_{eff} of "mask" approach using 45 nm node "metal 1" geometries depending on thickness and k-value of all functional films

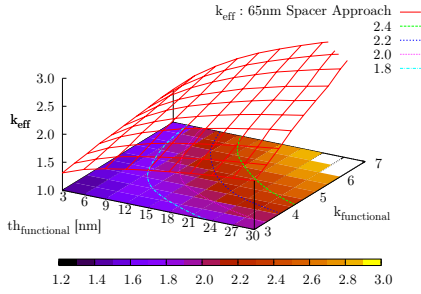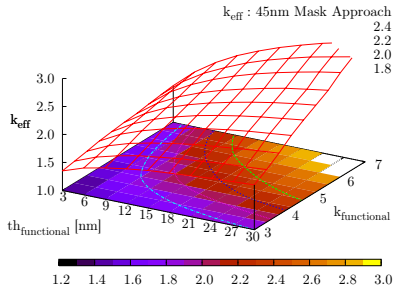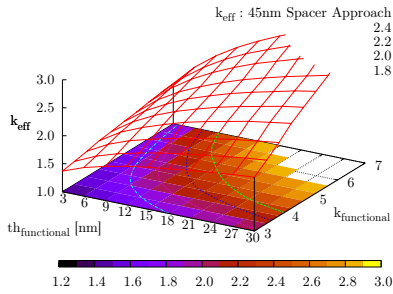*Fig 9: k_{eff} of "spacer" approach using 45 nm node "metal 1" geometries depending on thickness and k-value of all functional films*

2.2 and 2.4 show distinct combinations of both parameters.

5 Conclusions

- Two air gap approaches with sacrificial dielectrics ("mask" and "spacer") were successfully characterized concerning their effective k-value.
- FEM simulation was used for k_{eff} extraction.
- 65 nm and 45 nm node geometries were applied.
- Impact of thickness and permittivity of PECVD SiC:H films on k_{eff} were examined for metal 1 level geometries.
- k_{eff} is well adjustable by variation of both parameters.
- The received values fulfill the requirements of the ITRS 2005 for both approaches.

6 Acknowledgement

7 References

[1] K. Schulze, S.E. Schulz, M. Rennau, T. Gessner, Proceedings of the Advanced Metallization Conference (AMC) 2005, MRS Conf. Proc. AMC XXI, MRS Warrendale, PA, 2006p. 309-316

[2] K. Schulze, S.E. Schulz, M. Rennau, T. Gessner, Proceedings of the Materials for Advanced Metallization Conference (MAM) 2006, published in Microelectronic Engineering 83 (2006), pp. 2324-2328

Tab. 2: Geometries of ITRS 2005 for 65 and 45 nm node incl. stipulated values of Fig. 1 and Fig. 2

			Vertical Dimensions [nm]			Horizontal Dimensions [nm]			
			b_{METAL}	b_{GAP}	b_{SPACER}	h_{MASK}	h_{CAP}	$h_{DIELCTRIC}$	h_{STOP}
Mask-approach	65 nm	Metal 1	76	76	-	10	10	119	10
		Intermediate	98	98	-	10	10	166	10
		Min. Global	145	145	-	10	10	309	10
	45 nm	Metal 1	54	54	-	10	10	87	10
		Intermediate	68	68	-	10	10	112	10
		Min. Global	103	103	-	10	10	226	10
Spacer-approach	65 nm	Metal 1	76	76	8	10	10	119	10
		Intermediate	98	98	10	10	10	166	10
		Min. Global	145	145	15	10	10	309	10
	45 nm	Metal 1	54	54	5	10	10	87	10
		Intermediate	86	86	7	10	10	112	10
		Min. Global	103	103	10	10	10	226	10

Towards Atomic Layer Deposition Processes for Copper Thin Films

Waechtler, Thomas [1]; Schulz, Stefan E. [1, 2]; Roth, Nina [3]; Lang, Heinrich [3]; Gessner, Thomas [1, 2]

[1] Chemnitz University of Technology, Center for Microtechnologies, 09107 Chemnitz
[2] Fraunhofer Institute IZM, Reichenhainer Str. 88, 09126 Chemnitz
[3] Chemnitz University of Technology, Institute of Chemistry, 09107 Chemnitz

1 Introduction

Copper damascene metallization of ultra-large scale integrated (ULSI) circuits requires thin and conformal Cu seed layers before thicker films are deposited electrochemically for trench fill. Growing these seed layers by physical methods such as sputtering is becoming increasingly difficult with the continued shrinking of device dimensions. In contrast, atomic layer deposition (ALD) is able to create conformal and continuous ultra-thin films in deep trenches and three-dimensional structures due to its self-limiting deposition characteristic [1, 2]. Therefore, ALD Cu is not only interesting for future technology generations of ULSI circuits, but also for the metallization of MEMS devices and emerging approaches such as 3D integration.

However, ALD of elemental metals is not straight-forward. In case of Cu, the direct approach using a Cu source reagent and a reducing agent to obtain the elemental metal requires rather high temperatures [3, 4] or plasma processes [5, 6], leading to difficulties related to agglomeration of the films and reduced conformality. Therefore, hybrid techniques are favored that include making a Cu compound first which is then converted to Cu either as part of the actual ALD process or in a subsequent step. Such processes have been suggested by several groups either via copper nitride [7, 8] or oxide intermediates [9-13].

In addition, finding a suitable Cu precursor remains a central issue. Most Cu compounds such as Cu(I) halides or Cu(II) metal-organics are solids, posing challenges to precursor evaporation and delivery to the process chamber. On the other hand, most liquid metal-organic Cu(I) compounds contain halogens that can lead to reduced adhesion of the Cu films or etching of the substrate materials. Some Cu(I) precursors such as the novel Cu(I) amidinates [14-16] avoid these issues, but most of them require expensive synthesis routes.

Therefore, this work concentrates on ALD processes using a liquid Cu(I) β-diketonate which can readily be synthesized by standard methods. In contrast to approaches using fluorinated Cu compounds [8-10, 13], the current work deals with a fluorine-free precursor to avoid the undesired side-effects mentioned above. To obtain ultra-thin, continuous films, agglomeration must be avoided. Therefore, the experiments aim at ALD processes well below 200°C.

2 Experimental

For ALD experiments, a Cu(I) β-diketonate compound as shown in Fig. 1 was chosen with R and R' being non-fluorinated alkyl groups while L is an organophosphane Lewis base ligand.
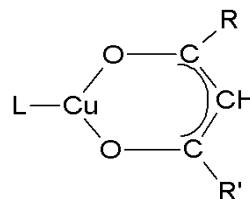
Fig. 1: General formula of a Cu(I) β-diketonate compound.

The precursor is liquid under standard conditions. Thus it can be supplied to the deposition chamber by liquid delivery without using additional solvents. For ALD, the substance was evaporated using a Bronkhorst liquid delivery system at temperatures from 85 to 100°C.

Following the approach to create copper oxide films by ALD, O_2, H_2O vapor or a mixture of both were used as the oxidizing agents, while Ar was applied as purge and carrier gas both for the precursor and the water vapor created in a bubbler. ALD was carried out at temperatures between 100 and 150°C using 100 mm Si wafers sputter-coated with TaN/Ta film stacks or TaN films as substrates.

3 Results and Discussion

ALD at 135°C on Ta substrates with O_2 or H_2O vapor as oxidizing agents resulted in discontinuous films with bad adhesion to the underlying Ta. In contrast, with a combination of O_2

and H_2O vapor ("wet O_2") the adhesion was strongly improved and continuous films were grown. This is confirmed by X-ray photoelectron spectroscopy (XPS) as shown in Fig. 2 (a) for the Ta4d5 signal.
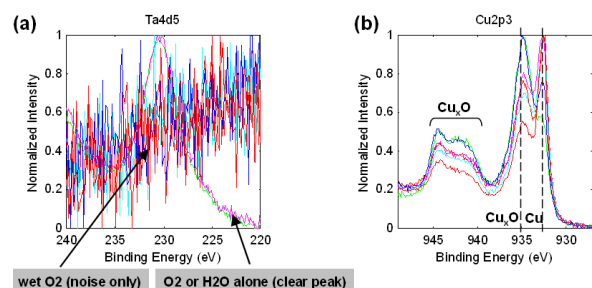

Fig. 2: XPS surface investigation of different ALD samples obtained with O_2, H_2O vapor and wet O_2 on Ta. Using wet O_2, continuous films are obtained and the Ta4d5 signal (a) disappears. In all cases, mixtures of elemental and oxidized Cu were obtained (b).

Fig. 2 (b) depicts the Cu2p3 spectra of such ALD films revealing that mixtures of elemental and oxidized Cu were grown. As depicted by Fig. 3, clusters were obtained overlying the continuous ALD film, most probably resulting from parallel CVD that leads to the formation of elemental copper.
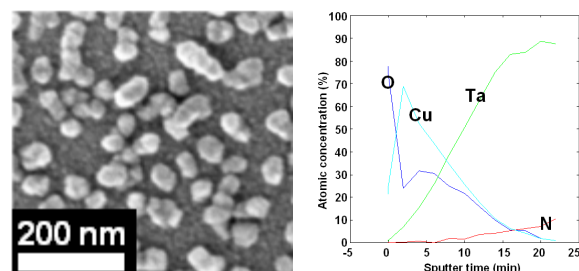

Fig. 3: SEM image (left) and XPS depth profile (right) after ALD on Ta with wet O_2 and 5 s oxidation pulse.

This effect could partially be mitigated by increasing the oxidation pulse time from 5 to 11 s, and it was largely suppressed on nitrogen-rich Ta with 11 s oxidation pulse, as seen in Fig. 4. The XPS spectra in Fig. 3 and 4 also show that the Ta surface tends to get oxidized during ALD. Therefore, a subsequent reduction process also needs to convert the oxidized interface back to metallic Ta.

Based on the experiments on nitrogen-rich Ta, ALD was further carried out on TaN substrates. Since TaN is less reactive to metal-organic precursors than Ta [17, 18] it is expected that parallel CVD effects can be suppressed more effectively. Essentially, smooth films were obtained at 135°C, as shown in Fig. 5. In contrast, the formation of clusters parallel to film growth was observed at temperatures around 145°C. This indicates that self-decomposition of the precursor starts at higher temperatures on TaN.

During ALD experiments on TaN at 135°C, the precursor pulse length was varied to study the saturation of the film growth. As depicted by Fig. 6, first results suggest the existence of a growth regime close to self-saturation, as the growth per cycle (GPC) is nearly independent of the precursor pulse length in the range of 2 to 8 s.
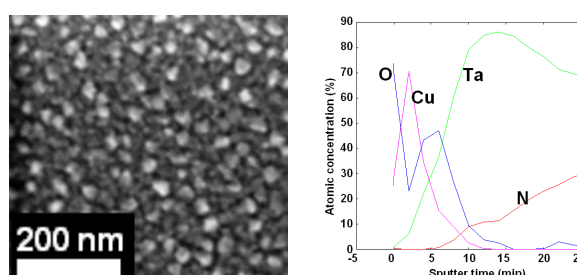
Fig. 4: SEM image (left) and XPS depth profile (right) after ALD on a nitrogen-rich Ta sample with wet O_2 and 11 s oxidation pulse.
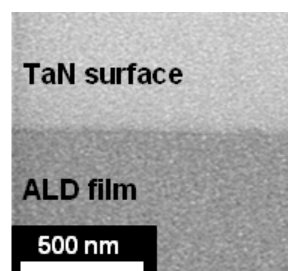
Fig. 5: ALD film grown at 135°C on TaN. The sample was partially etched to expose the TaN surface.
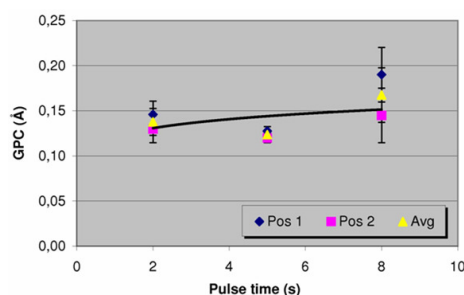
Fig. 6: Growth per cycle vs. precursor pulse length for ALD on TaN at 135°C.

4 Summary and Outlook

A liquid, non-fluorinated Cu(I) β-diketonate precursor was used for depositing Cu films via low-temperature thermal ALD of copper oxide using O_2, H_2O vapor, or wet O_2 as co-reactants. On Ta, films identified as mixtures of elemental

and oxidized Cu were obtained at 135°C. Due to beginning self-decomposition of the precursor, cluster formation was observed in parallel to the growth of continuous films. In contrast, on TaN the generation of clusters could largely be suppressed at 135°C and first results suggest that a self-saturated growth regime can be obtained, which is a major prerequisite for a working ALD process.

The next steps will include a more thorough investigation of the ALD processes and reducing the oxidic films to obtain elemental copper.

5 Acknowledgements

6 References

[1] M. Leskelä and M. Ritala, *Angew. Chem. Int. Ed.* **115**, 5548-5554 (2003)

[2] A. Hand, *Semicond. Int.* **26**, 46-51 (2003)

[3] T. Törndahl, M. Ottosson, and J.-O. Carlsson, *Thin Solid Films* **458**, 129-136 (2004)

[4] P. Mårtensson and J.-O. Carlsson, *Chem. Vap. Deposition* **3**, 45-50 (1997)

[5] A. Niskanen, A. Rahtu, T. Sajavaara, K. Arstila, M. Ritala and M. Leskelä, *J. Electrochem. Soc.* **152**, G25-G28 (2005)

[6] Z. Li, A. Rahtu, and R.G. Gordon, *J. Electrochem. Soc.* **153**, C787-C794 (2006)

[7] Z. Li and R.G. Gordon, *Chem. Vap. Deposition* **12**, 435-441 (2006)

[8] T. Törndahl, M. Ottosson and J.-O. Carlsson, *J. Electrochem. Soc.* **153**, C146-C151 (2006)

[9] R. Solanki and B. Pathangey, *Electrochem. Solid-State Lett.* **3**, 479-480 (2000)

[10] J. Huo and R. Solanki, *J. Mater. Res.* **17**, 2394-2398 (2002)

[11] P.J. Soininen, K.-E. Elers, V. Saanila, S. Kaipio, T. Sajavaara, and S. Haukka, *J. Electrochem. Soc.* **152**, G122-G125 (2005)

[12] P.J. Soininen, K.-E. Elers, and S. Haukka, US 6,482,740 B2 (2002)

[13] R.A. Powell and J.A. Fair, US 6,464,779 B1 (2002)

[14] B.S. Lim, A. Rahtu, and R.G. Gordon, *Nat. Mater* **2**, 749-754 (2003)

[15] B.S. Lim, A. Rahtu, J.-S. Park, and R.G. Gordon, *Inorg. Chem.* **42**, 7951-7958 (2003)

[16] Z. Li, S.T. Barry, and R.G. Gordon, *Inorg. Chem.* **44**, 1728-1735 (2005)

[17] S. Gandikota, S. Voss, R. Tao, A. Duboust, D. Cong, L.-Y. Chen, S. Ramaswami, and D. Carl, *Microelectron. Eng.* **50**, 547-553 (2000)

[18] E. Machado, M. Kaczmarski, P. Ordejón, D. Garg, J. Norman, and H. Cheng, *Langmuir* **21**, 7608-7614 (2005)

Impact of dielectric material and metal arrangement on thermal behaviour of interconnect systems

Schulze, Knut; Schulz, Stefan E.; Gessner, T.
Chemnitz University for Technology, Center for Microtechnologies, Chemnitz

1 Introduction

The development of advanced integrated circuits with improved performance and extended functionality requires the application and integration of new materials. The comprehensive characterization of material properties and an optimized design are essential especially for the interconnection system. However, improvements of the electrical behavior by introducing low and ultra low-k dielectrics or air filled cavities (air gap structures) can cause serious thermal problems. Therefore, a combined optimization including thermal simulation becomes important for present and future circuit design. Precise prediction of the thermal behavior of advanced interconnection systems requires a careful characterization of electrical and thermal properties of metals and dielectrics used. Though both porous dielectrics and air gap structures are promising candidates for the interlevel metal dielectric, one of the major concerns for their integration are Joule heating of the metal and the poor thermal conductivity of the dielectric [1]. The global heat flux within IC metallization systems is perpendicular to the silicon substrate, which is usually the actively cooled heat sink of the whole system. This direction of global heat flux is mainly caused by the huge ratio of footprint area to the stack thickness of such architectures. The heat flow of complex metallization systems of 45 nm node geometries and up to 5 differently densely packed metal levels was investigated using FEM simulation. Furthermore the impact of the following conditions was checked:

- Dielectric material (SiO_2, porous low-k material, air gaps) and integration scheme
- Availability of vias and via density
- Interconnect and via arrangement
- Thickness of additional functional films (hard mask films, etch stop films, …)

2 FEM Simulation of the thermal behaviour of 45 nm node interconnect systems

2.1 Simulation models

Fig. 1 shows a general schematic of interconnect system which was used for the thermal simulation. Five metal levels of dimensions according to the 45 nm technology node of the ITRS 2005 [2] requirements were investigated.
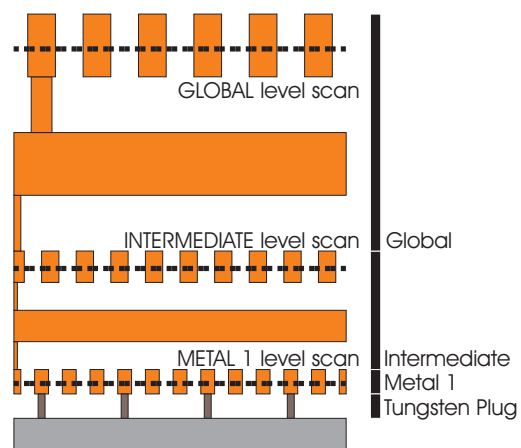
Fig. 1: General scheme of the simulated interconnect system of the 45 nm technology node and plotted scan paths (dotted lines) for temperature analysis

Additionally to the line adjustment the scan paths for temperature plots are shown in Fig. 1 (dotted lines). They are placed across the periodic metal lines of metal 1, intermediate, and global wiring. The following boundary conditions were used during the FEM simulation. A passivation stack consisting of 300 nm PECVD SiO_2 = 1.05 W/mK and 500 nm PECVD Si_3N_4 = 0.7 W/mK was applied on top of all structures. Heat dissipation at the surface of the passivation stack was therefore set to 0 W/m². The substrate temperature was constant. Symmetrical conditions were concerned for the side surfaces. This means that no heat exchange through these areas is assumed to occur. The results of the simulations were the temperature

increases in the interconnect systems compared to the substrate temperature. All simulated configurations/models are shown in Tab. 1 and Tab. 2. The sub-divisions include a variation of the dielectric material - air gaps (λ_{Air} = 0.026 W/mK) and PECVD SiO$_2$ (λ_{SiO2} = 1.05 W/mK) in Tab. 1, porous ultra low-k (λ_{low-k} = 0.15 W/mK, k = 2.2) dielectric in Tab. 2. Furthermore the integration scheme of the low-k case is varied in Tab. 2. In these cases "hybrid" means a low-k material integration to the metal

Tab. 1: Summary of all simulated air gap and SiO$_2$ architectures

levels and PECVD SiO$_2$ to the via levels. "Full low-k integration" defines a full integration of the low-k material to both via and metal levels of the interconnect systems. All functional films (used for patterning, hard mask, etc.) were stipulated to be PECVD SiC:H with a thermal conductivity of λ_{SiC} = 0.3 W/mK and a thickness of 10 nm for metal 1 level, 20 nm for intermediate dimensions, and 30 nm for global wiring (represented by the table rows identified with "SiC stop / cap" of the Tab. 1 and the

Tab. 2: Summary scheme of all simulated hybrid low-k and full low-k architectures

Tab. 2). For the evaluation of the impact of the SiC:H films, cases of zero-thickness SiC:H were introduced ("no stop / cap"). The schemes of the

left side of each table use vias ("Including vias") and the schemes of the right half no vias. Via integration is illustrated in two principle ways – "mismatched" and "matched vias". For "matched vias" the metal lines are contacted on top and at the bottom. On the other hand the "mismatched vias" have an alternation of top and bottom contacting. Both cases are similar, but there are differences in their thermal behaviour. Heat flux of "mismatched vias" through the metal areas (lines and vias) is interrupted in comparison to the "matched vias". This enforces a heat flux through the dielectrics and this increases the impact of different dielectrics/integration schemes. Independent of this, via-free architectures have been examined, too. These cases are shown on the right half of both tables, indicated by "without vias". Two types are shown. The "full filling" rows of both tables illustrate that all 5 metal levels of Fig. 1 contain dense metal lines. "Half filling" is characterized by alternating metal levels filled with dielectric material and metal levels filled with dense metal lines. They provide the most extensive dielectric areas of all simulation models. Joule heating caused by a constant current density in the interconnect lines was applied to all metal areas. These homogenous heat sources represent the loads of the simulations.

2.2 Simulation results
According to the models of Tab. 1 and Tab. 2, the absolute distributions of temperatures were simulated. These values are summarized in Fig. 2 and Fig. 3. The most obvious impact is caused if vias are not available.
"Without-Via" cases: The worst case is the full low-k integration in combination with half filling of the metal lines. Large areas of very low thermal conductivity are responsible for an intensive heat accumulation in the upper levels of the interconnect system. The temperature scans of Tab. 3 show discrete temperate levels for each metal level. This is caused by the absence of copper vias which take the main heat flux within each via level. The main heat flux occurs perpendicular to the Si substrate / heat sink. The temperature distributions within each metal level show no significant fluctuation (see Tab. 3). The maximum temperature increase is directly coupled to the size of the dielectric area and dielectric material (value of thermal conductivity). According to this, PECVD SiO$_2$

filled structures offer the lowest min/max temperature distribution - only insignificantly
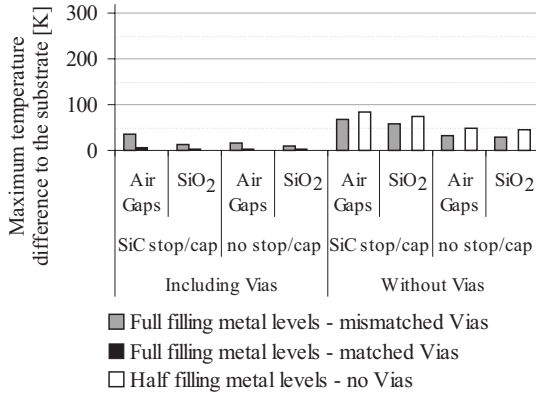

Fig. 2: Maximum occurring temperature rise of interconnect systems using air gaps or SiO_2 for dielectrics (see Tab. 1) depending on cap and stop film materials and via constellation
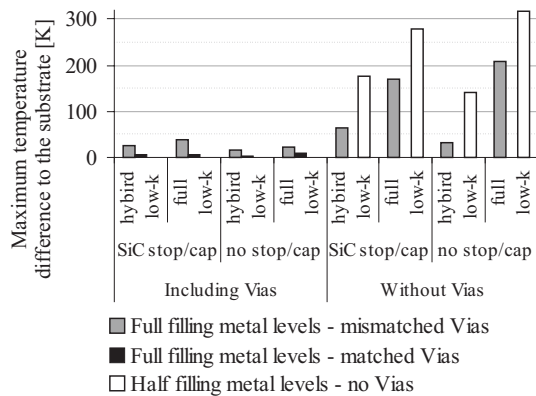

Fig. 3: Maximum occurring temperature rise of interconnect systems using low-k or full low-k integration scheme (see Tab. 2) depending on cap and stop film materials and via constellation

better than the air gap variants. Because of the discrete temperature levels (no inter-metal temperature gradient) in all these cases, there is no necessity for an inter-metal heat flux (assumed that air is exclusively used for IMD). Taking this into account, the low thermal conductivity of air does not deteriorate heat dissipation remarkably. The performance of air gap technology is nearly as good as conventional SiO_2. This evidence is supported by the results of Shieh et al. [3].

"Via" cases: Introducing metallic vias into the architectures reduces the temperature load to a minimum. The general via-constellation is exceedingly important. A "mismatched" via contacting is definitely more critical for the heat dissipation than a "matched" one (see Tab. 4).

As expected, interrupted ("mismatched") metal channels cause a heat accumulation directly at the dielectric "bridges" between the interconnects of each metal level (IMD areas). The increased maximum temperatures of the air gap cases and "mismatched" vias is an indication of the lowered thermal cross-talk of neighbouring lines in comparison to SiO_2 structures. This correlates to the publication of Schindler et al. [4]. Especially the results of these integration schemes without capping and stopping layers show comparable temperature values for the "matched" via cases, but distinct differences for "mismatched" via constellation. A "matched" via contacting causes comparable temperatures within 3 metal levels. The very low thermal conductivity of air is responsible for significant temperature gradients within each metal level and from level to level and shows clearly and precisely the reduced thermal crosstalk within these regions. This effect is superposed by the heat flux through the inter level dielectric PECVD SiO_2 between the upper and subjacent lying metal levels.

Impact of SiC:H stop / cap / mask films: The impact of SiC:H film thickness depends on the integration scheme and the integrated material. Because of the lower thermal conductivity of SiC:H in comparison to SiO_2 furthermore thinned SiC:H films give an improvement of heat dissipation for the SiO_2 and air gap based technologies (Fig. 2). In case of full low-k integration the SiC:H films are responsible for a slight reduction of the maximum temperature because of their higher thermal conductivity, $\lambda_{SiC} = 0.30$ W/mK, in comparison to values of porous low-k materials of about 0.15 W/mK.

3 Conclusions

A 5-level interconnect system of 45 nm technology node dimension was used for thermal FEM simulations. The impact of different dielectrics (air gaps, low-k, PECVD SiO_2) and different integration schemes on the maximum heating under homogeneous heat source load was investigated. Furthermore the influence of thermal conductivity and thickness of functional films was investigated. Selected metal line and via constellations were used to screen the advantages and disadvantages of every variant. The results have shown that selective air gap approaches have the potential to provide a thermal behavior comparable to SiO_2 based

interconnect systems. This is well founded since densely packed areas have a large portion of highly conductive metal materials, which take over the main heat conduction. The integration of new materials for an enhanced electrical performance of interconnect systems has been shown to cause a definite degradation of the thermal behavior of these systems in comparison to SiO_2 based structures. On the other hand the degree of this degradation is mainly affected by the interconnect arrangement itself. Well designed interconnect architectures including dummy structures of high thermal conductivity, well adjusted via distribution or even selective SiO_2 removal may minimize or almost compensate this loss of thermal performance.

4 Acknowledgement

5 References

[1] R. Streiter, H. Wolf, U. Weiss, X. Xiao, T. Gessner, Proc. of the Advanced Metallization Conference (AMC) 1999, MRS Conf. Proc. ULSI XV 2000, p. 335-342.

[2] International Technology Roadmap for Semiconducors, 2000-2005, Semiconductor Industry Association, San Jose, CA 2000-2005

[3] P. Shieh, L.C. Bassman, D.-K. Kim, K.C. Saraswat, M.D. Deal, J.P. McVittie, IEEE, IITC Conference 1998, pp. 125-127

[4] G. Schindler, A. Stich, Z. Gabric, W. Pamler, Proc. of the Advanced Metallization Conference (AMC) 2005, MRS Conf. Proc. AMC XXI, MRS, Warrendale, PA; 2006, pp. 255-261

Tab. 3: Scans of the temperature increase of 3 metal levels (metal 1, intermediate, global, see Figure 1) for a constant current density of all metal lines including vias, depending on cap and stop film material, in comparison to the silicon substrate (see Tab. 1 and Tab. 2 for the schemes)
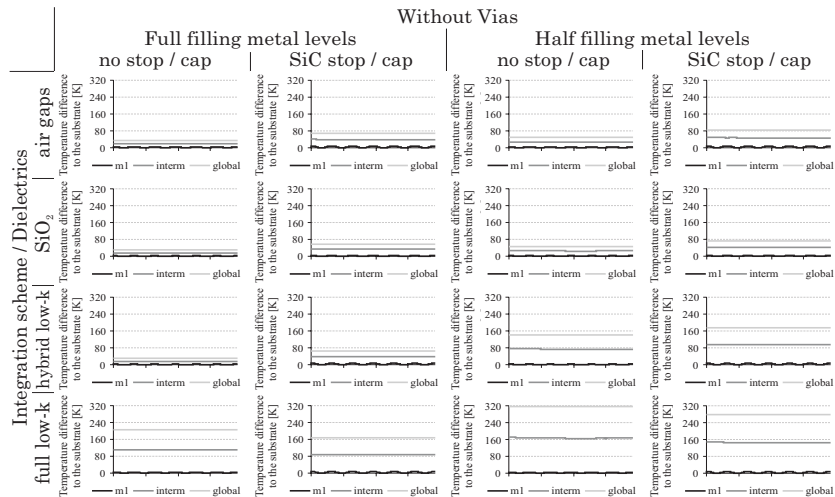
Tab. 4: Scans of the temperature increase of 3 metal levels (metal 1, intermediate, global) for a constant current density of all metal lines without vias, depending on cap and stop film material, in comparison to the silicon substrate (see Tab. 1 and Tab. 2)
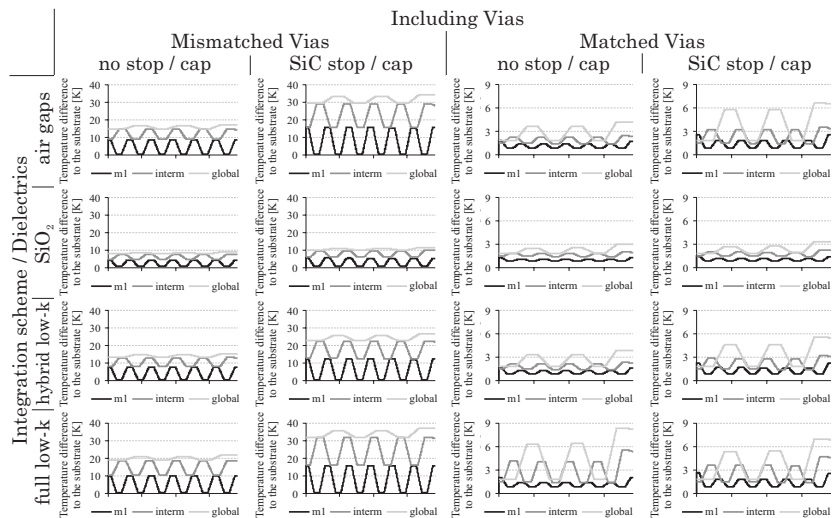
Characterization and modeling of dielectric isolation structures in a high-voltage semiconductor technology

Lange, A. [1]; Erler, K. [1]; Heinz, S. [1]; Ebest, G. [1]; Lerner, R. [2]; Eckoldt, U. [2]; Schottmann, K.[2]

[1]Chemnitz University of Technology, Faculty for Electrical Engineering and Information Technologies, Chair Electronic Devices; [2]X-Fab Semiconductor Foundries AG Erfurt

1 Introduction

During the last years the integration of high voltage circuits became more and more essential. This development is driven by the growing market for smart power integrated circuits which combine high voltage or high power devices and additional control circuitry on a single chip.

The supply voltages in these circuits often range from 3.3V for the controlling circuit up to several hundred volts. Therefore, the electric isolation between the different devices becomes crucial.

Classic bipolar or CMOS technologies widely rely on junction isolation, where a reverse-biased pn-junction is used to isolate the devices. While this isolation method can also be applied on high voltage circuits, there are significant drawbacks. The leakage current associated with this isolation is not zero and has very high temperature dependence. Additionally, the junction works as a voltage dependent capacity, limiting the maximum frequency of operation. The greatest downside in using junction isolation in high voltage circuits is the occupied physical space. The depletion region of the reverse biased junction becomes wider as the supply voltage increases, thus limiting the possible degree of integration.

Using a dielectric isolation technology to electrically separate single devices helps to overcome those drawbacks. This type of isolation provides very low leakage current and minimal space consumption. An overview of different dielectric isolation technologies can be found in [1].

In cooperation with the X-FAB Semiconductor Foundries AG, the electrical behaviour of such an isolation technology was characterized. Based on the results of this investigation, a simple device model for these isolation structures was created.

2 Dielectric isolation structures

The examined isolation structures were samples of a 1μm dielectric isolated smart power process provided by the X-Fab Semiconductor Foundries AG. The process features high voltage DMOS transistors along with CMOS transistors with different voltage levels and bipolar devices.

Fig. 1 shows a cross-section of the isolation structure used within this process. The vertical isolation is provided by a thick buried oxide. Lateral isolation is realized by a trench with very high aspect ratio.
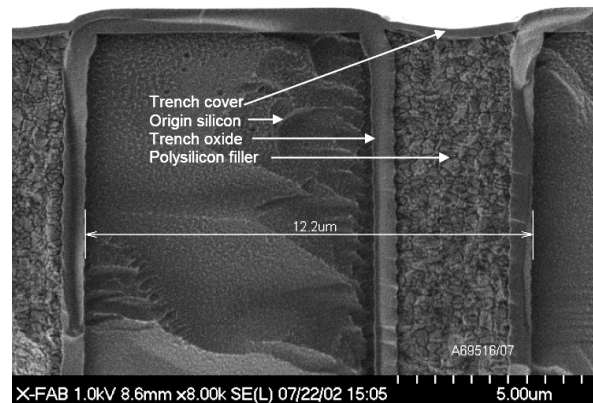
Fig. 1: Cross-section of finished trench with trench cover oxide [5]

The silicon at the trench sidewalls is highly doped and functions as low resistance contact area to a buried N+ layer. The sidewall oxide ensures the insulating capability. Finally, a polysilicon refill provides the mechanical stability of the structure.

The maximum operating voltage for the isolation structures are specified with 300V for a single trench. By using parallel trenches, the maximum voltage can be raised up to 700V for a triple trench.

3 Electrical characterization

The characteristics of the isolation structures were measured by a HP4062UX parameter test system. Because of the maximum applicable voltage with two of its high power SMUs in series of 400V, an additional Keithley Model 2410 high voltage SMU was used to provide the test

circuit with voltages up to 1100V. The measurements included the evaluation of the breakdown and lifetime characteristics, the determination of critical trench configurations and the analysis of the generic voltage and temperature dependence of the leakage current in these isolation structures.

The determined behaviour of these structures was quite complex. The leakage current shows a strong dependence on the history of electric stress the trench was exposed to. An unstressed trench initially shows a leakage current, which immediately decreases while stressing with constant voltage. We will refer to this effect as electric formation of the trench.

3.1 Electric formation

Fig. 2 shows the typical leakage current characteristic of an unstressed trench structure. As already mentioned, the leakage current initially decreases rapidly. The rate of decrease is clearly voltage dependent. In addition, an already formed trench undergoes a new formation process if stressed with a higher voltage than before.
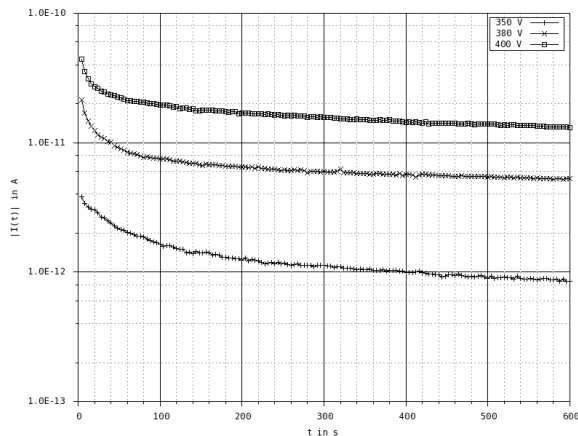
Fig. 2: Leakage current characteristic of the trench structure while stressed with constant voltage

Further investigations showed that there is also a dependence on the polarity of the applied voltage. A trench already stressed behaves like an unstressed trench if the polarity is reversed.

The underlying cause of this effect seems to be charging and discharging of traps in the sidewall oxide of the trench structure and will be further explained in section 4.

3.2 Leakage current characteristic

Fig. 3 shows an example of the generic characteristic of the trench leakage current at different temperatures. Because of the ongoing formation effect during measurement which can be seen in

the hysteresis of the curves, different structures had to be used for each device temperature. All devices were exposed to the same electric stressing before each measurement.
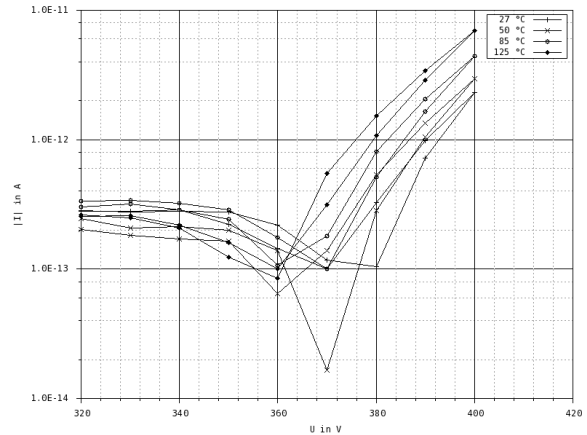
Fig. 3: I-V-Characteristic of the trench structures at different temperatures

The leakage current shows a strong, nearly exponential dependency on the applied voltage. The influence of the device temperature on the leakage current can also be seen.

4 A DC-model for the trench leakage current

With simulation being a key part in today's process of integrated circuit design, the existence of proper device models becomes crucial. This need also applies to parasitic circuit elements like isolation structures. For dielectric isolation technologies like the one investigated, such models don't exist yet.

4.1 Generic DC-model

As described, the isolation structures consist of two layers of silicon dioxide with a layer of polysilicon embedded between. Assuming that main voltage drop occurs above the oxide layer, the influence of the polysilicon on the static leakage current characteristic could be neglected.

Therefore, the leakage current was described by modelling the carrier transport through a single dielectric layer. In our case, tunnelling of electrons was determined as the main transport phenomena.

$$J = A \cdot E^2 \cdot \exp\left(\frac{B}{E}\right) \qquad (1)$$

Tunnel emission through a dielectric can be described by equation 1 with the constants A and B

depending on the height of the energy barrier and the electron effective mass in the dielectric [3].
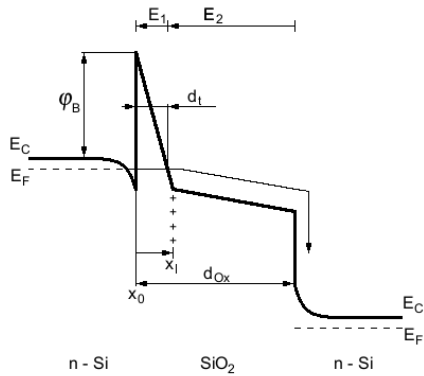
Fig. 4: Deformation of the energy barrier under influence of a positive sheet charge.

This equation is only valid for a triangular barrier. With charged traps inside the oxide layer, the energy barrier is deformed, changing the tunnelling distance (Fig. 4). For our model, the distribution was simplified as a sheet charge Q' close to the Si-SiO2 interface. In this case, the effective barrier height can be approximated as shown in equation 2.

$$\varphi_{B,eff} \approx \varphi_B - \frac{q \cdot Q' \cdot x_l}{\varepsilon_{SiO_2}} \tag{2}$$

The tunnelling probability itself is independent of the device temperature. However, the energetic distribution of electrons in the silicon close to the interface is temperature dependent. The slightly higher tunnelling probability of an electron occupying a higher energy level in the accumulated region of the semiconductor was empirically introduced into our model.
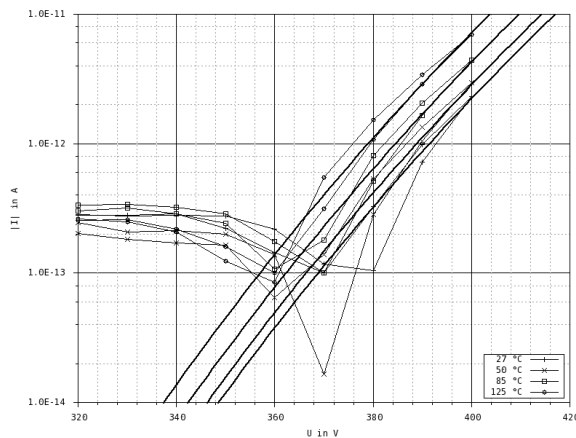
Fig. 5: Simulation results for the static DC-model

The results achieved with this model are shown in Fig. 5. On the downside, this model is only

valid for a trench which was already electrically stressed. The unstressed trench needs to be modelled in a different way.

4.2 Worst case model

Because of the rapid formation process of an unstressed trench, its characteristic can not be measured. The worst case model was therefore derived from the characteristics shown in Fig. 2. Based on the assumption made before, a simple model for the filling process of the positive charged traps was created.

$$\frac{dQ'(t)}{dt} = -\alpha \cdot \frac{I(t)}{q} \cdot Q'(t) \tag{3}$$

The differential equation shown in equation 3 leads to a time dependent expression for the trench leakage current which could be fitted to the results of our measurement (Fig. 6).
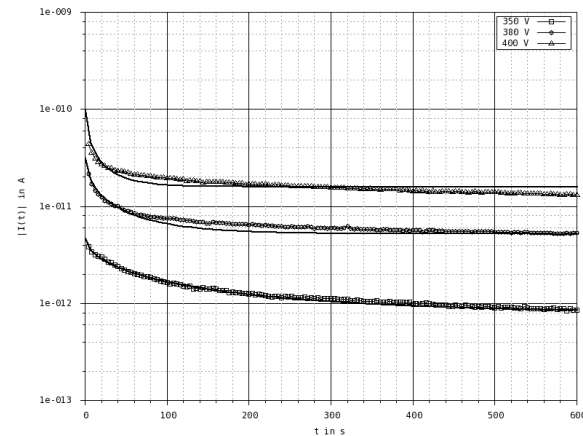
Fig. 6: Simulation results for the time dependent leakage current

From this expression, the final model for the unstressed trench could be derived.

5 References

[1]   Murari, B.; Bertotti, F.; Vignola, G.A.: *Smart Power ICs.* Springer 1995

[2]   Lange, A.: *Modellierung von Trenchisolationen.* Chemnitz University of Technology, 2006

[3]   Lenzlinger, M.; Snow, E.H.: *Fowler-Nordheim Tunneling into thermally grown SiO_2.* Journal of Applied Physics, Vol. 40, Nr. 1, pp. 278-283, January 1969

[4]   Snel, J.: *The doped Si/SiO_2-Interface.* Solid State Electronics, Vol. 24, p. 135, 1981

[5]   X-Fab Semiconductor Foundries: *XD10 - 1 µm DIMOS Application Note.* July 2005

Reliability of amorphous hydrogenated carbon films (a-C:H) in microelectronic applications

Klaus Schirmer[1], Josef Lutz[1], Stefan Steinhoff[2]

[1]TU Chemnitz, Fakultät für ET/IT, Professur Leistungselektronik und elektromagnetische Verträglichkeit,
[2]IXYS Semiconductor GmbH Lampertheim

1 Introduction

Reliability and long term stability are some of the most important requirements in modern microelectronic devices. For some high voltage applications the increasing demands on the electronic properties reveal the limits of silicon oxide as passivation layer. The implementation of hydrogenated amorphous carbon films as passivation layer for high voltage diodes requires among others the verification of the lifetime stability of its blocking capability.

2 Amorphous hydrogenated carbon

The extraordinary material properties like high hardness and chemical inertness offer a wide range of applications to amorphous hydrogenated carbon (a-C:H). Earlier investigations have demonstrated the applicability as passivation layer for silicon power devices [1].
PECVD deposited carbon forms a great variety of crystalline and disordered structures. The fraction of the graphitic sp^2 bonds and the diamond like sp^3 bonds in the growing film depends sensitively on the energy of the surface impinging ions [2].

3 Passivation

The passivation layer protects the pn-junction termination at the device surface against moisture an ion charges. Based on the high density of states in the band gap of a-C:H films, mirror charges can be created at the interface between the carbon film and the silicon substrate to suppress high electrical field peaks. This results in high breakdown voltage. The cross-section in fig.1 shows the floating field limiting rings that optimize the field distribution on the edge of the device. Compared to the thickness of SiO_2 coats the a-C:H passivation layer is rather thin (200nm).
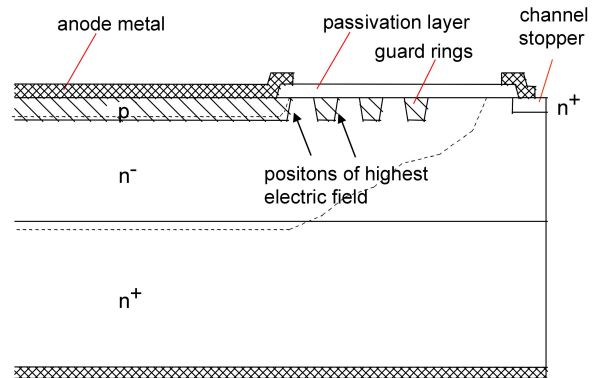
Fig. 1: Power device junction termination

4 Deposition

The most commonly used method for depositing carbon thin films consists in plasma enhanced vapour deposition (PECVD), with a monomer gas of C_xH_y. The application of helium backside cooling avoids temperatures over 140°C during the deposition process. Due to the major role of the ion energy the depositions were performed at three different self-bias voltages.
E_1, E_2 = 1,25 x E_1, E_3 = 1,43 x E_1
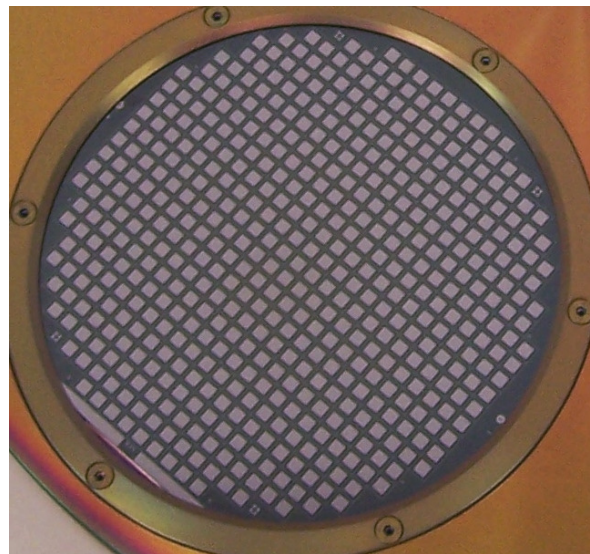
Pic.1: clamped diode wafer after a-C:H etching

According to the equipment adjustments for sufficient homogeneity the corresponding power densities resulted:

P_1, $P_2 = 1{,}74 \times P_1$, $P_3 = 2{,}69 \times P_1$

Deposition rates:

$R_{D1} = 30{,}0$ nm/min, $R_{D2} = 34{,}9$ nm/min,
$R_{D3} = 44{,}2$ nm/min

The structuring of a-C:H layers by means of an oxygen plasma was effected on the same equipment as the deposition. Metallization and packaging were performed by our collaboration partner IXYS Semiconductor GmbH, Lampertheim.

5 HTRB test

For semiconductor devices aging could lead to a change in the characteristic data or even to a failure. The 1000h high temperature reverse bias reliability test (HTRB) to proof the blocking stability bases on the IEC 60747. To differ from these standard our test condition were aggravated to $T_c = 150°C$ and 97% of voltage class. The blockage behaviour of nine diodes out of the three deposition variations is shown in fig. 2.
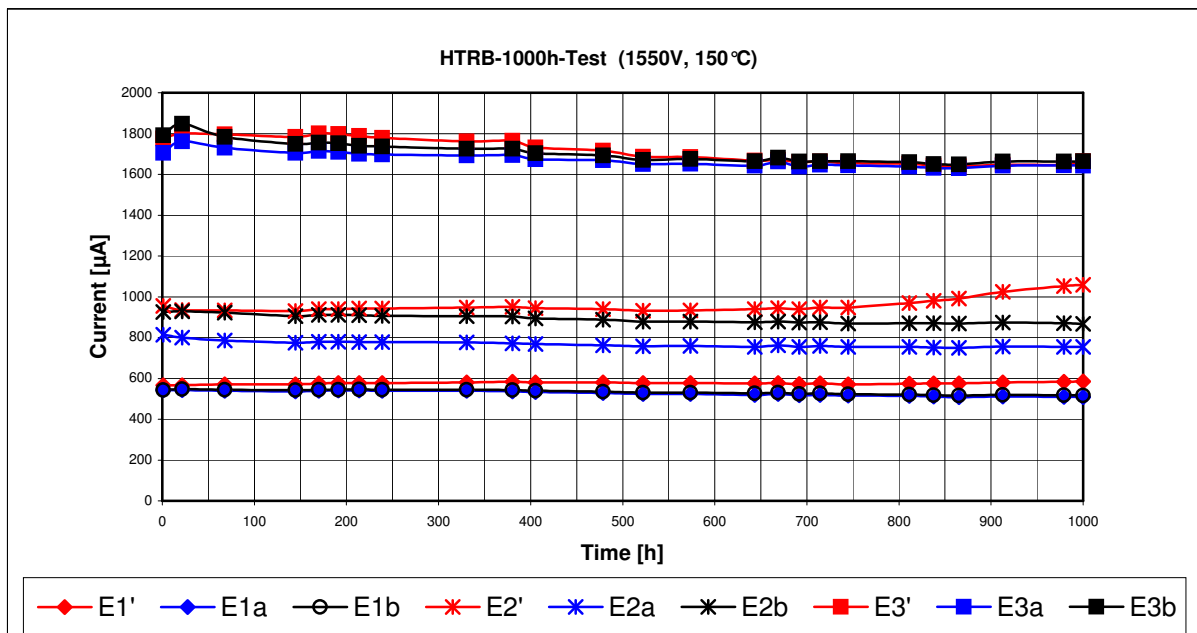
Fig. 2: Reverse current during HTRB test

Three diodes, E1', E2' and E3' are additionally polyimide coated. As expected the leakage current differs corresponding to deposition bias voltage right from the start. The only sample to with increasing leakage current within the test was E2'. The average values of the reverse currents are mentioned below.

U bias	$I_R[\mu A]$	deviation [%]
E1	550	-5.5
E2	900	-6.8
E3	1760	-5.3

6 Conclusions

The applied variations in deposition processing comply with conditions for industrial manufacturing qualification. Without additional polyimide coating all diodes indicate a stable

blocking behaviour. As the E1-process has shown the clearly lowest leakage current one might connive the required increase in deposition time. Further ongoing reliability tests will turn out the suitability of these a-C:H films under different conditions for the utilization as passivation layer in high power semiconductors.

7 References

[1]   R. Barthelmess et al, Proceedings of the ISPSD, 1998
[2]   J. Robertson, Diamond-like amorphous carbon, Material Science and Engineering R 37 (2002) 129-281

First- Principles calculations of the band gap of $Hf_xSi_{1-x}O_2$ and $Zr_xSi_{1-x}O_2$ alloys

E. Nakhmedov, E. Nadimi, Ph. Plänitz, F. Chiker, R. Öttking and Ch. Radehaus
TU Chemnitz
Department of Electrical & Information Engineering, Opto- and Solid State Electronics

Abstract

A generalized quasichemical method and the cluster expansion approach are applied to calculate the band gap of amorphous $Hf_xSi_{1-x}O_2$ and $Zr_xSi_{1-x}O_2$ alloys within the pseudopotential based density-functional theory. The dependence of the band gap of $Hf_xSi_{1-x}O_2$ and $Zr_xSi_{1-x}O_2$ compounds on the molar concentration x is computed to be nearly linear with small bowing parameter b.

1. Introduction

In order to increase the physical thickness of gate oxides, while maintaining or increasing the device performance, investigations of new insulator materials with high dielectric constants k are of vital importance for the microelectronic industry. Hafnia (HfO_2) and zirconia (ZrO_2) are promising candidates to replace silicon oxynitrides because of their higher dielectric constants, $\varepsilon \sim 20$ for hafnia and $\varepsilon \sim 25$ for zirconia, compared to $\varepsilon = 3.9 \div 7$ for SiO_xN_y. Experimental studies [1] show that, although the HfO_2 gate dielectric is thermodynamically stable in contact with Si, the ZrO_2 / Si interface is not stable against the formation of silicides. Nevertheless Hf and Zr silicates have shown [2] to be stable in direct contact with Si up to high temperatures.

Hf and Zr atoms usually substitute the silicon atoms in silicon dioxide crystals, yielding pseudobinary alloys of the form $Hf_xSi_{1-x}O_2$ or $Zr_xSi_{1-x}O_2$, where x is the atomic fraction of $X = Hf, Zr$ atoms. Nowadays the constituent SiO_2 and HfO_2 or ZrO_2 compounds, building up the ternary alloys $Hf_xSi_{1-x}O_2$ or $Zr_xSi_{1-x}O_2$, have been carefully studied by means of first principle methods [3-5]. To our knowledge there are not yet ab initio investigations on the x dependence of the band gap of $Hf_xSi_{1-x}O_2$ and $Zr_xSi_{1-x}O_2$ compounds.

The lack of translational symmetry of the atomic potentials in the amorphous hafnium- and zirconium- silicates requires special methods to develop first-principle computations. In this paper we apply a cluster expansion approach (CEA) [6] and the generalized quasichemical approximation (GQCA) [7] to calculate the structures and the electronic properties of $Hf_xSi_{1-x}O_2$ and $Zr_xSi_{1-x}O_2$ alloys by DFT based first principle pseudopotential methods.

2. Computational methods and technical details

Zr or Hf atoms usually substitute the silicon atoms in SiO_2 crystals. The alloy atoms Si and $X = Hf, Zr$ in the ternary $X_xSi_{1-x}O_2$ compounds randomly occupy their sublattice, whereas the O atoms constitute the other sublattice. As an initial cluster we choose an α-quartz unit cell with three SiO_2 molecules, and replace the silicon atoms in the cluster by Hf or Zr atoms. The possible clusters can be labelled according to the numbers j of substitutions as $X_0Si_3O_6$, $X_1Si_2O_6$, $X_2Si_1O_6$, and $X_3Si_0O_6$ with $X = Zr$ or Hf corresponding to $j = $ *0, 1, 2,* and *3*. Symmetry breaking along the c-axis in the hexagonal unit cell of α-quartz results in different energies for different configurations of e.g. one substitution in the $X_1Si_2O_6$ cluster. In the high temperature limit each cluster of $\{j,k\}$ with j substitutions is weighted with the probability [7, 8]

$$x_{j,k}(x) = g_{j,k}x^j(1-x)^{3-j}, \qquad (1)$$

where $g_{j,k}$ is the degeneracy factor.

The configurational average of the fundamental physical parameters $P_{j,k}$ is done according to the Connolly-Williams method [8]:

$$P(x) = \sum_j \sum_k x_{j,k} P_{j,k} , \qquad (2)$$

provided that every configuration $\{j,k\}$ is realized with the composition-dependent probability $x_{j,k}$.

In our computations we employ standard DFT+LDA theory implemented in the ABINIT code, where the charge density is represented in a plane-wave basis with periodic boundary conditions [9]. We use the Hartwigsen-Geodecker-Hutter (HGH) semicore-pseudopotential, which is expanded over a Gaussian basis set to describe semi-core electron states. Choosing a high cutoff energy (100 Ha) ensures the accuracy of structural and energetic properties.

3. Results and discussions

The total energy, the density of electronic states (DOS), the band gap E_g^j and the mean-square (rms) deviation $\Delta E_g(x)$ of the band gap were calculated for clusters with $j=0, 1, 2,$ and 3 substitutions, including the clusters of pure α-quartz as well as ZrO_2 and HfO_2 crystals. The configurational averaged values of $E_g(x)$ and $\Delta E_g(x)$ are obtained by applying the Connolly-Williams method, expressed by Eq. (2). Our computational studies show (see, Figs.1a and 2a) a nearly linear dependence of the band gap of $X_x Si_{1-x} O_2$ compounds with $X = Hf, Zr$, which varies between the band gaps $E_g(SiO_2)$ and $E_g(XO_2)$ of SiO_2 and XO_2 according to the following expression:

$$E_g(x) = (1-x) E_g(SiO_2) + x E_g(XO_2) - \qquad (3)$$
$$b x (1-x) .$$

The deviation of the alloy band gap in Eq. (3) from the linear interpolation between the band gaps of two constituents can be described by a parabolic fitting with a bowing parameter b. The quadratic fitting explicitly describes the band gap bowing, giving $b=1.723$ and $b=0.28$ for the bowing parameters of $Zr_x Si_{1-x} O_2$ and

$Hf_x Si_{1-x} O_2$ compounds, correspondingly.
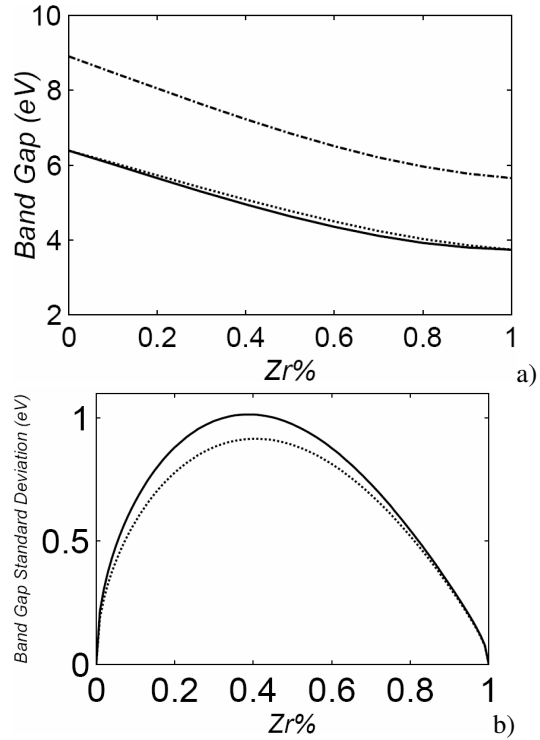
Fig.1 (a) The band gap of $Zr_x Si_{1-x} O_2$ alloys vs the composition. The continuous and the dotted curves denote DFT-LDA results with optimized and fixed supercell sizes, correspondingly. The dashed curve is the averaged energy gap scaled to the experimental values of the end-point crystals band gap. (b) The mean-square deviation of the band gap vs composition.

The calculations of $\Delta E_g(x)$ for $Hf_x Si_{1-x} O_2$ and $Zr_x Si_{1-x} O_2$ compounds reveal strong fluctuations in the rms. As it can be seen from Figs.1b and 2b, the maximal values of $\Delta E_g(x)$ for both alloys are centred around $x_0 = 0.4$. The mean-square deviation for $Zr_x Si_{1-x} O_2$ alloy reaches $1\ eV$ around $x_0 = 0.4$, which is approximately 20% of the DFT-LDA value, whereas it is $0.68\ eV$ around $x_0 = 0.4$ for the $Hf_x Si_{1-x} O_2$ compound, taking 13% of the DFT-LDA band gap.

It is well known that the DFT-LDA approximation systematically underestimates the band gap, and therefore, the quasiparticle GW contributions are necessary to correct the band gap to reasonable values. We suppose that a linear dependence of the quasiparticle corrections on the composition is valid for $Zr_x Si_{1-x} O_2$ and $Hf_x Si_{1-x} O_2$ compounds. Under this assumption we have scaled the band gaps of

$Zr_xSi_{1-x}O_2$ and $Hf_xSi_{1-x}O_2$ alloys to the experimental band gaps of the end-point crystals.
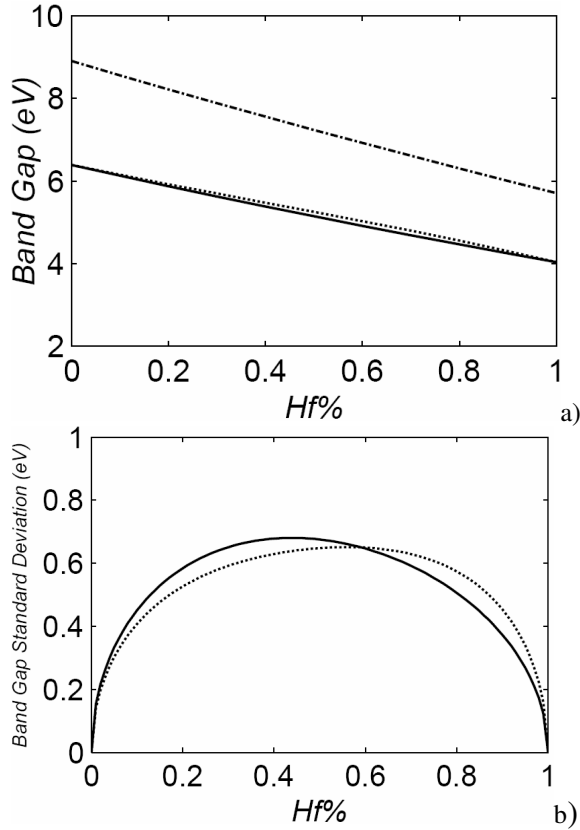

Fig.2: (a) The band gap of $Hf_xSi_{1-x}O_2$ alloys vs the composition. The continuous and the dotted curves denote the DFT-LDA results with optimized and fixed supercell sizes, correspondingly. The dashed curve is the averaged energy gap scaled to the experimental values of the end-point crystals band gap. (b) The mean-square deviation of the band gap vs the composition.

The rescaled values for the averaged energy gap $E_g(x)$ are plotted in Figs.1a and 2a by dashed curves.

The structure parameters and the unit cell volume of each cluster get specific values which differ from those of other clusters. The clusters in a real structure are randomly distributed "filling" the amorphous bulk material. In this case the volumes of the clusters are relaxed to some average value, creating at the same time an internal stress due to alloying. To find the excess stress we calculate the clusters energies in two steps. In the first step the total energy $\varepsilon_{j,k}$ is calculated by optimizing the atomic positions as well as the unit cell sizes. In the second step, the average unit cell sizes,

$$r_i(x) = \sum_j \sum_k x_{j,k} \, r^i_{j,k}, \quad i = 1, 2, 3,$$ for a given

concentration are calculated. Equating the cluster sizes to their average values, the energy $\varepsilon^{fix}_{j,k}$ for the cluster with fixed cell sizes $r_i(x = j/n)$ is calculated. In the second step of calculations the atomic coordinates are relaxed again until the Hellmann-Feynman forces vanish. The difference between the averaged values of the total energies per volume $\dfrac{\varepsilon^{fix}(x) - \varepsilon(x)}{\vartheta(x)}$ characterizes the internal excess stress due to alloying.

To understand how the excess stress affects the band gap, we have calculated the band gap of the ordered clusters with fixed cell sizes and determined the averaged band gap $E^{fix}_g(x)$, illustrated in Figs. 1a and 2a by dotted curves. The changes in the rms, depicted in Figs. 1b and 2b, are not significant too.

The band gap of hafnium and zirconium silicate films measured by x-ray photoelectron spectroscopy (XPS), was shown [10] to depend linearly on contents. Nevertheless the optical band gap of the Hf silicate film measured in Ref. [11] reveals a considerably high bowing $b \sim 4 \, eV$, which seems to be connected with an indirect character of the band gap.

4. Conclusions

In this paper we have calculated the band gap, the bowing parameter and the rms of the band gap, as well as the internal stress in the pseudobinary $Zr_xSi_{1-x}O_2$ and $Hf_xSi_{1-x}O_2$ alloys. We applied the cluster expansion approach (CEA) and the generalized quasichemical approximation (GQCA) to calculate an evident dependence of the physical characteristics on the molar fraction x by the DFT-LDA first principle method. Our results show that the band gap depends nearly linearly on x, having a small bowing. The results obtained for the band gaps are consistent with those experimentally observed in Ref. [26] for hafnium and zirconium silicate films.

References:

[1]   M. Gutowski, J. E. Jaffe, C.-Li Liu, M. Stoker, R. I. Hegde, R. S. Rai, and P. J. Tobin, Appl. Phys. Lett. Vol. 80, Nr.11, pp. 1897- 1899(2002).

[2] G. D. Wilk, R. M. Wallace, and J. M. Anthony, J. Appl. Phys., Vol. 87, Nr. 1, pp. 484-492 (2000); J. Appl. Phys. Vol. 89, Nr. 10, pp. 5243-5275 (2001).

[3] Y. P. Li and W. Y. Ching, Phys. Rev. **B**, Vol. 31, Nr.4 , pp. 2172-2179 (1985).

[4] J. E. Jaffe, R. A. Bachorz, and M. Gutowski, Phys. Rev. **B,** Vol. 72, Nr.11, pp.144107-1 -144107-9 (2005).

[5] B. Kralik, E. K. Chang, and S. G. Louie, Phys. Rev. **B ,** Vol. 57, Nr.12 , pp. 7027-7036 (1998).

[6] S. H. Wei, L. G. Ferreira, J. E. Bernard, and A. Zunger, Phys. Rev. **B,** Vol. 42, Nr. 15, pp. 9622-9649 (1990).

[7] A. Sher, M. van Schilfgaarde, A.-B. Chen, and W. Chen, Phys. Rev. **B,** Vol. 36**,** Nr. , pp. 4279 (1987).

[8] J. W. D. Connolly and A. R. Williams, Phys. Rev. **B,** Vol. 27, Nr.8, pp. 5169 -5172 (1983).

[9] M. C. Payne, M. P. Teter, D. C. Allan, T. A. Arias, and J. D. Joannopoulos, Rev. Mod. Phys., Vol. 64, Nr. 4, pp.1045-1097 (1992); http://www.abinit.org

[10] H. Kato, T. Nango, T. Miyagawa, T. Katagiri, and Y. Ohki, International Workshop on Gate Insulator (IWGI) 2001, Tokyo, pp. 166-167.

[11] A. Callegari, E. Cartier, M. Gribelyuk, H. F. Okorn-Schmidt, and T. Zabel, J. Appl.Phys., Vol. 90, Nr.12 , pp.6466 -6475 (2001).

The effect of Nitrogen doping on the tunneling effective mass of electrons in ultrathin SiO$_2$ gate insulator

E. Nadimi[1], C. Golz[2], M. Trentzsch[2], L. Herrman[2], K. Wieczorek[2], and C. Radehaus[1]

[1] TU Chemnitz Department of Electrical & Information Engineering, Opto- and solid state electronics
[2] AMD Saxony LLC & Co. KG, Wilschdorfer Landstraße 101, D-01109 Dresden

1 Introduction

Intolerably high gate leakage current in MOSFETs with ultrathin SiO$_2$ dielectric requires the use of high-k gate dielectrics in the next generation of MOSFETs as predicted by the international technology roadmap for semiconductor (ITRS) [1]. However, silicon oxynitride has been used in the last years as an intermediate solution toward high-k gate dielectric. Low concentration of interface defects and higher dielectric constants in comparison to those of silicon oxide, as well as higher resistance against the boron penetration into the channel are the most superior properties of silicon oxynitride. This makes it the first choice for the 11 Angstrom EOT technology node for a relatively long time. Therefore, characterizing the physical parameters of silicon oxynitride gate dielectrics is of great importance.

2 Extracting the tunneling effective mass of electron

Several theoretical and experimental studies have been conducted to investigate the characteristic parameters of silicon oxynitride as a function of the nitrogen concentration. One of the most efficient experimental approaches to determine the ultrathin oxide and oxynitride parameters is fitting the calculated gate leakage current to experimental curves [4,5]. This method is widely applied to carrier effective mass extraction in ultrathin gate dielectrics [6]-[10]. However, using different models and approximations in the calculation of gate tunnel current has ended up with a wide range of electron effective mass in the silicon oxynitride. Parameter free density functional Theory (DFT) based on first principle methods within the local density approximation (LDA) have been applied to calculate the band gap, the effective mass and the dielectric function of a sample [2]. However,

there is no strong justification of using the effective mass of carriers extracted at the bottom/top of conduction/valence band for tunneling carriers, which tunnel through aperiodic structures with energies within the band gap. As Fukuda et al. [6] suggested, there are two different values for tunneling and band effective mass of electrons (m*$_T$ =0.35, m*$_c$=0.60). On the other hand, several authors reported thickness dependent effective masses for electrons in ultrathin dielectric layers [5,7,8]. This thickness dependence could not be addressed with ab initio calculations of bulk super cell methods with periodic boundary condition.

Doping of a SiO$_2$ crystal by nitrogen atoms changes the band structure and consequently the effective mass of electrons in silicon oxynitride. Recently Mao et al. [2] and Ng et al. [4,5] addressed this issue using first principle calculations and I-V fitting, respectively. The effective masses extracted from this ab initio calculated band structure in Ref. 2 are pretty high, perhaps due to dangling bonds in the structure. However, thermal processes during the integration of MOS transistors anneal the structures and lead to a strong reduction of dangling bonds; therefore calculations based on structures with dangling bonds are questionable.

Ng et al. [4,5] have determined the barrier height and the effective mass simultaneously by fitting I-V measurements to the analytical expression of DT and FN tunneling currents for thin and thick oxides layers, respectively. However expressing the tunneling current analytically requires many approximations.

To overcome these difficulties we propose a new quantum mechanical model [11] for the calculation of the tunneling current within the effective mass approximation. The accuracy of our self-consistent Schrödinger-Poisson (SP) method prevails much more over the accuracy of the quasi-classical approximation resulting in the analytical expressions of DT and FN currents.

The leakage current measured at AMD Saxony for MOSFETs with SiO_xN_y gate oxide of different thicknesses and nitrogen concentrations are fitted to those calculated according to our method. The tunneling effective mass of electrons is then extracted as a function of thickness and nitrogen concentration.

The main parameters required for the calculations are the conduction band offset at the Si/SiO_xN_y interface, the dielectric constant of the SiO_xN_y layer, and the tunneling electron effective mass. The values of conduction band offset and dielectric constant are considered to vary linearly between the values of SiO_2 and Si_3N_4. The linear behavior of conduction barrier height and dielectric constant have been verified by experimental works [3] and used by other authors [10]. The conduction band offset of 3.15 and 2.1 eV and relative dielectric constant values of 3.9 and 7.5 have been used for SiO_2 and Si_3N_4 respectively.

The nitrogen concentration and the physical thickness of the samples are extracted with X-Ray photoemission spectroscopy (XPS). Although XPS is less precise for thick layers, it is a reliable and precise method for ultrathin layers (t_{ox}<3 nm) [12]. In general, the ellipsometry is more precise than XPS for pure silicon dioxide layers, but it is not suitable for oxynitride layers with unknown nitrogen concentration, because the result of ellipsometry thickness measurement depends on the nitrogen concentration in the layer. On the other hand using the XPS method, the thickness and the nitrogen concentration could be extracted at the same time. These two parameters are extracted using X-ray with an energy of 1486.6 eV.

3 Results and discussion

We studied 9 different samples. The physical characteristics of the samples are listed in table 1. The calculated gate currents are fitted to the experimental values at 1 V gate voltage. This point is around the working point of transistors in today's CPUs and this fitting results in a good agreement for the whole range of 0-2 V. Figure 1 shows the calculated current in comparison with the experimental data for samples numerated as 2, 4 and 7 with 0.1%, 6.9%, and 17.2% nitrogen concentrations correspondingly. Excellent agreement between measured and simulated curves is obtained using $0.92m_0$, $0.59m_0$, and $0.68m_0$ for the electron

tunneling effective mass with m_0 being the free electron mass. The electron tunneling effective mass extracted for the other samples are listed in the Table 1.
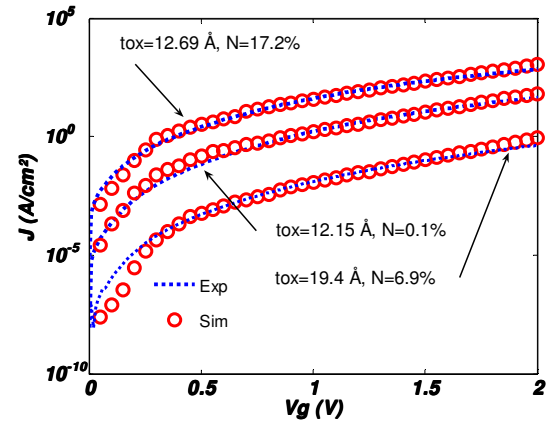
Fig. 1: measured and simulated gate tunnel current for samples 2, 4 and 7

Silicon dioxide gates of samples 1-3 contain the nitrogen concentration of 0.1%, which is just in the limit of a contamination. Comparison of these samples shows a strong dependency of electron tunneling effective mass on the layer thickness. As the thickness decreases the effective mass increases due to compressive stress in the oxide layer at the SiO_2/Si interface. It has been reported that the oxide layer within ~ 1 nm from the Si/SiO_2 interface has a higher density than the bulk oxide layer and consequently the Si-O-Si bonds are compressively strained near the interface [13]. On the other hand, Eriguchi et al. [14] have experimentally found that the tunnel current through the oxide layer with less built-in compressive stress near the interface is higher as in the reverse case. This implies that the more strained oxide has a lower tunnel current or apparently a higher effective mass.

The same discussion can be applied to the samples with higher nitrogen concentrations. For example, comparing sample 5 and 6 with almost the same concentration of nitrogen shows the same trend of increasing the effective mass by decreasing the layer thickness. Samples 8 and 9 reveal a similar trend for higher nitrogen concentrations.

As mentioned above, the electron tunneling effective mass is also a function of the nitrogen concentration. Samples 2 and 7 have almost the same physical thickness of 12.15 Å and 12.69 Å but different nitrogen contents of 0.1% and 17.2% respectively. Calculations result

in an effective mass of 0.92 m_0 for sample 2 but 0.68 m_0 for the 7th sample, which shows that, increasing the concentration of nitrogen reduces the effective mass in silicon oxynitride. Comparison of the samples 3 and 8 also shows the same behavior.

This result are in consistent with other works [2], [9], reported for the electron tunneling effective mass in light nitrided silicon oxides.

The effective mass values obtained in our calculation are slightly higher than values reported e.g. by Simonetti et al. [8] but lower than the values reported by Mao et al. [2]. Simonetti et al. reported a value of ~0.72 m_0 for a 10 Å thick silicon oxide layer. The discrepancy seems to be due to the physical thickness extraction method. The thickness measured with XPS is known to be smaller than the values extracted from ellipsometry, TEM or capacitive methods [15]. The underestimation of the thickness results in slightly higher values for effective mass extracted in our case. However the clear tendency of an increased effective mass in thinner layers and a decreased effective mass with increasing nitrogen content is obvious.

In Ref. 8 a linear dependency of the effective mass on the dielectric thickness is suggested. The dependence of the effective mass on the nitrogen concentration in our study is not strong, in contrast to exponential relation reported in Ref. 2., and could be considered linear. In the first step we suggested a linear dependence of the effective mass on both the thickness and the nitrogen concentration of a sample:

$$m*/m_0 = a + b.t_{ox} + c.N\% \qquad (1)$$

The values of effective mass are interpolated to the above linear function targeting the lowest sum of squared absolute errors over all samples.

The values of the coefficients are calculated to: a = 1.215850, b = -0.026908 and c = -0.010805. The maximum and mean values of relative error are 0.0496 and 6.57×10^{-5} respectively. In the second step we add a term to include the correlation between concentration and thickness in the linear interpolation of the effective mass:

$$m*/m_0 = a + b.t_{ox} + c.N\% + d.t_{ox}.N\% \qquad (2)$$

Interpolating the data with the same method results in the following values a=1.310044, b=-0.023529, c=-0.034048, d=0.000874 for the coefficients, and 0.0343 and 3.29×10^{-4} for the maximum and mean relative errors respectively. As it can be seen, the correlation coefficient d is relatively small and the relative error is as high as that in the first interpolation. Therefore, we can conclude that the thickness dependency of the effective mass is not strongly correlated with the nitrogen concentration dependency.

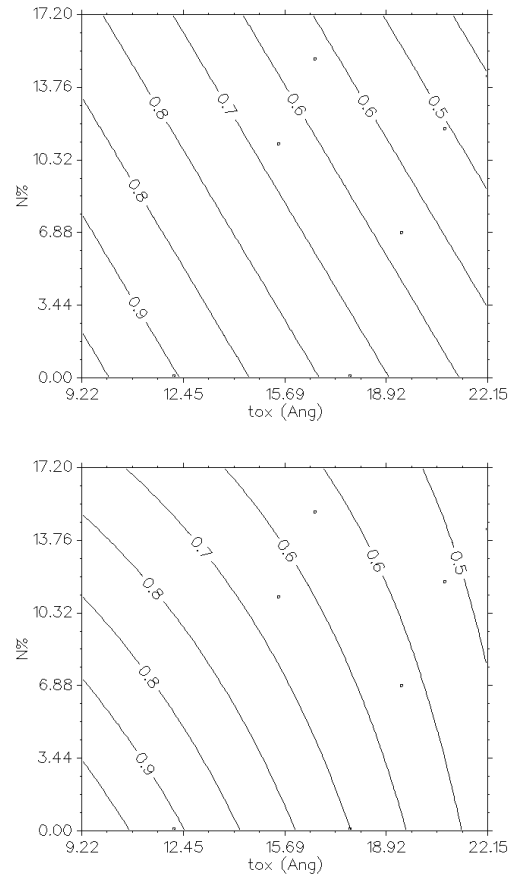Fig. 2: the contour illustration of not correlated (up) and correlated (down) linear interpolation.

The contour plots of two interpolation functions are depicted in figure 2. The contour curves in figure 2 clearly show that the thickness dependency is stronger than the nitrogen concentration dependency. Nevertheless, in the correlated case the nitrogen dependency prevails against the thickness dependency for thinner layers.

4 Conclusions

The tunneling effective mass of electrons in ultrathin silicon oxynitride layer is extracted from gate tunnel current in NMOS structure. Different samples with different thickness and nitrogen concentration are used to study the thickness and nitrogen concentration dependencies of effective mass.

The extracted effective masses show a strong dependency on the thickness of ultrathin layers. The effective mass tends to increase with decreasing the layer thickness. On the other hand, doping nitrogen to silicon oxide reduces the effective mass. The interpolations show a week correlation between the thickness dependency and the nitrogen concentration dependency of the effective mass. The interpolation functions can be used to suggest proper values for the effective mass of a sample with a specific thickness and nitrogen concentration at least in the range of the existing samples.

Table 1: the extracted tunneling effective mass for different samples

sample	t_{ox} (Å)	N%	m*
1	9.22	0.1	0.98
2	12.15	0.1	0.92
3	17.74	0.1	0.71
4	19.4	6.9	0.59
5	15.47	11.1	0.65
6	20.77	11.8	0.54
7	12.69	17.2	0.68
8	16.63	15.1	0.60
9	22.13	14.3	0.51

5 Literatures

[1]   The International Technology Roadmap for Semiconductors. Available: http://public.itrs.net

[2]   L. F. Mao, Z. O. Wang, J. Y. Wang, and G. Y. Yang, S*emicond. Sci. Technol.*, Vol. 20, pp. 1078-1082, 2005.

[3]   X. Guo, and T. P. Ma, *IEEE Electron Devices Lett.*, Vol. 19, Nr. 6, Jun. 1998.

[4]   C. Y. Ng, T. P. Chen, C. Q. Sun, and S. Fung, *J. Appl. Phys.*, Vol. 96, Nr. 10, pp. 5912-5914, Nov. 2004.

[5]   C. Y. Ng, T. P. Chen, and C. H. Ang, *Smart Mater. Struct.*, Vol. 15, pp. S39-S42, 2006.

[6]   M. Fukuda, W. Mizubayashi, A. Kohno, S. Miyazaki, and M. Masatak Hirose, *Jpn. J. Appl. Phys.*, Vol. 37, pp. L1534-L1536, Dec. 1998.

[7]   Khairurrijal, W. Mizubayashi, S. Miyazaka, and M. Hirose, *J. Appl. Phys.*, Vol. 87, Nr. 6, pp. 3000-3005, Mar. 2000.

[8]   O. Simonetti, T. Maurel, and M. Jourdain, *J. Appl. Phys.*, Vol. 92, Nr. 8, pp. 4449-4458, Oct. 2002.

[9]   Y. C. Yeo, T. J. King, and C. Hu, *IEEE Trans. Electron Devices*, Vol. 50, Nr. 4, pp.1027-1035, Apr. 2003.

[10] P. A. Kraus, K. Z. Ahmed, C. S. Olsen, and F. Nouri, *IEEE Trans. Electron Devices*, Vol.52, Nr. 6, pp. 1141-1147, Jun. 2005.

[11] E. Nadimi, C. Radehaus, E. P. Nakhmedov, and K. Wieczorek, *J. Appl. Phys.*, Vol. 99, pp. 104501 1-7, 2006.

[12] J. R. Shallenberger, D. A. Cole, S. W. Novak, and R. L. Moore, *Ion Implantation Technology Proceedings*, Vol. 1, pp. 79-82, 1999.

[13] N. Awaji, S. Ohkubo, T. Nakanishi, Y. Sugita, K. Takasaki, and S. Komiya, *Jpn. J. Appl. Phys.,* Part 2, Vol. 35, pp. L67-L70, Jan. 1996.

[14] K. Eriguchi, Y. Harada, and M. Niwa, *IEDM Tech. Dig. 1998*, pp.175-178.

[15] M. P. Seah *et al.*, *Surf. Interface Anal.,* Vol. 36, pp. 1269-1303, 2004.

The application of Higher Order Derivatives Method for parametric component-level simulations of MEMS

Kolchuzhin, Vladimir [1]; Mehner, Jan[2]; Doetzel, Wolfram[1]

[1]Chemnitz University of Technology, Department of Microsystems and Precision Engineering

[2]Fraunhofer Institute for Reliability and Microintegration, Department Multi Device Integration

1 Introduction

Finite element techniques have become state of the art for component design of MEMS. Physical effects related with electromagnetic, mechanical, fluid and thermal fields in complex devices are accurately described for static, harmonic and transient load situations [1].

Drawback of existing FE techniques is that those algorithms can only analyze a single model configuration with specified dimensions and physical parameters. In practice, designers long for the influence of parameter variations on the structural response in the same way as known from analytical methods. Currently, parametric models of complex devices are extracted by numerical data sampling and subsequent fit algorithms, Fig.1. Each sample point must be obtained by a separate FE run whereby the change of geometrical dimensions is realized by mesh morphing or re-mesh functionality. Usually one needs between several ten to some hundreds of sample data in order to capture the influence of design parameters accurately [1].

The article demonstrates the new parametric approach [2] to design of coupled domain systems (e.g. sensors and actuators) where strain energy and capacitance functions relate interactions between electrostatic and structural domains.

2 Description of the Method

The key idea of the new approach, which account for parameter variations in a *single* FE run, is to compute not only the governing system matrices of the FE problem but also their partial derivatives with regard to design variables, Fig.1. Difficulties arose mainly from the fact that extraction of high order derivatives becomes numerical unstable and time consuming.

In contrast to symbolic differentiation which propagates mathematical functions, novel approaches make use automatic differentiation algorithms which process numerical values extracted at the initial position. Chain differentiation rules describe how to combine partial derivatives and binomial coefficients in order to form elementary mathematical operations and where to store results in 3-D arrays. Finally, Taylor vectors of the goal function can be expanded covering the system response in the vicinity of the initial position with regard to design parameters, Fig. 1.

3 Conclusion

The algorithms support linear static and harmonic analyses of structural, thermal and electrostatic domains and sequential couple-field problem, Fig. 2.

Especially for case studies of different geometrical dimensions, sensitivity analyses of manufacturing tolerances and model export for EDA one needs fast and accurate models which capture the parameter relationship. Special emphasis was put on strain energy and capacitance extraction for reduced order modeling of MEMS. Benefits of variational technologies compared to ordinary data sampling procedures become obvious for large complex and multi-parameter problems. Response functions provide not only capacitance data but also the first and second derivatives needed for Maxwell force and electrostatic softening computations [1].

4 References

[1] Mehner,J.; Bennini,F.; Doetzel,W.: *CAD for Microelectromechanical Systems*. System Design Automation: Fundamentals, Principles, Methods, Examples, Kluwer Academic Publ., pp. 111-132, 2000.

[2] Kolchuzhin,V.; Mehner,J.; Gessner,T.; Doetzel,W.: *Parametric Simulation of MEMS Based on Automatic Differentiation of Finite Element Codes*. "MSM2006", v. 3, pp. 507-510.
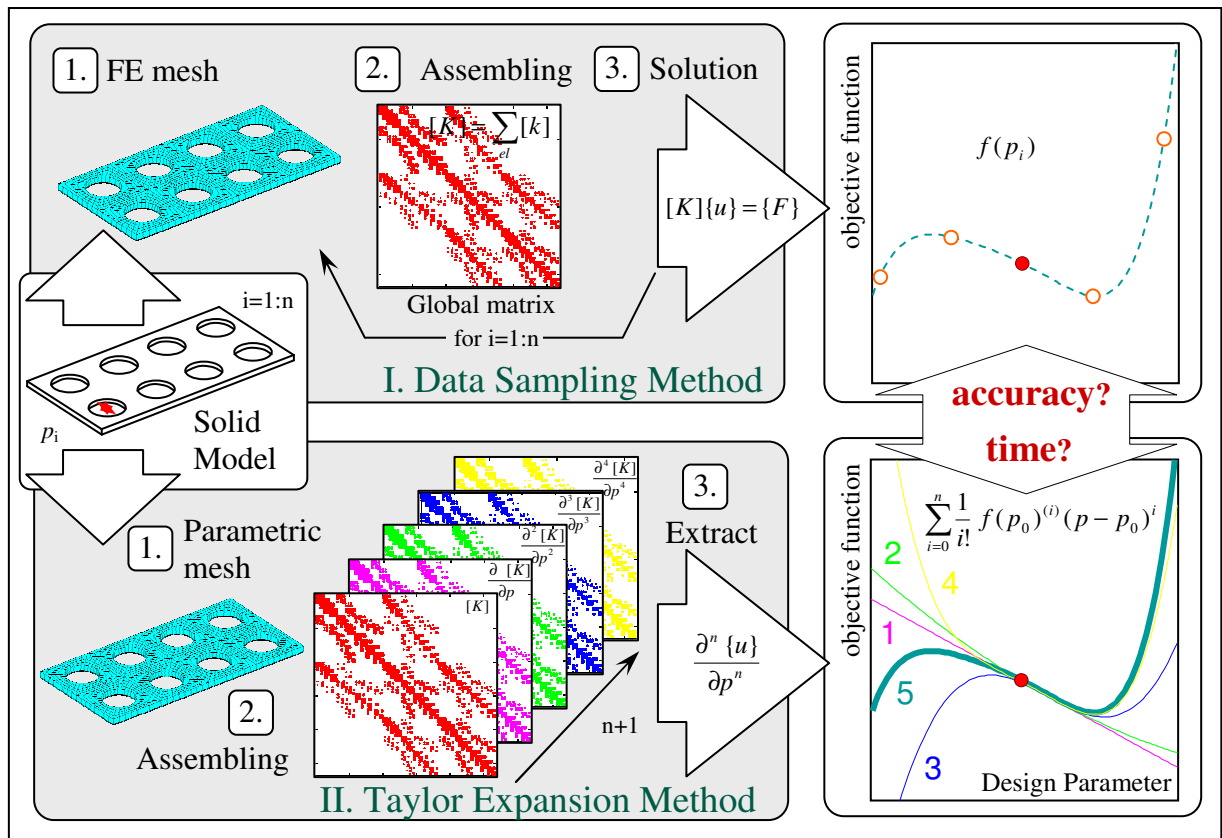
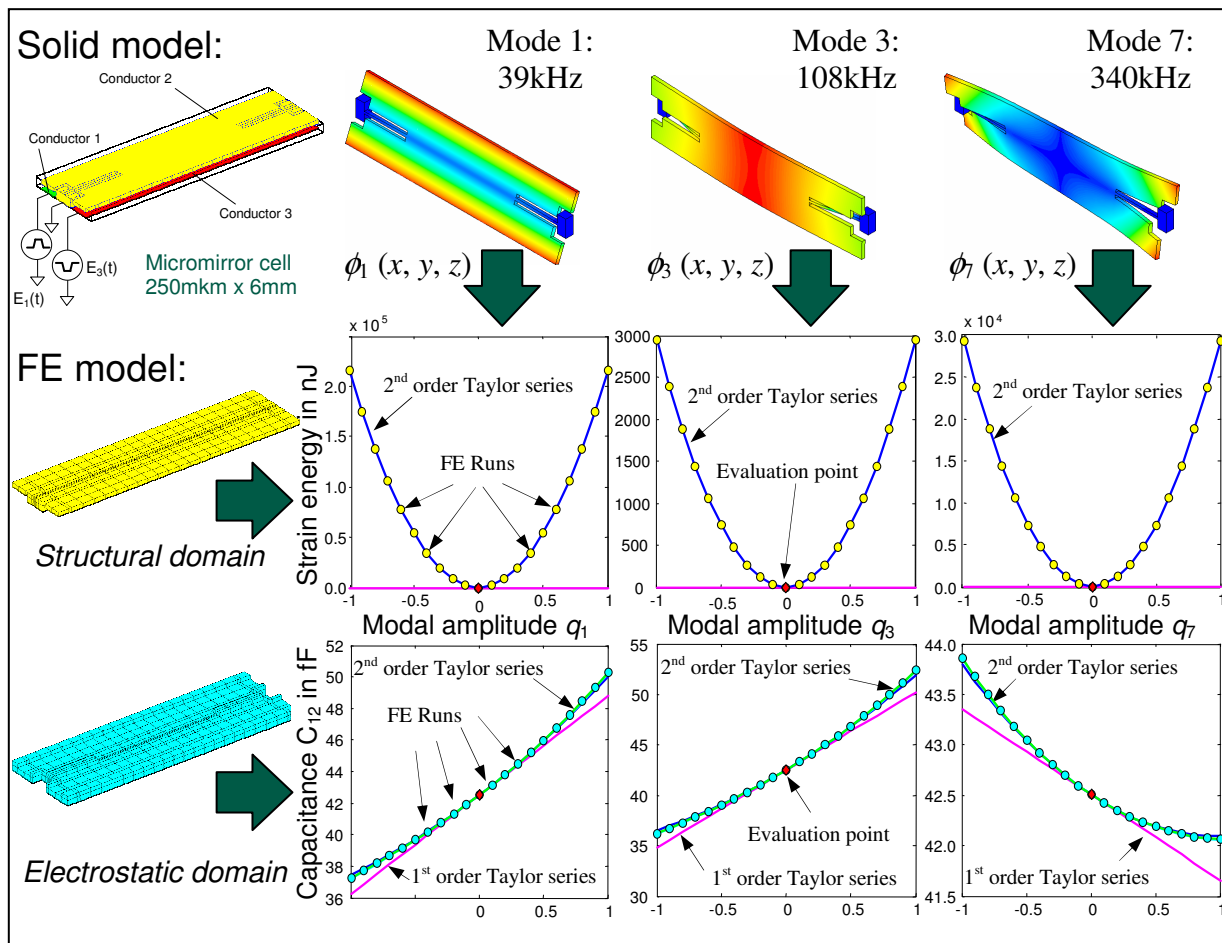*Fig. 1: Flow chart of ordinary and parametric FE techniques*

Fig. 2: Accuracy of parametric FE techniques compared to ordinary FE sampling for generation of ROM

Near Infrared MOEMS Spectrometer

Saupe, Ray[1]; Otto, Thomas[2]; Weiß, Alexander [1]; Stock,Volker [3]; Gessner, Thomas[1,2]
[1]Chemnitz University of Technology, Center for Microtechnologies,
[2]FhG-IZM Chemnitz, Dep. MDI
[3]COLOUR CONTROL Farbmesstechnik GmbH

1 Introduction

Near Infrared (NIR) spectroscopy has developed to an important and useful analysis method over the past years. The existence of compact, portable devices offers a lot of applications and possibilities. Compact devices, mostly based on detector arrays, are quite costly caused by the expensive Indium Gallium Arsenide (InGaAs) detector arrays. By using MOEMS the set-up can be realised much more efficiently.

2 Functional principle & Setup

The MOEMS Spectrometer is realized in a simple optical set-up according to a Littrow alignment. The central component of this set-up is a scanning micro mirror [1] which design has been optimized for the spectrometer. The properties of the Micro mirror strongly influence the performance of the spectrometer system. With a large active surface and a tilt angle a high throughput and broad working range will be achieved. A plate warp less than a fraction of the optical wavelength ensure accuracy of the optical image. The functional principle can be described as follows: infrared radiation, emitted from a quartz tungsten halogen lamp, is absorbed by a sample and enters a fiber optic. The sample is presented either in transmission mode or in diffuse reflection. After entering the fiber the radiation launch the spectrometer through the entrance slit. A deflection mirror reflects the radiation toward a spherical mirror, which collimates the incident radiation and reflected it towards the micro mirror. Then the radiation is reflected to a diffraction grating, which divides it into its spectral components. According to the wavelength dependent reflection angle of the micro mirror the desired component of diffracted light reaches the exit slits via both micro mirror and collimator. Behind the spatially separated exit slits two single element detectors and transimpedance amplifiers are arranged, which convert the mono-

chrome radiation into electrical signals for further data processing [2].

3 Packaging

The spectrometer housing (Figure 1) is made by using rapid prototyping methods. Using rapid prototyping while the design process allows a fast and flexible development, whereby almost all electrical, mechanical and optical components are easy to embed. This enhances consequently the quality and takes advantages over conventional assembled packages.
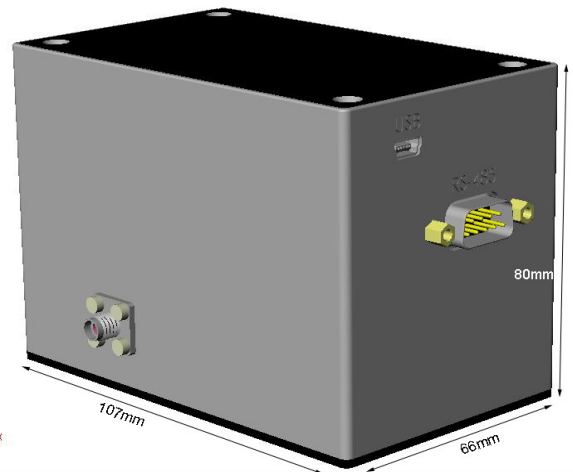
Figure 1: Spectrometer package manufactured by selective laser sintering

4 Experimental results

Figure 2 shows the signal stability (amplitude, wavelength) and the average stray light during a long term measurement campaign measured with a spectral filter. Permanent observation of the mirror angle by a position sensor increases thereby the reproducibility. Measuring the wavelength reproducibility a shift ($\Delta\lambda$) less than 0,05 nm was recorded. Furthermore the amplitude deviation (ΔT) is better than 0,1%. Stray light was determined by the measurement with edge filters. The minimization of stray light is important in connection with Lambert Beer's law since the linearity between absorbance and

Figure 2: Transmission spectra (band pass filter with peak position @1400nm)

concentration gets lost. The resulting standard deviation 0,086 (0,1%) was mainly improved by integrated stray light traps . SNR of approx. 4000 to 1 by a basic measurement could also be achieved. It can be improved further by averaging to about the square root of the original values.

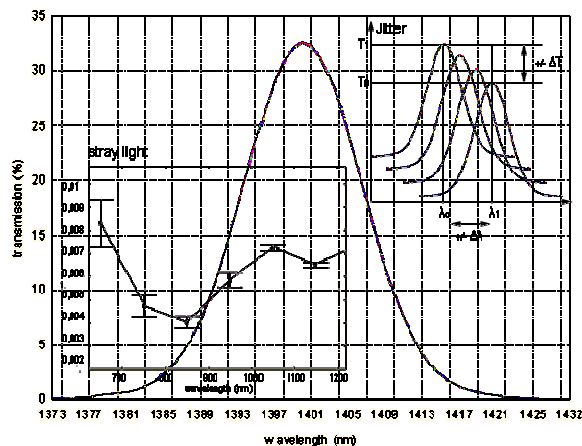| Parameters	NIR-Spectrometer
wavelength range	660 – 2100nm
spectral resolution	< 12nm
SNR @ single measurement	4000:1
repeatability	± 0,05nm
dimensions (mm)	107x66x80
primary measuring time	2ms

Table 1: Specifications

5 Applications

The micro mirror spectrometer has been applied extensively to various practical problems. One of those in foodstuff is the detection of meat quality. Therefore different meat species (beef, turkey hen, pork and chicken) and diverse storage methods were analyzed with regard to identification and degradation effects. In this connection chemometric models, e.g. PCA, PLS and ANN with promising results were evaluated.

In addition, applications to industrial process control have been realized. Some nameable are:

- Identification of textiles
- Identification of polymers (for sorting problems)
- Quantification of process gases (methane, ethane, butane, propane, carbon dioxide)

Also applications in medical sciences like the non invasive diagnostic of digestion disorders were accomplished. Purpose of this clinical study was to determine fat (r=0,98) and water (r=0,96) content in faeces. This first evaluation study was important for evidence of malassimilation and for estimating the efficacy of treatment with pancreatic enzymes. Further clinical studies should estimate more critical parameters and substances.

Another realized more physical measurement scenario is the spectroscopic ellipsometry for determining film thicknesses. Here the required accuracy of $\delta t < 0,2nm$ could be achieved.

Future works mainly for home care applications can be seen in non-invasive glucose sensing or determination of metabolic disorders.

6 Summary

In this work the functional principle, experimental results and some applications of the micro mirror spectrometer was presented. Flexible setup, portability, cost efficiency and short scan time are features, which offer advantages compared to conventional spectrometers. The overall measurement results e.g. in food, polymer and textile science or clinical chemistry shows the applicability of the MOEMS spectrometer. Thus the small sized and competitive NIR device could assist economic efficiency in many application fields.

Further versions of the system working within a wavelength range up to 2500 nm are already in development. By further enhancing the opto-mechanical design, a performance improvement in terms accuracy and repeatability may be achieved.

7 References

[1] W. Dötzel, T. Gessner, R. Hahn, C. Kaufmann, K. Kehr, S. Kurth, J. Mehner; *Silicon Mirrors and Micromirror Arrays for Spatial Laser Beam Modulation*, Dig. Of Tech. Papers of 1997 International Conference on Solid-State Sensors and Actuators, Vol. 1 pp. 81-84, Chicago, 1997
[2] T. Otto, R. Saupe, U. Fritzsch, V. Stock, R. Bruch, T. Gessner, *Novel Dual-detector micro spectrometer*, San Jose, 2005, Proceedings of SPIE Vol. 5719, pp.76-82

Microcoils for NMR Spectroscopy of Biological Sample Material

Leidich, Stefan[1]; Hofmann, Lutz[1]; Kurth, Steffen[2]; Kaufmann, Christian[1]; Gessner, Thomas[1,2]
[1]Chemnitz University of Technology, Center for Microtechnologies
[2]Fraunhofer Institute for Reliability and Microintegration, Dept. Multi Device Integration

1. Introduction

NMR spectroscopy is an important analysis technique with widespread application in research, medicine and industry. However, the analysis of mass limited samples like purified primary stem cell populations requires very high sensitivity of NMR hardware. Using different kinds of miniaturized coils in NMR resonators has led to improvement in sensitivity [1]. The microcoil presented here addresses four important aspects of NMR micro spectroscopy – high sensitivity by using low resistance copper conductors and therefore high Q factor, homogenous RF magnetic field by using Helmholtz coil configuration, reduction of NMR background signals and minimization of the static magnetic field distortion by proper selection and shaping of construction materials.

2. Design

According to fig. 1, the design consists of two layers of windings and additional cylindrically shaped silicon elements on top and bottom. One of the major concerns of micro NMR is the low spectral resolution caused by distortion of the static magnetic field (B_0-field) due to different magnetic susceptibilities χ of construction materials. In contrast to ref. [2] the substrate and the sample container are shaped cylindrically. Known from physics, cylindrical shape mitigates the distortional influence of matter on homogenous magnetic fields since all spherical shapes as well as long cylinders provide homogenous field in their inside.

The mean radius of the coils is approximately equal to the separation of the coil layers. The resulting Helmholtz configuration produces homogeneous RF magnetic field (B_1-field) necessary for pulse sequence experiments. Fig. 2 shows the B_1-field normalized to coil current plotted over the capillary length and cross section, respectively. The B_1-field distribution is directly related to the signal intensity contributed by each elementary sample volume.
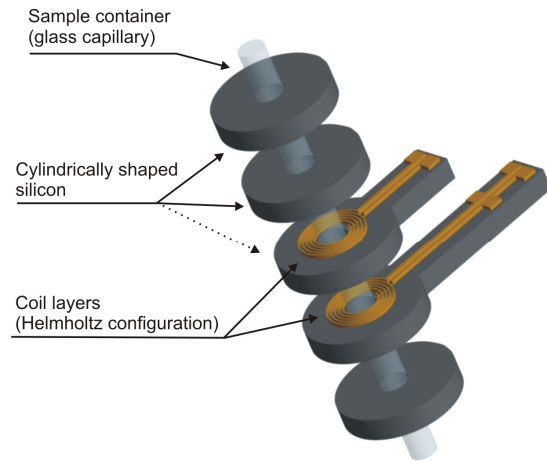
Fig. 1: Microcoil for NMR spectroscopy

Using numerical integration technique it can be shown that 90% of the maximal possible signal intensity (infinite sample length) is generated by an effective sample cylinder of ~1000 µm length. In correspondence with the capillaries inner diameter of 200 µm this results in 31.4 nl active sample volume.
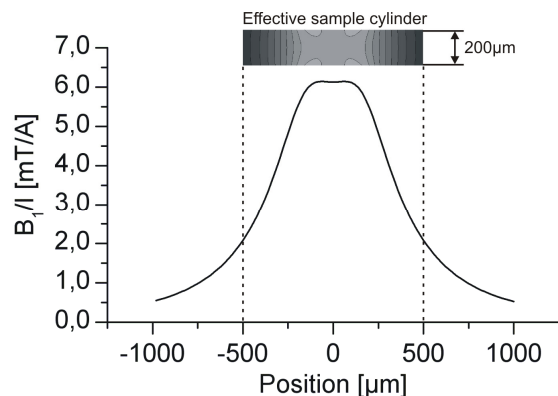
Fig. 2: B_1-field vs. elementary sample volume position (position direction normal to coil plane); inset: surface plot of B1-field intensity, cross section through effective sample cylinder

3. Fabrication Technology

The fabrication process of the coil is optimized to deal without remanent polymers like SU8, which is commonly used for planarization of

thick conductors, necessary for high Q factor. Polymers consisting of carbon and hydrogen cause NMR background signal (^{1}H/^{13}C NMR) and B_0-field distortions. For this reason, the connection from the inside winding to the feed line is placed into an etched cavity. The process is schematically shown in fig. 3.

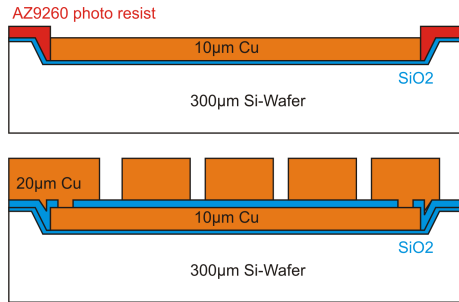*Fig. 3: Fabrication sequence of coil conductors*

The cavity is structured using KOH wet etching and is filled by electroplated copper in photo resist moulds. The first available coils provide 20 µm thick copper traces and copper filled cavities of 10 µm depth. Coils with different diameters have been fabricated. Fig. 4 shows a SEM micrograph of a coil with 155 µm inner diameter (D_i). The final cylindrical shape and the dicing are achieved by dry etching.

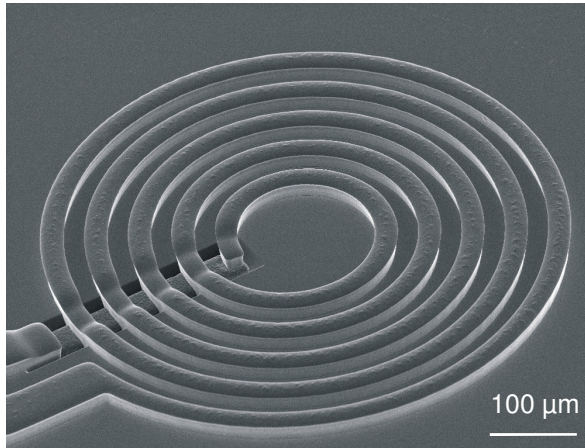*Fig. 4: SEM micrograph of fabricated coil (D_i=155 µm)*

3. Results

For RF characterization a vector network analyzer with signal-ground on wafer probes is used. Thru-Open-Short-Match (TOSM) calibration has been performed using commercial calibration standards on ceramic substrate. Measured scattering parameters (fig. 5) are transformed into an analytically described Pi-circuit model [3].
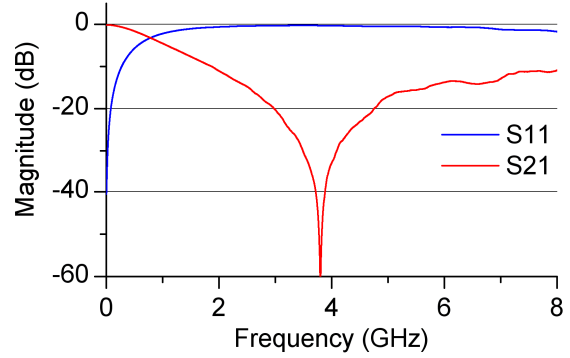
Fig. 5: Measured S-Parameter of the coil (D_i=430 µm)

The quality factor (Q factor) is calculated according to the commonly used definition (1) [3]. This formulation considers magnetic and electric energy stored in the field, and therefore yields a Q factor of zero at self resonance. The Q factor over frequency of a 5 turn, 430 µm inner diameter, 20 µm conductor width and 30 µm spacing coil is shown in fig. 6. The fitted model provides 20 nH inductance, a Q factor of 26 (at 750 MHz) and self resonance frequency of 2.8 GHz.

$$Q(\varpi) = \frac{\mathrm{Im}\left(Y_{\pi 11}(\varpi)^{-1}\right)}{\mathrm{Re}\left(Y_{\pi 11}(\varpi)^{-1}\right)} \qquad (1)$$
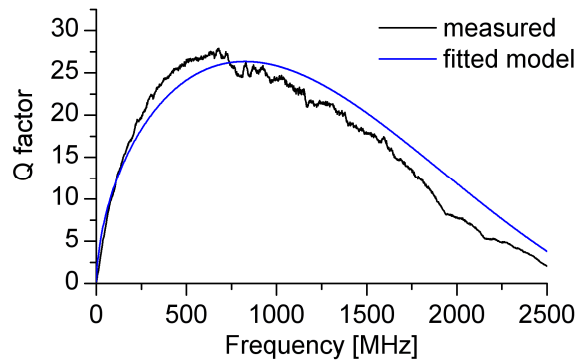
Fig. 6: Q factor of measured coil and fitted model

References

[1] P. J. M. van Bentum, J. W. G. Janssen, et. al.: *Toward Nuclear Magnetic Resonance µ-Spectroscopy and µ-Imaging.* The Analyst, vol. 129, pp. 793–803, 2004

[2] C. Massin, F. Vincent, et al.: *Planar Microcoil-Based Microfluidic NMR Probes.* J. Mag. Res., vol. 164, pp. 242–255, 2003

[3] P. Arcioni, R. Castello, et. al.: *An Innovative Modelization of Loss Mechanism in Silicon Integrated Inductors.* IEEE Trans. Circ. Sys., vol. 46, no. 12 , pp. 1453–1460, 1999

A MEMS friction vacuum gauge

Tenholte, D.[1]; Kurth, S.[2]; Hiller, K.[1]; Kaufmann, C[1]; Geßner, T.[1,2]; Dötzel, W.[1]

[1]Chemnitz University of Technology, Faculty of Electrical Engineering and
Information Technology, D-09107 Chemnitz, Germany

[2]Fraunhofer IZM, Dep. Multi Device Integration, D-09126 Chemnitz

1 Introduction

A lot of new MEMS based vacuum gauges have been developed by scaling down conventional working principles during the last years [1].

In high and fine vacuum, friction gauges are used as reference sensors and for calibration measurements. The damping of an oscillator by energy emission to the surrounding gas depends on the effective viscosity of the gas, which hinges on the pressure. An utilization of the dependency of damping by ambient pressure in MEMS, customized for vacuum measurement, is described by Kurth [2] and by Bianco [3].

We have developed a new MEMS friction vacuum gauge which expands the advantages of common friction gauges. Besides the perspicuous smaller size a benefit of the new sensor to common ones is its sensitivity above 1 mbar nearly up to ambient pressure. The sensor consists only of glas, silicon and aluminium, so it can be used for measurements in environments with temperatures of up to 350° C.

2 Assembly and working principle

The working principle of the sensor is based on the pressure depending gas friction. The essential part of the sensor is a torsional oscillating plate with a nearby wall. For detecting the vacuum pressure we utilise two different kinds of pressure depending damping: For higher pressures where the gas can be considered as a continuum, the squeeze damping is the pressure dependent one. For low pressures, where the gas can not be considered as a continuum, the molecular damping is pressure dependent.

The structure of the sensor is shown in Fig. 1. It consists of a 25 µm thick, 3x3 mm^2 oscillating plate which is mounted in the centre of the chipframe by two 325 µm long torsional springs. The gap between oscillator and the electrodes on the carrier amounts 5 µm. Below the oscillating plate is a hole in the carrier wafer for reducing the damping at higher pressures so the plate will oscillate and not be overdamped at any pressure.
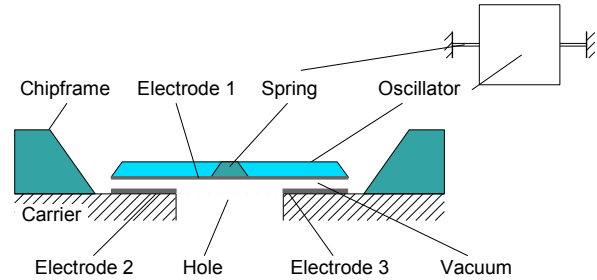
Fig. 1: Cross sectional view of the sensor

The damping of the oscillator can be determined by evaluating the free damped oscillation. Due to a driving voltage between the oscillator (Electrode 1) and one of the ground electrodes (Electrode 2, resp. Electrode 3) the oscillator tilts around its rotation axis. After switching off the driving voltage, the damped oscillation

$$\varphi(t) = \hat{\varphi}\, e^{-\delta t} \cdot \cos(\omega_d t) \tag{1}$$

is measured. The decay constant δ of the system is determined by detecting the maxima of the oscillation and calculating their logarithm. These values result in a straight line which gradient is the decay constant:

$$\ln \varphi(t) = \ln \hat{\varphi} - \delta t \tag{2}$$

Depending on the pressure, the decay constant can be calculated by averaging from several 10 to several 1000 measured values which reduces the influence of noise. The conversion to pressure is done by means of a calibration curve.

3 Simulation

Because of the narrow gap of 5 µm between oscillator and electrodes, the squeeze effect appears nearly up to ambient pressure. Due to the hole under the oscillator and the small amplitude of oscillation, the motion of the plate towards the electrode has to be regarded as translational. Methods for numerical analysis of the squeeze damping for two parallel, towards moving plates are among others presented by van Kampen [4].

For lower pressures, the mean free path of the gas molecules is much larger than the gap between oscillator and electrodes. In this pressure

area the molecular damping occurs. The equations derived by Li [5] for calculating the molecular damping, refer to a paddle formed structure, considered as a mathematical pendulum with lateral dimensions. The oscillator plate of our sensor can be approximated as two on their hinge concatenated paddles.

At the lower end of the pressure range, pressure independent kinds of damping like intrinsic and thermo compression damping reach the magnitude of the molecular damping.

On the basis of the developed simulation model the sensor geometry has been optimized, so that the measurement range is as wide as possible and the sensor is sensitive nearly up to ambient pressure.

4 Measurement results

The sensor has been installed inside a vacuum system and the damping of the oscillator has been measured as a function of the ambient pressure.
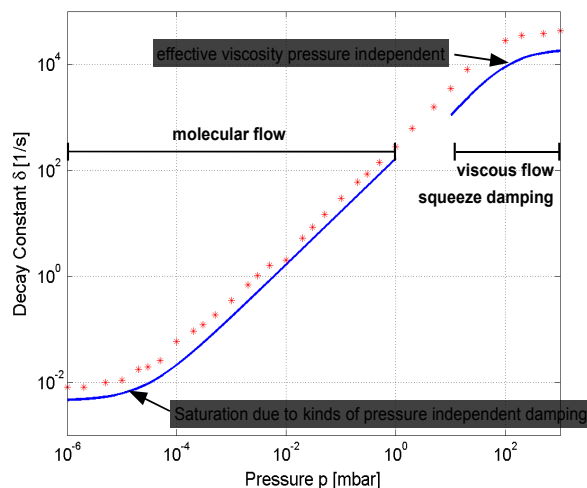

Fig. 2: Simulated decay constant for the optimized sensor compared to measurement results

Fig. 2 shows the results of the measured decay constant in comparison to the simulated one. As to see, simulation and measurement match very well. The sensor is sensitive for a pressure range of over 8 decades from 10^{-5} to 10^3 mbar. The measurements have been iterated a couple of times to verify the repeatability, and no significant deviations have occurred.

The sensor consists only of glas, silicon and aluminium. To determine the behavior of the sensor at high temperatures, it has been fixed on its bond wires within a copper pipe, that was heated at one end by a halogen lamp. One can assume that the temperature inside the pipe will be
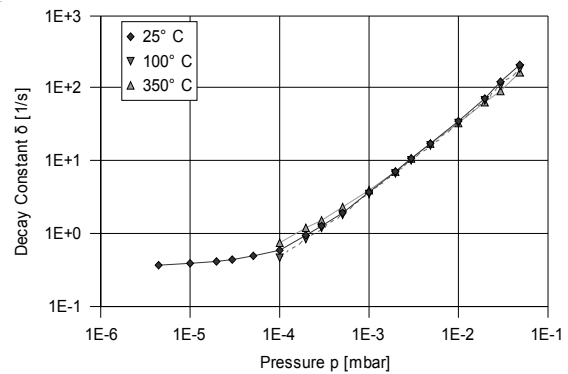
Fig. 3: Pressure dependency of the decay constant at various temperatures

homogeneous after one hour due to heat radiation.

The results of these measurements are shown in Fig. 3. Only a small influence of the temperature on the damping in the range of less than 10% of the actual value could be observed. We suppose that these small deviations issue from the used reference Pirani-Gauge.

5 Conclusions

We have developed a new MEMS friction vacuum gauge with a measurement range of about 8 decades nearly up to ambient pressure. The sensor can be used in high temperature environment up to temperatures of 350° C. The deviation from measurement value can be assumed of less than 5%.

6 References

[1] S. Wilfert, C. Edelmann: *Miniaturized vacuum gauges*; J. Vac. Sci. Technol. A, Vol. 22, No. 2, Mar/Apr 2004, pp. 309-320

[2] S. Kurth et al.: *A micromachined pressure gauge for the vacuum range based on damping of a resonator*, Proc. of SPIE 2001, Vol. 4559, pp. 103-111

[3] S. Bianco et al.: *Silicon resonant microcantilevers for absolute pressure measurement*; J. Vac. Sci. Technol. B, Vol 24, No. 4, Jul/Aug 2006, pp. 1803-1809

[4] R. P. van Kampen, R. F. Wolffenbuttel: *Modeling the mechanical behavior of bulk-micromachined silicon accelerometers*; Sensors and Actuators A64 (1998), pp. 137-150

[5] Bingqian Li et al.: *The theoretical analysis on damping characteristics of resonant microbeam in vacuum*; Sensors and Actuators 77 (1999), pp. 191-194

Active Smart RF-ID Label for Transportation Monitoring

Reuter, Danny[1]; Bertz, Andreas[1]; Wiemer Maik[2]; Geßner, Thomas[1,2]

[1] Chemnitz Univ. of Technology, Center for Microtechnologies

[2] Fraunhofer Institute for Reliability and Microintegration, Departement MD&E

1 Introduction

Within the project "ASIL", an active radio frequency identification (RFID) label for the monitoring of shock and inclination during transportation processes is being developed. For this purpose the requirements on the inertial sensors, measuring shock and inclination, are different to common applications. Therefore, the technology and the design for the transducer element have to be modified and a packaging technology has to be developed.

The goal of the project is the integration of inertial sensors in already existing RFID labels. The specific tasks are the limited energy supply and the demand for a very thin and flexible system by low manufacturing costs. The low energy consumption is realized by a specific measurement procedure. The reduction of the chip height is obtained by modifying the device technology and integration of a novel thin film encapsulation method.

2 Technology of the sensing device

To achieve the ambitious requirements for the RFID label, we use the Air gap Insulated Microstructures (AIM) technology for sensor fabrication [1]. The capacitive working principle enables low energy operation, the high aspect ratio of the structures allows high sensitivity, and hence the required dynamic range.

For enabling flip-chip assembling of the system Nickel or palladium has to be bumped on the contact pads by electroless plating. Therefore the metallization system of the AIM technology has to be modified regarding the material and the passivation. The aluminum is replaced by an AlSiTi alloy as seed layer for the plating process. Exposed surfaces of interconnection lines have to be passivated by dielectric material to avoid deposition of the plated metal.

In figure 1 the improved process steps are compared to the previous technology. Before the patterning of the metal, an additional PE-CVD SiO layer has been deposited and is used as hard mask for the metal etch process. With the subsequent structuring of the insulation stack, the passivation layer is opened above the contact pads in order to create contact windows for the plating process. Another SiO layer is deposited by PE-CVD as mask for the deep reactive ion etching (DRIE) of the silicon structures. As a result of the isotropic deposition but anisotropic removal of the SiO, a spacer oxide remains at the sidewalls of the metal layer and is used as sidewall passivation.
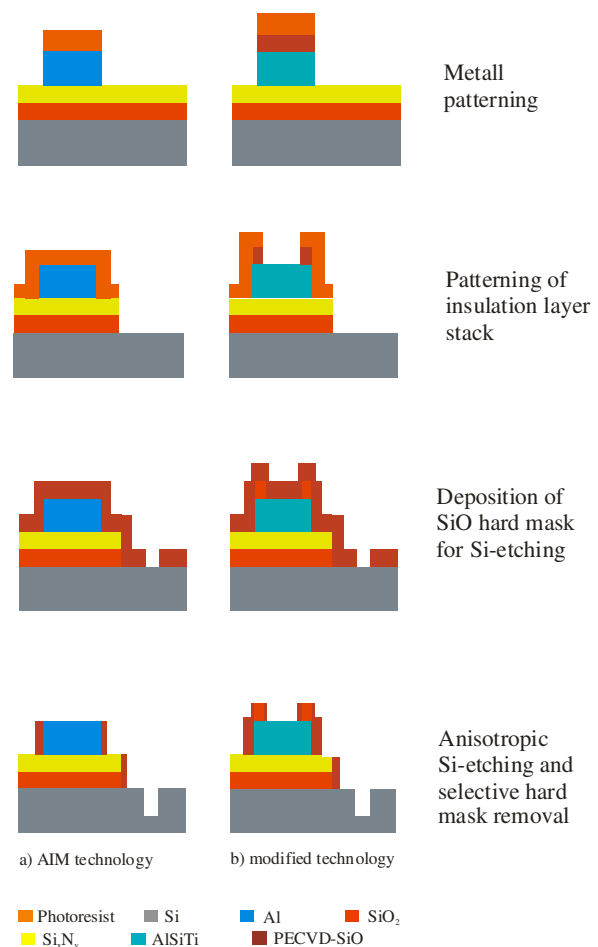

Fig. 1: Schematic drawing of the conventional and the modified AIM technology; the modification enables plating of nickel bumps on the contact pads

3 Thin film encapsulation of the inertial sensor

The size of the label will be the format of a cash card. Therefore the height of the subsystems and hence the silicon dies is limited. So far, the sensors are packaged by bonding a silicon wafer to the sensor wafer using seal glass. To meet the terms regarding the chip height, it is necessary to process thin substrates or grind and polish the wafer stack to the final thickness. Furthermore, the seal glass bonding is chip area consuming, due to the wide bonding frame.

A novel approach is using surface micro-machining processes for creating thin film caps. These thin film encapsulation (TFE) technologies are based on a sacrificial layer which is covering the microstructures during deposition of the encapsulating film. [2, 3] The sacrificial layer is removed via access holes, which are sealed hermetically during a final deposition step (fig. 2).
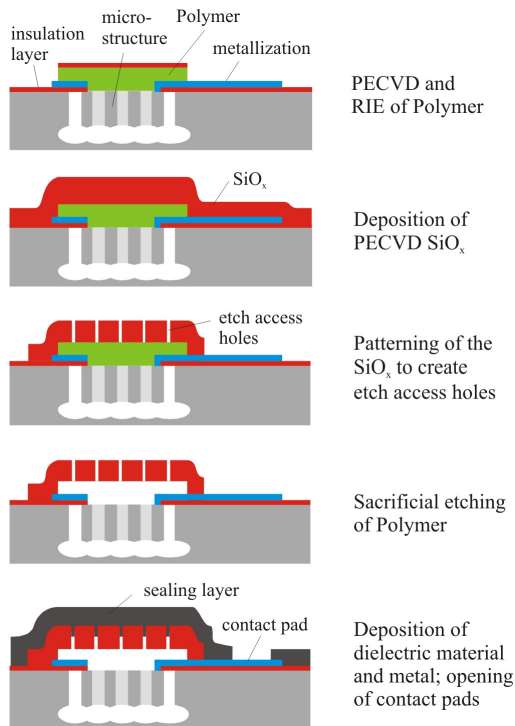

Fig. 3: Schematic process flow of the PECVD Polymer based thin film encapsulation technique

Mostly SiO_2 is used as sacrificial material [2], however this is not process compatible to the AIM technology. Organic materials, which can be easily removed in oxygen plasma, are an interesting alternative. Therefore we are using a PECVD polymer which is temperature stable up to 400°C utilizing subsequent PECVD processes.

In order to demonstrate the technology, test structures were fabricated. Figure 3 shows the SEM micrograph of a throughout dry processed thin film encapsulated silicon structures.
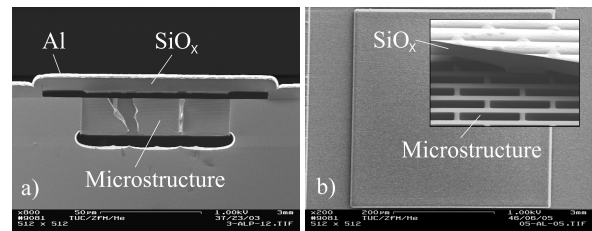
Figure 4. SEM of sealed MEMS structures a) cross-section of 100x100 µm² cap b) top and detail view of 400x400 µm² cap

Since the sealing is realized during PECVD, the process pressure is maintained in the cavity of the micro package. The deflection of the cap due to the pressure difference between the ambient and the cavity can be measured with an interferometer, proofing the successful sealing of the thin film cap (fig. 4).
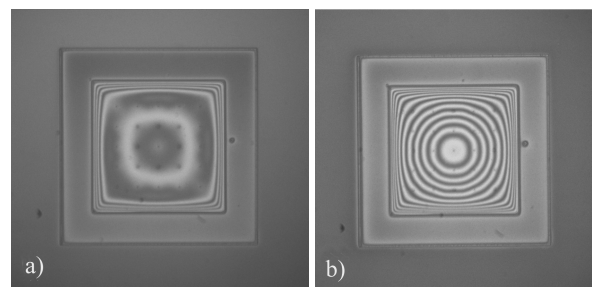
Figure 4. Interferometric contour image (λ = 514,7 nm) of a 400x400 µm2 plate a) released SiOx membrane with 1.5 µm thickness b) after sealing with 7 µm SiOx; the maximum deflection is 0.25 µm (due to residual stress) and 1.54 µm (due to one atmosphere pressure difference) respectively

References

[1] Lohmann, C.; Reuter, D.; Bertz, A.; Gessner, T.: *High Aspect Ratio Micromachining using the AIM Technology*, chapter in the book: The World of Electronic Packaging and System Integration, pp. 544-548, 2005.

[2] A. Partridge et al., "New Thin Film Epitaxial Polysilicon Encapsulation for Piezoresistive Accelerometers", *in Proc. of IEEE Conference on MEMS 2001,* pp. 54-59, 2001.

[3] Woo-Tae Park: *Wafer-Scale Film Encapsulation of Micromachined Accelerometers*, Proc. Transducers '03, Boston, June 8.-12., 2003.

Laser Frequency Trimming of Micro Mirror Devices

J. Bonitz[1], J. Mehner[2], C. Kaufmann[1], K. Bleul[3], J. Hänel[3], T. Gessner[1,2]
[1]Center for Microtechnologies, Chemnitz University of Technology
[2]Fraunhofer Institute for Reliability and Microintegration, Department Multi Device Integration
[3]3D-Micromac AG, Chemnitz

Introduction

Fabrication technologies of Micro Mirror Devices (MMD) cause tolerances in device dimensions and consequently on key parameters like the resonant frequency. Frequency trimming of MMD's is a promising approach to overcome these manufacturing tolerances, to tune sensors and actuators for certain operating conditions and it promises an increasing yield in MEMS technology.

Post fabrication frequency trimming is commonly applied to micromechanical resonators [1,2,3] or gyroscopes [4]. Different techniques like plasma etching [2], ion bombardment [3] or laser ablation [1,4] are used for this approach. The biggest disadvantage of these techniques is a relatively low maximum frequency change in the range of 0.02 % [1] to 4.5 % [4].

Simulation

Within this project a new trimming technology with higher efficiency is developed. Additional trimming elements are added at frequency influencing mirror components like mirror plate and torsion spring.
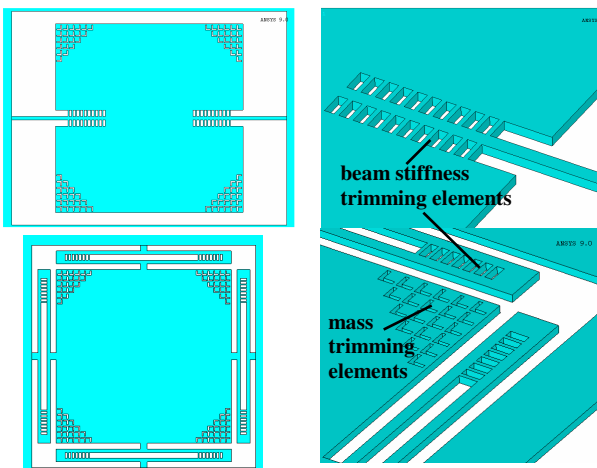
Fig. 1: FEM layout of the devices with a detailed view of the trimming elements (above: 1D-mirror, below: 2D-mirror)

A removal of these elements by laser cutting at the mirror plate effects a frequency increase because of mass reduction, whereas the removal at the torsion beams effects a frequency decrease because of a lower beam stiffness. Figure 1 shows the FEM layout of the devices with a detailed view of the trimming elements for a 1-dimensional and 2-dimensional micro mirror, respectively.

The FEM simulated frequency changes of the trimmed structures are shown in Table 1. Thereby large maximum frequency changes can be reached (up to 31.3 %) at very fine increments (0.4 %). Because of this fact, this method offers a very fine, previously calculable frequency tuning by a systematic combination of the trimming variants.

Table 1: Simulated frequency changes for 1- and 2-dimensional micro mirrors

Trimming	Relative frequency change	
	1D mirror	2D mirror
Frequency increase by mass removal at the mirror plate → removal of all 21 trimming elements → removal of one trimming element	+ 9.1 % + 0.5 %	+ 7.8 % + 0.4 %
Frequency decrease by changing the spring length → removal of all 10 trimming elements → removal of one trimming element	- 20.5 % - 2.9 %	- 31.3 % - 6.3 %

Micro Mirror Fabrication

The Micro Mirror Devices are fabricated by silicon bulk technology. The main fabrication steps are shown in Figure 2.
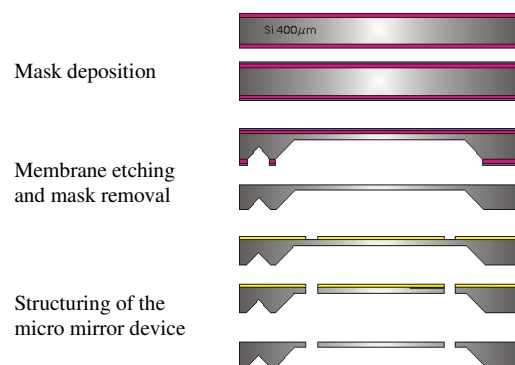
Fig. 2: Fabrication steps of the MMD

Laser micromachining

The silicon laser micro cutting was done by an ultra short pulsed laser with an UV wavelength. Ablation by laser radiation causes always the generation of debris. This contamination of the sample surface has to be avoided because clean surfaces are necessary for the optical used mirror areas and for possible subsequent wafer bonding processes. Having a mean free path of less than 200 μm, particles condensed on the surface of the sample around the cutting edge area. So contamination because of debris is a problem by laser micro cutting under ambient pressure. As solution the use of fine vacuum has proven to be an appropriate method to avoid particle deposition on the micro mirror and to reach a clean surface.

The trimming process combines laser treatment and frequency measurement as an integral technology (Fig. 3) and can be carry out in waver level.
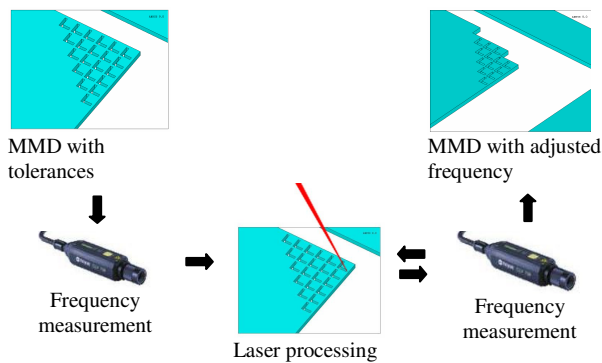
Fig. 3: Principle workflow of the laser trimming process

Measurements

To verify the simulation values all trimming elements were successively trimmed with subsequent frequency measuring. The results are shown in
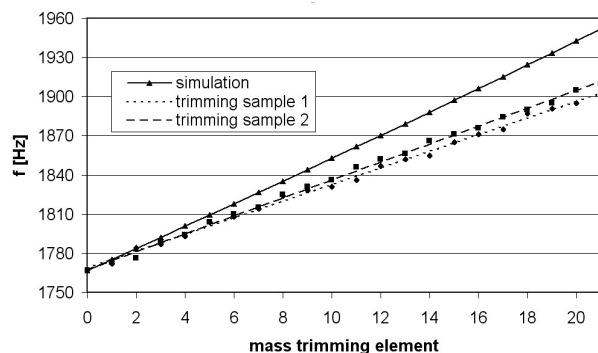
*Fig. 4: Frequency curve for the trimming of all **mass elements** compared to the simulation values*

Figure 4 and 5 for the trimming of mass and beam stiffness elements of a 1-dimensional mirror. The measured values are in good agreement with the simulated frequencies. Only a slight deviation is visible.
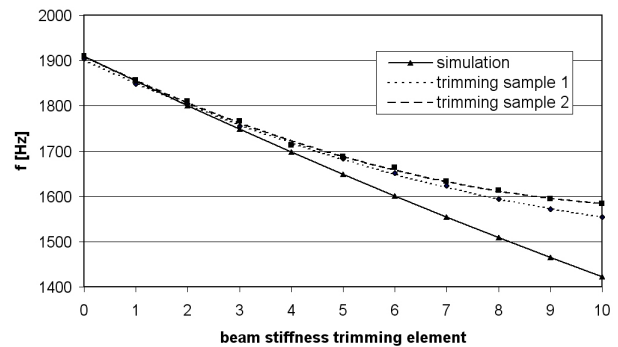
*Fig. 5: Frequency curve for the trimming of all **beam stiffness elements** compared to the simulation values*

Figure 6 shows light microscopy images of completely trimmed micro mirrors.
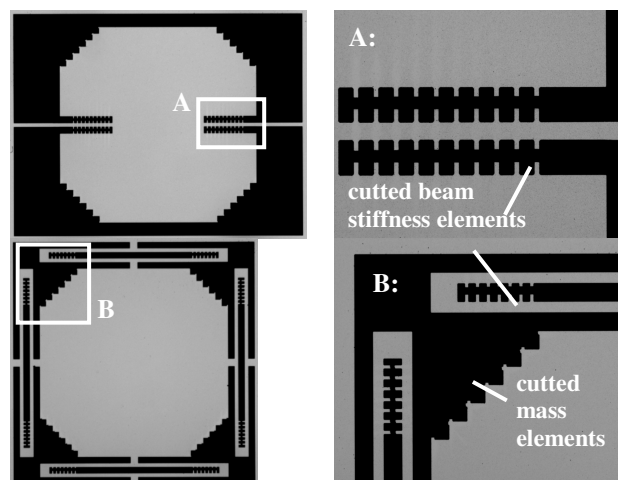
*Figure 6: Light microscope images of completely trimmed MMD's with enlarged views of the trimming elements. (above: 1D-mirror, below: 2D-mirror)*

References

[1] M.A. Abdelmoneum et al., "*Location-Dependent Frequency Tuning of vibrating micromechanical resonators via Laser trimming*", *Proc. of the IEEE Int. Frequency Control Symposium*, 23-27 Aug, 2004, pp. 272-279

[2] K. Weiss, M. Tupaj, "*SAW resonators frequency trimming by plasma etching*", *European Frequency Time Forum*, 5-7 March 1996, IEE Conference Publication No 418, pp. 155-158

[3] V.S. Aliev et al., "*Precision frequency trimming of SAW and STW resonators using Xe+ heavy ion bombardment*", *IEEE Transactions on Ultrasonics, Ferroelectrics and Frequency Control*, Vol. 41, No. 5, 1994

[4] S. Günther et al., „*Laser Trimming of a Silicon Tuning Fork Gyroscope*", *Proc. Eurosensors*, September 17-20, 2006, paper M2B-P15

MEMS Scanners for raster scanning laser projection

Christian Kaufmann[1], Steffen Kurth[3], Hendrik Specht[2], Ramon Hahn[1], Jan Mehner[3],
[1] Chemnitz Univ. of Techn., Faculty of Electrical Engineering and Information Technology, ZfM
[2] Chemnitz Univ. of Techn., Faculty of Electrical Engineering and Information Technology, MGT
[3] FhG-IZM Branchlab Chemnitz, Dep. MDI

1 Introduction

In recent years the field of display technologies has been underlain enormous changes. Classical technologies like the cathode ray tube have been replaced and new fields of application have been opened up by new technologies like LCD, DMD or LCOS. This trend will be continued in future. One important contributor will be the arising MEMS based Laser Display Technology (LDT) due to its advantages regarding picture quality, flexibility, potential for miniaturization and low cost. In this paper an experimental raster scanning laser display system will be presented which is capable of handling image data in XGA resolution from a standard DVI/VGA interface.

2 Scanners

Raster scanning of the intensity modulated laser beam is a very straight approach for laser projection with high resolution. It requires extremely fast scanning in one axis (fast axis) and time linear deflection of the beam in the perpendicular axis (slow axis) respectively. Consequently, two different single axis micro scanners are applied in the display reported in following.

2.1 Electrostatic fast axis scanner

In order to achieve a high diffraction limited resolution and a high scanning frequency, the approach followed here is based on a two degrees of freedom resonator. The scanner consists of a mechanically active part made of crystalline silicon and a glass bottom (Fig. 1). The circularly shaped mirror with 2.2 mm diameter is excited by a driving plate which is elastically connected to the mirror plate. The glass bottom with an opening in the region beneath the mirror and a part of the driving plate carries driving electrodes. Mirror and driving plate built basically a two degrees of freedom system where a magnitude amplification of 50 occurs at the resonant frequency of the second resonant mode which is used for operation. As a result, the relatively low deflection of driving

plate in comparison to the mirror makes a very small electrode gap size possible.
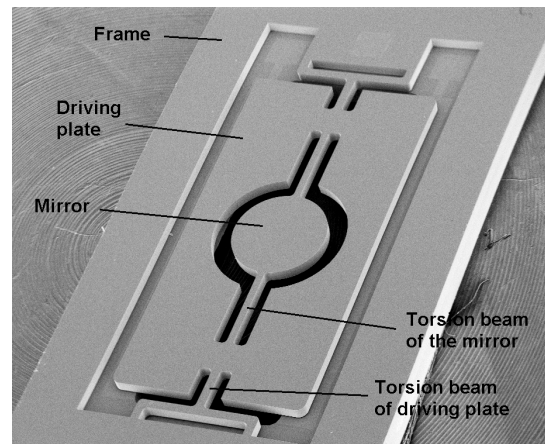
Fig. 1: SEM image of the fast axis scanner

It leads to a high electrostatic force and low influence of damping caused by the air flow in the electrode gap on the Q-factor of the used resonant mode. Applying up to 370 dc bias voltage and 190 volt ac, the mirror is excited to resonate at 24 kHz with $\pm 5°$ mechanical deflection. A mechanical Q-value of 5,500 ensures extremely low scan jitter and makes it easy to synchronize the clock of the image processing electronics.

2.2 Electromagnetic scanner for slow axis scanning

Since the incoming laser beam is already scanned in the fast axis, the slow axis scanner has to provide 11mm x 2.5mm mirror size (Fig. 2). One of the main criterions is to achieve large scan angle and shortest retrace time of the saw tooth shaped motion of this scanner. The optically active area is surrounded by a planar coil whose magnetic field interacts with the field of two permanent magnets where the actuator is mounted in-between. The electro dynamic working principle offers the possibility to apply driving current multi times over the normal value during retrace time. Due to the fact that a high resonant frequency of the actuator is

advantageous, special care was taken to minimize the moment of inertia. This results in a small thickness of the structure. A relaxation trench on each long side of the optical active area decouples it from the planar coil regarding to thermal induced stress. A mechanical deflection of $\pm 5°$ is achieved applying 7.5 volt. The resonant frequency of tilt mode is 820 Hz.
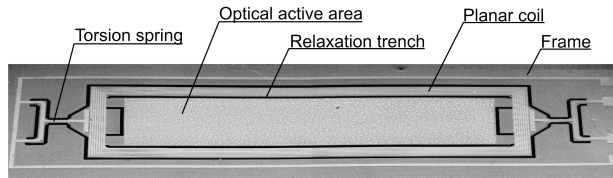
Fig. 2: SEM of slow axis scanner (silicon part only)

3 Display system

The scanners are arranged in a compact optical design, as shown in Fig. 3, which was optimized in terms of minimum distortions of the resulting image and maximum optical efficiency.
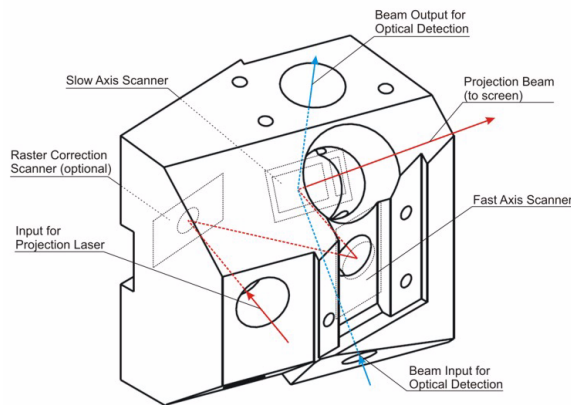
Fig. 3: Schematic drawing of scan engine

All course of beam parameters are molded into a scanner carrier making optical adjustment work almost unnecessary during assembly. The optical engine also contains a directly modulated 635 nm projection laser which can be easily replaced by a RGB laser module in future to make the system capable of projecting full color images.

To run the optical engine, special driving circuitry including a pixel stream converter is required. A schematic of the signal flow is shown in Fig. 4. The resonant driven fast axis scanner determines the line rate (and the related pixel clock) of the system and – together with a phase locked loop – it serves as a time base for the output side of the pixel stream converter. The

input side of the latter one consists of a DVI/VGA interface which comes with its own time regime. Thus the architecture of the pixel stream converter, which has been implemented on a FPGA, is designed to allow full asynchronous operation of both input and output side. Furthermore it performs a real time pixel sequence inversion of every second line to make bidirectional line scanning possible.
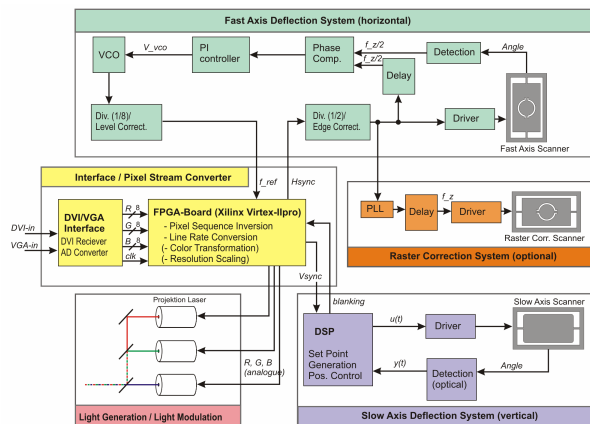
Fig. 4: Signal flow diagram
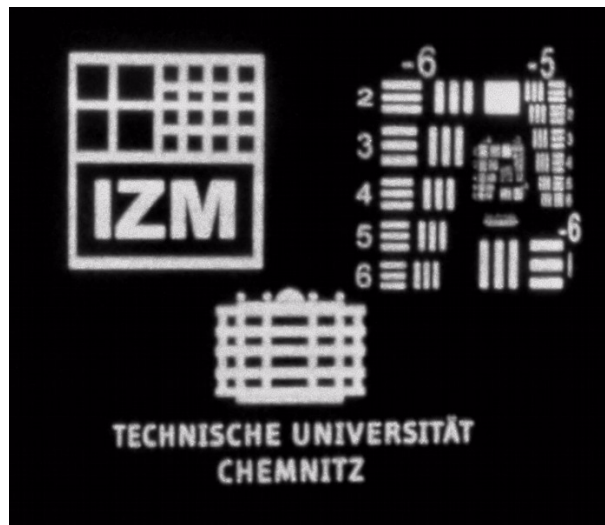
Fig. 5: Example of test image

The picture quality achieved by the current monochrome version of the laser display system exceeds the requirements of typical PDA applications (Fig. 5). By replacing the laser light source in future, a full color version will achieve picture quality sufficient for mobile entertainment.

X-ray collimators of microstructured silicon

Frühauf, Joachim[1]; Gärtner, Eva[2]; Straube, Holger[1]; Zschenderlein, Uwe[1]

[1]TU Chemnitz, Faculty for Electrical Engineering and Information Technology, Workgroup Materials in Electrical Engineering and Electronics; [2]SiMETRICS GmbH, Limbach-Oberfrohna

1 Introduction

Soller collimators are important elements in X-ray diffraction systems to filter an almost parallel beam. Since the energy dispersive technique (ED-XRD) needs no expensive and space-consuming goniometer device, this method in particular provides the possibility of building small and cost-saving XRD-systems. In the course of further miniaturisation, small and microstructured collimators are requested [1]. The silicon microtechnique offers a wide range of high developed integrated processes to achieve such a microstructure. The photolithography in combination with the wet etching of silicon ensures the high accuracy needed. In spite of its low absorption coefficient but due to its low thermal coefficient of expansion, silicon is suited for this application.

2 Design and technology

2.1 Principle

A Soller collimator basically consists of a series of high absorbing membranes, that are layered parallel with a defined air slit between them. The principle of the collimation is shown in Fig 1. To filter the beam within two planes, a second collimator is needed, which is twisted by 90° to the first one in beam direction.
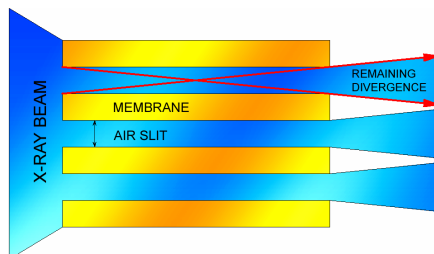
Fig 1: Schematic principle of a Soller collimator

The remaining beam divergence depends on the ratio of slit width and membrane length. Thus, the geometry must be reduced congruently to preserve its divergence properties. In preferably compact collimators both, membrane thickness and slit width, have to be microstructured then.

2.2 Requirements and design

The Soller collimator should be used in ED-XRD devices. It ought to collimate X-rays up to 40 keV on the primary side. The remaining divergence should be less than 0.6°, considering a ratio of slit width and membrane length of 1:100. Therefore, with a given maximum collimator length of 10 mm, the maximum slit width is limited to 100 µm. To ensure a reasonable primary beam intensity, the membrane shouldn't be thicker than 100 µm. That requires a Au-metallisation (2 µm) to accomplish a high X-ray-absorbing membrane. The beam to collimate has a maximum diameter of 4 mm.

The structured chips must be stacked up to a complete Soller collimator, which will then be fixed. It is subsequently ready for assembling into an ED-XRD device.
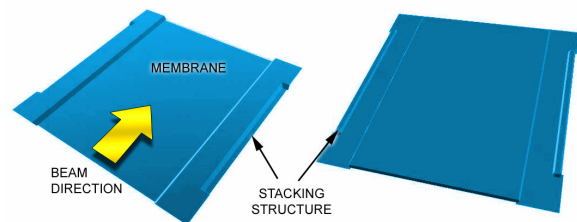
Fig 2: Chip (left: front; right: back) with membrane structure and stacking structure simulated by SIMODE.

Fig 3:90°-twisted aligned chips to prevent a preferred deflection of the wafer.

A front mask and a back mask were designed, containing several windows for the membrane structure and the stacking structure (Fig 2). Additional windows were made for perforations,

avoiding sawing into the membrane during the dicing process. The chip size was selected with 10 x 10 mm. To prevent a preferred deflection direction of the wafer, the chips masks were twisted by 90° to each other (Fig 3).

2.2 Preparing steps

The preparation is based on 300 µm-4"-wafers (Si, p-type, {100}, 0.039 Ωcm). It were 52 Chips placed on one such wafer. The structuring steps are shown in Fig 4. Succeeding the photo-lithographic process, the front side and later both sides are wet etched with KOH.
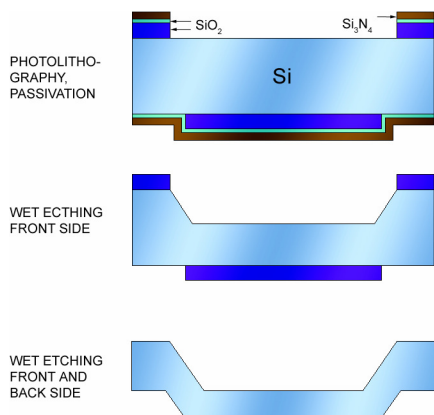
Fig 4: Schematic structuring process (extremely simplified, without stacking structure)

Afterwards the wafer is thermally oxidised followed by metallising with 20 nm Ti (adhesive layer) and 2 µm Au (absorber layer). In advance of the sawing process, a resist has to be coated to protect the sensitive surface from fouling with and penetrating of sawdust.

2.3 Assembling

After the dicing process and the removal of the resist, 22 single chips are stacked up to a collimator (Fig 5) under a stereo microscope.
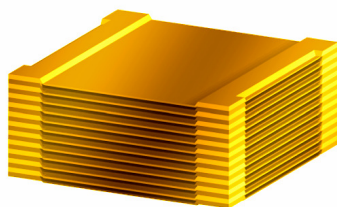
Fig 5: Schematic Soller collimator consisting of 22 Chips (alternating bright and dark) .

The stack gets a stable top and bottom chip. It's fixed afterwards by gluing a mounting chip on the left and right side (Fig 6). This stack in Fig 6 is now stable and save for handling. Usually it's assembled now into a special carrier which is then installed into the ED-XRD device.
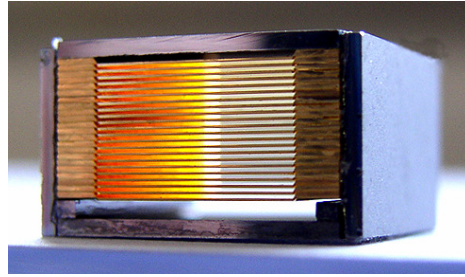

Fig 6: Fixed stack (22 Chips) with a stable top and bottom chip as well as a mounting chip left and right

3 Results

3.1 Characterisation and Conclusion

The single chips as well as the complete stack were optical measured. The warping and the notching of the membrane lies below four microns. The membrane thickness reaches values from 100 up to 109 µm and the width of the air slit lies between 101 and 107 µm. The design of the stacking structure allows horizontal movement between two stacked chips of maximum 30 µm. Therefore it can be found lateral shearing in the collimator stack. This is not critical since it has no influence on the parallel membrane layering. As the most critical process can be seen the sawing, that results often in little bulging of Au at the chip's corners. This can have an influence on the stacking distance between the chips causing nonparallel membrane layering.

After their successful manufacturing the first Soller-collimators will be tested now in an ED-XRD-System gaining the effective collimation characteristics.

4 Acknowledgements

5 References

[1] ARNHOLD, R.; KÄMPFE, B.: Application of Energy-Dispersive X-Ray Diffraction for Mobile Analysis. Proc.EDXRS 2002, 16.-21. June 2002, Berlin, Germany, pp 8

[2] STAUDE, M.: Student research project: "Entwurf eines Spaltsystems zur Parallelisierung von Röntgenstrahlung". TU Chemnitz, Juli 2006

MICROFLUIDIC BUBBLE ACTUATORS BASED ON HYDROGELS

Joerg Nestler[1], Karla Hiller[1], Thomas Otto[2] and Thomas Gessner[1,2]
[1]TU Chemnitz, Center for Microtechnologies (ZfM), Chemnitz, Germany
[2] Fraunhofer IZM Chemnitz, Dept. Multi Device Integration, Chemnitz, Germany

1 Introduction

Dosing and pumping small amounts of liquids is essential for the proper functionality of many Lab-on-Chip applications. Thus, fully integrated pumps and valves at an affordable price are desired to control the flow of a sample liquid, buffers or reference solutions. The electrochemical generation of gas bubbles by electrolysis offers a great opportunity for cheap actuators with large deflection, high pressure and precise control of dosed volumes. Such bubble actuators have already been successfully demonstrated for microfluidics. A possible working principle is shown in Fig.1 However, the integration of a liquid (e.g. water) can be critical for mass fabrication and may also cause problems concerning long-term stability.

A hydrogel based on poly (acylic acid) sodium salt (PAAS) was therefore investigated for its applicability as electrolyte, which combines the electrolytic and gas generating properties of water based electrolytes with a good processibility by screen printing or stencil printing. It is available at very low cost and non-toxic.
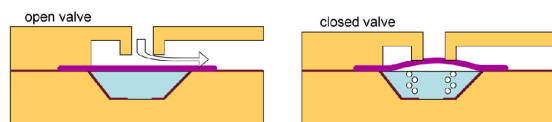
Fig. 1: Schematic of a bubble actuated valve based on electrolysis. A chamber, which contains a water-based electrolyte, is contacted by two electrodes and covered by a deflectable membrane. In this work, a hydrogel is used as electrolyte (instead of a liquid).

2 Theory

The electrolysis of water is the dissociation of water molecules into oxygen and hydrogen gas by means of an electric current. The reaction is given by:

Anode: $2H_2O \rightarrow 4H^+ + 4e^- + O_2$ (gas)

Cathode: $2H_2O + 2e^- \rightarrow 2OH^- + H_2$ (gas)
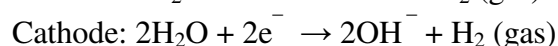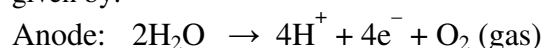
Using pure (de-ionized) water, this reaction is very slow. Increasing the ion content in the water for a given voltage increases the conductivity and thus the speed of the reaction. Crosslinked PAAS is a so-called super absorbing polymer which is able to dramatically swell in water. The swollen state is referred to as a hydrogel, which mainly consists of up to 99 wt% of water, but has a very high viscosity. When PAAS is brought in contact with water, the weakly bonded sodium is split off, leaving negatively charged polymer chains and movable sodium ions:
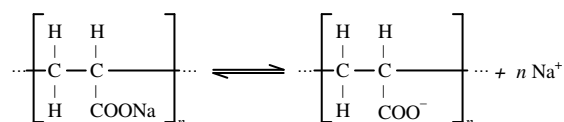
Using this effect, PAAS not only "thickens" the water, but also increases its ion content, thus leading to a much faster electrolytic reaction at moderate voltages.

3 Experimental

Silicon and COC were used as substrate materials for the actuators. Gold was sputtered and structured to form electrodes. Chambers around the electrodes where subsequently formed by SU8 lithography, leading to cavity heights between 80µm and 360µm.

Gels with three different PAAS concentrations (0.7wt%, 0.42wt% and 0.35wt%) were prepared using crosslinked poly (acrylic acid) and deionised water. The first of these mixtures has rubber-gel like properties, whereas the last one is still more "liquid-like".
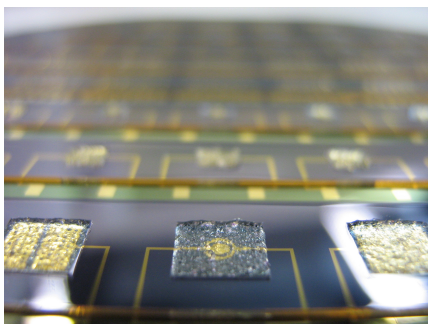
Fig. 2: Cavities filled with hydrogel using stencil printing as a batch process on a 4" substrate.

The SU8-chambers were filled with the PAAS gel - either manually or by stencil printing on wafer scale (Fig. 2) - and sealed with a tape membrane of a thickness of 70µm (Fig. 3)
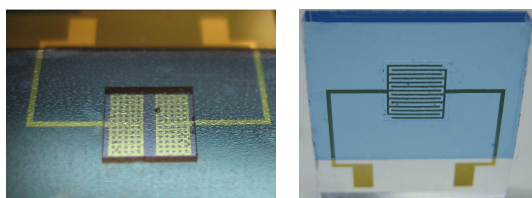
Fig.3: Membrane covered and gel filled actuators on silicon (left) and COC (right)

4 Results

The membrane deformation and deflection was measured by a stripe projection system. The dynamic properties such as the speed of deflection were measured by an auto-focus profilometer both for different electrode geometries and gel compositions.

The actuators with chamber areas of 3x3mm², an interdigital electrode configuration ("int") and a PAAS concentration of 0.7wt% reached a deflection of more than 300µm within a time of about 12s at a voltage of 5V.

Different electrode configurations were investigated (Fig. 4). As expected, the interdigital electrodes show the best performance due to the much lower resulting resistance of the electrolytic cell, which consequently leads to a higher current and faster gas generation for a fixed voltage.

Comparing the results for the different electrode designs with the influence of PAAS concentration (Fig. 4), it can be found that the performance of the actuator cell is mainly improved by a proper electrode design rather than a certain PAAS concentration. However,

also the higher conductivity at higher PAAS concentrations due to the larger amount of sodium ions can be clearly seen in Fig. 4.
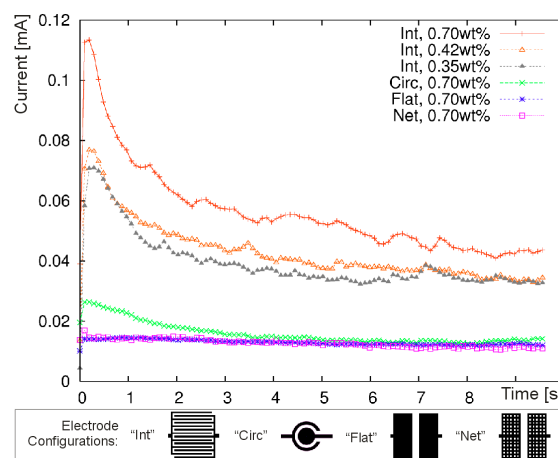
Fig. 4: Current through a gel-filled actuator cells with an area of (3x3) mm², a chamber height of about 360µm and a voltage of 5V for different PAAS concentrations in wt% and electrode configurations (bottom)

5 Conclusions

A PAAS based hydrogel has been successfully proved as a electrolytic material for a micro bubble actuator. It offers the potential of simple integration while increasing the ion content of the electrolytic solution at the same time. Next steps will focus on tailoring the actuator for microfluidic actuation in fully integrated point-of-care devices. This will include transferation of the technology to polymeric materials and the investigation of using the generated gas directly for driving of fluids. This will allow to drive fluids through microchannels over a very long distance with low power consumption and without heat generation.

6 Acknowledgements

7 References

[1] Nestler, J. et al: *Microfluidic Actuators based on hydrogels*, Proc. MicroTAS 2006 Conference, pp 757ff, Tokyo, Japan (2006)

A new technology platform for fully integrated polymer based micro optical fluidic systems

J. Nestler[a], K. Hiller[a], T. Gessner[a], L. Buergi[b], J. Soechtig[b], R. Stanley[b], G. Voirin[b] , S. Bigot[c],
J. Gavillet[d], S. Getin[d], B. Fillon[d], M. Ehrat[e], A. Lieb[e], M.-C. Beckers [f], D. Dresse [g]

[a] Center for Microtechnologies, Chemnitz University of Technology, Chemnitz, Germany
[b] CSEM Centre Suisse d'Electronique et de Microtechnique SA, Zurich, Switzerland
[c] Cardiff University, Cardiff, United Kingdom
[d] Comissariat à l'énergie atomique (CEA), Grenoble, France
[e] Zeptosens – a division of Bayer (Schweiz) AG, Witterswil, Switzerland
[f] Eurogentec S.A.,Seraing, Belgium
[g] Centre Hospitalier Regional de la Citadelle, Liège, Belgium

1 Introduction

The development of lab-on-chip (LoC) devices for bio analytical applications has been tremendously increasing during the past decade. Most of these devices are being fabricated by use of silicon or glass because processes for these materials are well known and surface properties of these materials are easy to match the requirements of biotechnology. However, since one core application of LoC devices are point of care applications, a strong demand on low-cost solutions for disposable LoCs has developed.

The use of expensive materials inhibit a high level of integration for point-of-care devices. Thus, most of the functionality is currently transferred to the "reader" – the controlling unit – instead of being integrated into the chip. Since the micro-macro interfaces between the chip and the reader are always difficult to handle, reader costs increase and sensitivity decreases. Thus, low-cost approaches for Lab-on-Chips have to be investigated which allow a high level of integration at an affordable price. Polymer materials show a high potential for cost efficient production of Lab-on-Chips not only as substrate materials but also as active components such as sensors and actuators.

To reach this goal, the development of a polymer based technology platform has been started within the European project "SEMOFS", which aims to integrate active optical sensors as well as micro fluidic actuators in a polymer cartridge. [1] Fig. 1 shows the different aspects of the platform. Miniaturized Surface Plasmon Resonance (SPR) has been chosen as optical detection method for the label-free detection of proteins. As active optical components, the integration of polymer light-emitting diodes (PLEDs) and polymer photodiodes (PPDs) for such a sensor application is investigated. Polymer micro fluidic actuators will be part of the system as well as a special surface modification to avoid protein adsorption on the walls of the fluidic channels.
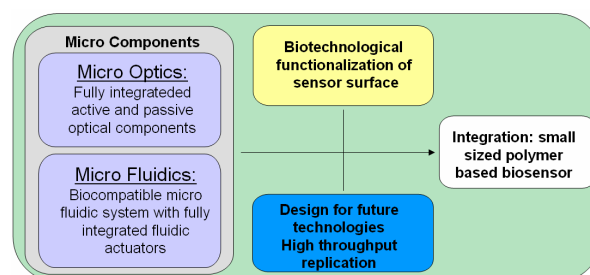
Fig. 1: Different aspects of the SEMOFS biosensor platform

2 Micro optical concept

The ***surface plasmon resonance (SPR) principle*** uses biochemical interactions at the sensor surface, which are monitored by observing the resonant behaviour of surface waves at a thin metal film (usually Au). This resonant mode will couple with the evanescent wave in the waveguide. When molecules are bound on the sensitive surface on top of the metal layer, the refractive index is slightly changed. This leads to a shift of the absorption peak with respect to wavelength (see Fig. 2).

Polymer Light Emitting Diodes (PLED) and ***polymer photodiodes*** (PPD) are potentially very attractive light sources and detectors for (disposable) lab-on-chip applications. The devices are ultra-flat (< 500 nm) and compatible with bendable substrates.
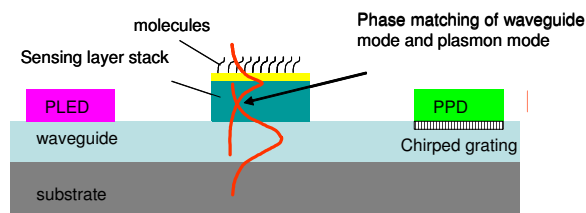
Fig. 2: Illustration of the surface plasmon resonance principle and the integrated optical system

PLEDs and PPDs can be produced by purely additive print processes at room-temperature and can thus be monolithically integrated into almost any system.

3 Microfluidics concept

The *passive microfluidics system* encloses hydrophilic channels for inlet and sample volume definition, hydrophobic channel segments (passive valve), the channel system around the sensitive areas, inlet ports and waste compartments. Furthermore, to avoid the usage of external interfaces for micro fluidics except of the sample inlets/outlet ports, *integrated micro fluidic actuators for valves and pumps* are desired for PoC devices. The integration of these actuators has to be realized within the technological platform and therefore be based on polymers. At least two polymer layers with integrated actuator elements will be bonded together, hereby the channels must be sealed. Different actuation principles have been evaluated. The actuators should not influence or depend on the fluid properties and should be able to displace comparably large fluid volumes. Especially for the targeted protein based application, high temperatures should be avoided.

The *electrochemical generation of a gas* offers a good possibility to generate pressures and thus large displacements in microfluidic systems. However, if the gas is – for example - generated by electrolysis of a liquid, the issue of "how to integrate an actuation fluid like water" in a large scale production had not been solved yet. Thus, in SEMOFS a special hydrogel is currently being investigated as electrolyte, which combines a low material price, intrinsic electrolytic properties as well as the possibility to be integrated by large scale fabrication methods like screen printing or stencil printing. First membrane covered actuator prototypes have been fabricated and characterized. [2]

4 Surface functionalisation

Both the surface of the microfluidic channels and the sensing surface must exhibit special properties with regard to the fluids and bio molecules. As for the sensing area, the surface must be hydrophilic, and the marker molecules should bind (immobilise). This is normally reached with oxide materials and has been successfully proven with HfO_2 and SiO_2 layers, tested on glass substrates. In the microfluidic channels, however, both *hydrophilic and hydrophobic* regions are desirable, with no binding or sticking should occur. Experiments were performed to test the non-fouling properties of conventional plasma deposited layers (SiOx, SiOC, Teflon-like). Binding occurred both on the hydrophilic and hydrophobic surfaces, thus these layers are not suitable in the microfluidic channels. However, by changing the chemistry, finally *non-fouling surfaces* could be deposited, and still the surface behaviour can be tuned from hydrophilic to hydrophobic. As a next step, such layers will be tested together with the micromachined channels.

5 Acknowledgements

6 References

[1] Nestler, J. et al: *A new technology platform for fully integrated polymer based microoptical fluidic systems,* Proc. 4M2006 – 2nd Conference on Multi Material Micro Manufacture, Grenoble, France (2006)

[2] Nestler, J. et al: µTAS: *Microfluidic Bubble Actuators based on hydrogels*, Proc. MicroTAS 2006 Conference, pp 757ff, Tokyo, Japan (2006)

5 Cooperations with industry and universities

Partnerships with the following institutes and companies were continued and / or established in 2006:

- Advanced Micro Devices (AMD), Sunnyvale & Austin, USA and Dresden, Germany
- Aktiv Sensor GmbH, Stahnsdorf, Germany
- Alpha Microelectronics GmbH, Frankfurt (Oder), Germany
- AMTEC GmbH, Chemnitz, Germany
- Anfatec Instruments, Oelsnitz, Germany
- Applied Materials, Santa Clara, USA and Dresden, Germany
- ALSTOM Transport Tarbes, France
- ASMEC Advanced Surface Mechanics GmbH, Radeberg, Germany
- Atmel Design Center, Dresden, Germany
- AUDI AG, Ingolstadt, Germany
- BASF AG, Ludwigshafen, Germany
- BMW AG Munich, Germany
- Robert Bosch GmbH, Reutlingen & Stuttgart, Germany
- Cabot Microelectronics Europe
- CAD-FEM GmbH Grafing, Germany
- CiS Institut für Mikrosensorik gGmbH, Erfurt, Germany
- Colour Control Farbmeßtechnik GmbH, Chemnitz, Germany
- DaimlerCrysler AG, Research Lab Ulm & Sindelfingen, Germany
- Danfoss Silicon Power, Schleswig, Germany
- Digital Instruments – Veeco Instruments, Mannheim, Germany
- DILAS Diodenlaser GmbH
- EADS Deutschland GmbH, Corp. Res. Ctr. Germany, Dept. Microsystems, München, Germany
- Endress und Hauser Conducta GmbH & Co. KG, Germany
- Eupec GmbH Warstein, Germany
- FACRI , Research Institute, Xi´an, China
- Fahrzeugelektrik Pirna GmbH, Pirna, Germany
- FHR Anlagenbau GmbH, Ottendorf-Okrilla, Germany
- First Sensor Technology GmbH, Berlin, Germany
- FLEXIVA automation & robotics, Amtsberg, Germany
- Forschungszentrum Rossendorf, Germany
- Freiberger Compound Materials GmbH, Freiberg:
- Fujitsu Microelectronic GmbH, Dreieich-Buchschlag, Germany
- GEMAC mbH Chemnitz, Germany
- GF Messtechnik Teltow, Germany
- Gesellschaft für Prozeßrechnerprogrammierung mbH (GPP) Chemnitz, Germany
- GHF IWM Halle
- Gyrooptics Company Ltd., St. Petersburg, Russia
- Heinrich-Hertz-Institut Berlin, Germany
- Hitachi Ltd., Japan
- Institut für Festkörper- und Werkstofforschung e.V. IFW Dresden, Germany
- IMEC, Leuven, Belgium
- Infineon Technologies AG, Munich and Dresden, Germany
- InfraTec GmbH, Dresden
- ITIM International Training Center for Material Science, Vietnam
- IXYS Semiconductor GmbH, Lampertheim, Germany
- Jenoptik-LDT GmbH, Gera , Germany
- Kyocera Fineceramics GmbH

- L.A.A.S-C.N.R.S Toulouse, Prof. Dr. D. Esteve, France
- LETI, Grenoble, France
- LG Thermo Technologies GmbH
- Lionix, Enschede, Netherlands
- LITEF GmbH, Freiburg, Germany
- Lucent Technologies, Nürnberg, Germany
- Massachusetts Institute of Technology, Cambridge / Boston, Mass., USA
- Max-Planck-Institut (MPI) für Mikrostrukturphysik Halle, Germany
- Mechanical Engineering Laboratory AIST, MITI, Dr. Mitsuro Hattori and Chisato Tsutsumi, Tsukuba, Ibaraki, Japan
- memsfab GmbH, Chemnitz, Germany
- Merck KGaA, Darmstadt, Germany
- Mesa Research Institute, Prof. J. Fluitman, Twente, The Netherlands
- Microtech GmbH, Gefell, Germany
- Mitsui Engineering and Shipbuilding Co. Ltd., Japan
- Motorola, Phoenix, Arizona ,USA / Munich, Germany
- MPA NRW Materialprüfungsamt Nordrhein-Westfalen, Germany
- Nex Systems, Wilmington, MA. , USA and Berlin, Germany
- NICO Pyrotechnik, Trittau, Germany
- NXP (founded by Philips), Corporate Research, Eindhoven (NL) & NXP Crolles (F)
- OEC GmbH, Germany
- Panasonic Plasma Display Dev. Lab., Inc., Highland, New York, USA
- Physikalisch-Technische Bundesanstalt Braunschweig (PTB), Germany
- Philips Applied Technologies, Eindhoven, The Netherlands
- PLASMACO Inc. Highland, New York, USA
- Preh GmbH, Bad Neustadt, Germany
- Qimonda AG, Dresden, Germany
- Raytek GmbH Berlin, Germany
- Ricoh Company, Ltd., Yokohama, Japan
- Rohm and Haas Electronic Materials, Marlborough, USA
- Roth & Rau Oberflächentechnik GmbH, Wüstenbrand, Germany
- RWE Schott Solar GmbH, Alzenau, Germany
- Sarnoff Europe, Aalter, Belgium
- Schenker Deutschland AG, Dresden, Germany
- Schott Mainz & Schott Glas Landshut, Germany
- Sentech Instruments GmbH, Berlin, Germany
- SICK AG, Waldkirch & Ottendorf-Okrilla, Germany
- SF Automotive GmbH, Freiberg, Germany
- Siegert TFT GmbH, Hermsdorf, Germany
- Siemens A&D ATS2 Nürnberg und AT Regensburg, Germany
- Siemens VDO Automotive AG, Limbach-Oberfrohna
- SiMetricS Silicon Metrological Components and Standards GmbH, Limbach-Oberfrohna
- Institut für Solarenergieforschung Hameln-Emmerthal, Germany
- Sony Corp., Semiconductor Business Unit, Japan
- ST Microelectronics, Crolles, France
- Suss Microtec AG Vaihingen, Munich and Sacka, Germany
- Dr. Teschauer AG, Chemnitz, Germany
- Thales-Avionics, Valence and Orsay, France
- TRW Airbag Systems GmbH & Co. KG, Aschau/Inn, Germany
- X-Fab Gesellschaft zur Fertigung von Wafern mbH, Erfurt, Germany
- ZMD Dresden, Germany
- 3D-Micromac AG, Chemnitz, Germany

Universities:

- Johannes Kepler Universität Linz, Austria
- Atominstitut Universität Wien, Austria
- Chongqing University, Chongqing, China
- Fudan University, Shanghai, China
- Shanghai Jiao Tong University, China
- TSINGHUA University, Beijing, China
- Xiamen University, Xiamen, China
- University of West Bohemia, Pilsen , Czech Republic
- Technische Universität Braunschweig, Germany
- Universität Bremen, Germany
- HTW Mittweida, Laserapplikationszentrum, Germany
- TU Dresden, Germany
- TU Ilmenau, Germany
- Universität Erlangen, Germany
- Universität Essen, Institut für anorganische Chemie, Germany
- Universität Hannover, Germany
- Westsächsische Hochschule Zwickau (FH), Zwickau, Germany
- TU Budapest, Hungary
- University of Tokyo, Res. Ctr. for Adv. Science & Technology (RCAST), Japan
- Tohoku University, Sendai, Japan
- University of Delft, Netherlands
- University of Twente – MESA, Netherlands
- Warsaw University of Technology (WUT), Warsaw, Poland
- Nowosibirsk State University, Russia
- North Caucasus State Technical University, Stavropol, Russia
- Technological University Singapore, Singapore
- Royal Institute of Technology, Stockholm, Sweden
- University of Hertfordshire, UK
- Cardiff University, Cardiff, UK
- State University of New York at Binghamton, USA
- Portland State University, Portland, Oregon, USA
- Rensselaer Polytechnic Institute (RPI), Troy, N.Y., USA
- University of Nevada, Reno, USA
- University of California at Berkeley, Berkeley Sensor and Actuator Center, USA
- Case Western Reserve University, Cleveland, Ohio, USA
- University of Colorado at Boulder, USA
- University of Delaware, Newark, USA
- Hanoi University of Technology, Vietnam

6 Equipment and service offer

The ZfM facilities include 1000m² of clean rooms (about 30% of them class 10 to 100). Modern equipments were installed for processing of 100 mm and 150 mm wafers as well as design and testing laboratories providing the basis for the following processes, partly in cooperation with the Fraunhofer Institute IZM, branchlab Chemnitz:

- Design (Workstations)
- Mask fabrication 3" ... 7" / Electron beam lithography / Proximity and contact double-side
  lithography
- High temperature processes: Diffusion / Thermal oxidation / Annealing / RTP

- Etching (dry: Plasma- and RIE-mode & wet: isotropic / anisotropic → equipment: Alcatel MCM, SECON XPL 251, STS Multiplex ICP-ASE, Metal Etch DPS Centura & ARIAS silicon wet etching box for etchants based on KOH and TMAH)
- Chemical vapor deposition MOCVD (Precision 5000 [Cu, WN, TiN])
- Chemical vapor deposition PECVD (Precision 5000 [SiO_2, Si_3N_4, CF-Polymer, SiCH, SiCOH, SiCNH])
- Physical vapor deposition PVD (FHR 150x4, CLC 9000)
- Chemical mechanical polishing CMP
- Wafer bonding: silicon direct, anodic, eutectic, glass frit
- Testing (SEM, AFM, electrical, mechanical …)

The ZfM provides the following services :

    R & D

(e.g. Si processes, technology, development of sensors and actuators, metallization)
- Thermal oxidation of silicon wafers
- PVD (Cr, Au, Ag, Ti, TiN, Ta, Cu , Pt, Co, Al, W, TiW, $AlSi_x$,CrNi, Pyrex)
- CVD: PECVD / LPCVD (600° C ... 900° C)
  (SiO_2 , Si_3N_4 , Polysilicon, $Si_xO_yN_z$, Cu-MOCVD, TiN-MOCVD, SiCOH, SiCH)
- PECVD (diamond-like Carbon films, a-C:H)
- Dry etching (Si, SiO_2 , Si_3N_4 , Polysilicon, Silicides, Al, refr. metals, TiN, Cr, DLC, lowk dielectrics)
- Wet etching (SiO_2 , Si_3N_4 , Si, Polysilicon, Al, Cr, Au, Pt, Cu, Ti, W)
- Wafer lithography / Electron beam lithography / Mask fabrication (3" ...7" Cr mask)
- Design & simulation (technology, process....)
  Software: ANSYS, SIMODE, PHOENICS, SIMBAD, EVOLVE ,
          Etch mask design tool EMADE
- Parametric testing: Waferprober, HP Testsystem
- Design of low power and low noise, analogue-mixed signal integrated circuits
- Design of integrated high-voltage circuits
- Characterization of analogue-mixed signal circuits up to 500 MHz
- Characterization and modelling of devices from low-voltage and high-voltage micro technologies

and in **analytical fields** such as
- Scanning electron microscopy SEM / EDX
- Atomic force microscopy AFM (D 3000)
- Variable angle spectroscopic ellipsometry (Sentech SE-850, UV-VIS-NIR)
- Laser profilometry (UBM, TENCOR FLX-2900)
- Surface profilometer (TENCOR alpha step 200, Dektak 3)
- US-Microscope
- Zug-/Druckprüfmaschine Zwick 4660 universal
- Perkin-Elmer DMA 7e dynamic mechanical analyser
- Micromechanical testing instrument (Sartorius and PI)
- Lifetime scanner SEMILAB WT-85

In cooperation with the Fraunhofer Institute IZM, branchlab Chemnitz:

- STS „Multiplex ICP" etch tool for deep silicon etching
- Wafer bonding (silicon fusion bonding, anodic bonding, eutectic bonding, Seal-glass-bonding, adhesive bonding)
- CMP AMAT & OnTrak-cleaner (Copper, Silicon, SiO_2)
- Test measurements for MEMS

7 Education
7.1 Lectures

Electronic Devices and Circuits
Elektronische Bauelemente und Schaltungen
Lecturer: Prof. Dr. G. Ebest

Electrical Engineering / Electronics
Elektronik
Lecturer: Prof. Dr. C. Radehaus

Design Technology and Production Engineering
Konstruktions- und Fertigungstechnik
Lecturer: Prof. Dr. W. Dötzel

Materials Science in Electrical Engineering
Werkstoffe der Elektrotechnik / Elektronik
Lecturer: Prof. Dr. J. Frühauf

Fundamentals of Electronics
Grundlagen der Elektronik
Lecturer: Prof. Dr. G. Ebest

Electronic Devices
Elektronische Bauelemente
Lecturer: Prof. Dr. G. Ebest

Optoelectronics
Optoelektronik
Lecturer: Prof. Dr. C. Radehaus

Semiconductor Device Technology
Technologien der Mikroelektronik
Lecturer: Prof. Dr. T. Gessner, Dr. S. E. Schulz

Solid State Electronics and Photonics
Festkörperelektronik und - photonik
Lecturer: Prof. Dr. C. Radehaus

Electrophysics
Elektrophysik
Lecturers: Prof. Dr. C. Radehaus

Fundamentals, Analysis and Design of Integrated Circuits
Integrierte Schaltungstechnik
Lecturer: Prof. Dr. G. Ebest

Physical and Electrical IC Design
Physikalischer und elektrischer Entwurf
Lecturer: Prof. Dr. G. Ebest

Analog Integrated Circuit Design
Integrierte analoge Schaltungstechnik
Lecturer: Prof. Dr. G. Ebest

Microtechnologies / Materials and Technologies of Microsystems and Devices
Mikrotechnologien / Werkstoffe und Technologien der Mikrosystem- und Gerätetechnik
Lecturers: Prof. Dr. J. Frühauf, Prof. Dr. T. Gessner

Renewable Energy
Solare Energietechnik,
Lecturers: Prof. Dr. G. Ebest, Prof. Dr. U. Rindelhardt

Optocommunication
Optokommunikation
Lecturer: Prof. Dr. C. Radehaus

Electrooptics
Elektrooptische Bilderzeugung
Lecturer: Prof. Dr. C. Radehaus

Device Technology
Gerätekonstruktion
Lecturer: Prof. Dr. W. Dötzel

Microsystems
Mikrosystemtechnik
Lecturer: Prof. Dr. W. Dötzel

Reliability and Quality Assurance
Technische Zuverlässigkeit / Qualitätssicherung
Lecturer: Prof. Dr. W. Dötzel

Control Engineering (Microsystem Technology)
Prüftechnik (Mikrosystemtechnik)
Lecturers: Dr. J. Markert, Dr. S. Kurth

Technical Optics
Technische Optik
Lecturer: Dr. B. Küttner

Computer Aided Design
CAD
Lecturer: Dr. J. Mehner

Semiconductor Measurement Techniques
Halbleitermeßtechnik
Lecturers: Prof. Dr. C. Radehaus, Prof. Dr. M. Hietschold

Electrical Drives
Elektrische Antriebe / Gerätetechnische Antriebe
Lecturers: Prof. Dr. W. Hofmann, Dr. R. Kiehnscherf

Integrated Circuit Design
Schaltkreisentwurf
Lecturers: Prof. Dr. D. Müller, Prof. Dr. U. Heinkel

System Design
Systementwurf
Lecturer: Prof. Dr. U. Heinkel

EDA-Tools
EDA-Tools
Lecturer: Prof. Dr. U. Heinkel

Rapid Prototyping
Rapid Prototyping
Lecturer: Prof. Dr. U. Heinkel

Components and Architectures
Components and Architectures
Lecturer: Prof. Dr. G. Herrmann

Computertechnologie
Computer Technology
Lecturer: Prof. Dr. G. Herrmann

Mikroprozessorsysteme
Microprocessor Systems
Lecturer: Prof. Dr. G. Herrmann

Design and Calculation of Power Electronic Systems
Entwurf und Berechnung leistungselektronischer Systeme
Lecturer: Prof. Dr. J. Lutz

Industrial Electronics
Industrielle Elektronik
Lecturer: Prof. Dr. J. Lutz

Power Electronics
Leistungselektronik
Lecturer: Prof. Dr. J. Lutz

Semiconductor Devices in Power Electronics
Bauelemente der Leistungselektronik
Lecturer: Prof. Dr. J. Lutz

Process and Equipment simulation
Prozesssimulation / Equipmentmodellierung
Lecturers: Prof. Dr. T. Gessner, Dr. R. Streiter

Interconnect Processes and Technology – Back-end of Line (BEOL) Processing
Lecturers: Prof. Dr. T. Gessner, Dr. S. E. Schulz

7.2 Student exchange programmes

SOCRATES / ERASMUS
I.S.M.R.A. – Ecole Nationale Supérieure d`Ingénieurs Caen, France
Technical University of Cluj-Napoca, Romania
Katholieke Universiteit Leuven / IMEC, Belgium
Danmarks Tekniske Universitet, Lyngby, Denmark
Ecole des Mines de Nancy, Nancy, France
University of Oulu, Finland
Universite de Rennes I, France
Technical University of Lodz, Poland
Royal Institute of Technology Stockholm, Sweden
University of West Bohemia, Pilsen , Czech Republic
Hristo Gendov, University of Burgas, Bulgaria

ISAP Programme (DAAD)
University of Delaware, Newark, USA
University of Nevada, Reno, USA
Portland State University, Portland, USA
DAAD
University of Hanoi, Vietnam

7.3 Project reports/ Diploma theses / PhD

Project reports

Bach, D.:   Charakterisierung und Funktion von RFID-Systemen.

Bleul, K.:   Konstruktion, Auslegung und Aufbau eines Demonstratormoduls für das Lasertrimmen von Siliziummikroaktoren

Erler, C.:   Entwurf und Realisierung einer Rotationsvorrichtung für MAS Kernmagnetische Resonanz-Spektroskopie von biologischem Probenmaterial mit Mikroresonatoren

Grillberger, M.:   Ein neuronales Interface für mögliche in vivo Applikationen

Günnel, H.:   Entwicklung von Technologien für das chemisch-mechanische Polieren von dünnen Si- und SiO_2-Schichten

Herrmann, M.:   Meßtechnische Charakterisierung von Drehratensensoren in BDRIE-Technologie

Kirch, M.:   Lasermikrobearbeitung

Klier, T.:   Echtzeitfilterung von verrauschten Beschleunigungssignalen in der Inertialmesstechnik

Lasch, M.:   Neu- und Weiterentwicklung von mechanischen Komponenten für die industrielle Verarbeitung von sub-µm körnigem Pulver in einer Anlage zum Lasermikrosintern

Lichtenberger, M.:	Erweiterung des Steuerteiles einer Laserdiodensignalquelle
Noeth, N.:	Temperaturstabile Metallisierungssysteme für SOI-Drucksensoren
Päßler, F.:	Konzept und Funktionsnachweis eines mikrofluidischen Aktor-Prinzips in Polymersubstraten
Pügner, T.:	Machbarkeitsstudie zur Dickenbestimmung von Funktionselementen in der Volumenmikromechanik mittels transmittiertem Licht
Reichmann, B.:	Entwicklung und Test eines geregelten zweiachsigen Scannsystems
Sachse, M.:	Entwurf eines Beschleunigungssensorarrays basierend auf der AIM Technologie
Schade, R.:	Design of a Slit System for Collimation of X-Rays.
Schaufuß, J.	Elektrostatische Sonden zur mechanischen Anregung von MEMS auf Waferlevel
Schmidt, A.:	Modifikation und Entwicklung von CMP-Prozessen zur Herstellung von Cu-basierten Leitbahnsystemen für Bauelemente der künftigen Technologieniveaus
Schüller, M.:	Simulation von Sputterprozessen mit Kalypso und T2
Vogel, J.:	Entwicklung eines fluidischen Mikroaktors auf Basis von Mikrosphären
Wetzel, S.:	Bonding of Si-Chips on Bulk Silicon Bodies
Wittig, A.:	Strukturoptimierung eines Beschleunigungssensorarrays
Wolf, N.:	Entwicklung einer Abform- und Packagingtechnologie für Silikone
Wünsch, D.:	Design of a Silicon Spring System for Generation or Calibration of the Force in Instruments of Hardness Testing.
Ziegler, P.:	Automatisierte Funktionskontrolle von kapazitiven Inertialsensoren auf Waferebene

Diploma works

Ahner, N.:	Entwicklung eines gap-fill Prozesses für die Applikation von spin-coating Materialien Advisors: Dr. S. Frühauf, Dr. S.E.Schulz
Carstens, J.	Implementierung eines Testmaskendesigns für die Prozessentwicklung bei der Maskenherstellung Advisors: Dr. F. Schurack, Dr. A. Bertz
Erler, C.:	Theoretische Untersuchungen zur Kraftwirkung elektrischer Wechselfelder auf polarisierbare Partikel und Nachweis der Kraftwirkung mit dem Rasterkraftmikroskop Advisors: Prof. W. Dötzel, Dr. Gastrock iba Heiligenstadt
Evangelinou, S.:	Design of a Silicon Spring System for Guiding of the Indenter in Instruments of Hardness Testing Advisor: Prof. J. Frühauf

Golz, C.:	Evaluierung von ultradünnen Gatedielektrika mit hohem Stickstoffgehalt Advisor: Prof. C. Radehaus
Grillberger, M.:	Untersuchung des Planarisierungsverhaltens des Cu-CMP Prozesses Advisors: Prof. T. Gessner, Dr. S.E. Schulz, DI R. Seidel
Hofmann, L.:	Entwicklung und Charakterisierung einer Technologie zur Herstellung von planaren Mikrospulen mit hohem Aspektverhältnis Advisor: DI S. Leidich
Kabadshow, I.:	Parallele Fast Multiploe Methode (FMM) mit Gradientenberechnung Advisor: Prof. Radehaus
Keutel, T.:	Zyklische Belastung von Doppelschichtkondensatoren Advisor: Dipl.-Ing. H. Mehlich
Lange, A.:	Modellierung von Trenchisolationen. Advisor: Prof. Ebest
Leistner, T.:	Entwicklung eines Messaufbaus zum Test und Betrieb von mikro-mechanischen, druckabhängigen Resonanzschwingerstrukturen aus Silizium zur Zuverlässigkeitsbewertung verkapselter Sensorelemente Advisors: DI H. Specht, DI J. Frömel
Ludewig, T.:	Plasma enhanced low temperature wafer level bonding of silicon to glass wafers Advisors: Dr. M. Wiemer, DI M. Gabriel
Luf, A.:	Eine integrierte Sensorausworteschaltung nach dem Prinzip der Delta-Sigma-Modulation. Advisor: Dr. Heinz
Morschhauser, A.:	Technologieentwicklung zur Polymermetallisierung Advisor: DI J. Nestler
Nowack, M.:	Galvanische Abscheidung von Dünnschichtkappen für Mikrostrukturen Advisors: DI I. Schubert, DI D. Reuter
Richtsteiger, A.:	Parameterregelung mehrphasiger Prozesse für das tiefe Siliziumätzen Advisors: Dr. A. Bertz, DI M. Küchler
Schäfer, T.:	Herstellung anwendungsbezogener SiO_2-Grabenstrukturen im sub-µm-Bereich durch RIE und ICP Advisors: Dr. A. Bertz, Dr. I. Mönch
Scheffler, K.:	Entwurf und Aufbau einer Polymer-Solarzelle auf Basis einer Polymer-Fulleren-Mischung Advisors: Dr. T.Otto, Prof. J.Grimm, DI R.Saupe
Schneider, L.:	Miniaturisiertes zweiachsiges frequenzselektives Schwingungsmess-Systems basierend auf MEMS-Resonatoren Advisors: Dr. Billep, Dr. Scheibner Siemens AG
Schreiber, M.:	Untersuchung von Abform- und Fügeprozessen für thermoplastische Polymere Advisors: Prof. T. Gessner, Dr. T. Otto
Schulze, A.:	Analyse und Entwurf von Resonatorstrukturen in BDRIE-Technologie zur experimentellen Charakterisierung von Dämpfungseffekten sowie zur Abschätzung der Herstellungskosten Advisors: DI Forke, Dr. Hiller, DKffr. Schmidt
Schwerdtner, R.:	Entwicklung von Verfahren zur Erzeugung von oberflächennahen Mikrostrukturen in Polymerschichten und –substraten für Anwendungen der Nanolithografie und Mikrofluidik mittels Heißprägen Advisor: DI Frömel
Seidel, R.:	Magnetisch betätigte Mikrospiegel Advisor: Dr. Markert
Staude, D.:	Verschließen von Poren („pore sealing") bei porösen ultra-low-k Dielektrika mit Plasmaprozessen Advisor: Dr. S. E. Schulz

Veit, B.:	Untersuchung verschiedener Doppelschichtkondensatoren und Ableitung eines Modells für einen Netzwerksimulator
	Advisor: Dr. M. Bodach
Weiß, A.:	Strukturanalyse und Branchendefinition für ein NIR-MEMS-Spektrometer und Evaluierung an einem Beispiel der klinisch-chemischen Diagnostik
	Advisors: Dr. T. Otto, DI R. Saupe
Wittig, A.:	Untersuchung aktueller Konzepte zur elektronischen Öldruckregelung an Verbrennungsmotoren
	Advisors: Prof. Dötzel, Dr. Kiehnscherf, Ohnesorge IAV GmbH Chemnitz

PhD / Habilitation

Dr.-Ing. Ronald Neubert   March 29, 2006
"Entwicklung eines neuen Farbmessverfahrens"
TU Chemnitz, Fakultät ET/IT

Dr.-Ing. Christian Lohmann   June 29, 2006
„Beiträge zur Entwicklung einer Technologieplattform für die Herstellung von oberflächennahen Mikrostrukturen mit hohen Aspektverhältnissen"
TU Chemnitz, Fakultät ET/IT

Dr.-Ing. Mirko Bodach   June 30, 2006
„Energiespeicher im Niederspannungsnetz zur Integration dezentraler, fluktuierender Energiequellen"
TU Chemnitz, Fakultät für ET/IT

Dr.-Ing Raed Amro   July 21, 2006
"Power cycling capability of advanced packaging and interconnection technologies at high temperature swings"
TU Chemnitz, Fakultät für ET/IT

Dr.-Ing. Steffen Heinz   August 24, 2006
„Integrierte Hochvolt-Ansteuerelektronik für Mikroaktoren mit elektrostatischem Antrieb"
TU Chemnitz, Fakultät für ET/IT

Dr.-Ing. Ramona Ecke   December 11, 2006
"Abscheidung (CVD) und Charakterisierung W-basierter Diffusionsbarrieren für die Kupfer-metallisierung"
TU Chemnitz, Fakultät für Maschinenbau

8 Colloquia / Workshops at the Institute

January 10, 2006
Prof. Masayoshi Esashi, Tohoku University, Dept. of Nanomechanics, Sendai, Japan
"MEMS in Japan"

June 28, 2006
Prof. Dr.-Ing. Hans-Heinrich Gatzen, Universität Hannover, Institut für Mikrotechnologie
„Magnetische Mikroaktoren"

July 13, 2006
Dipl.-Phys. Matthias Herrmann, TU Chemnitz, Fakultät für Naturwissenschaften
„Mechanische Eigenschaften von Schichtsystemen: Simulation und Experiment"

October 27, 2006
CMP Users Meeting
Organizer : Fraunhofer IZM / Fraunhofer ISIT / VDI/VDE

November 1, 2006
Dr.-Ing. Holger Erth , Sächsisches Textilforschungsinstitut e.V. , Chemnitz
„Textilien als Funktionsträger in technischen Einsatzgebieten"

9 Scientific publications 2006

Amro, R.; J. Lutz, J. Rudzki, R. Sittig, M. Thoben: *Power Cycling at High Temperature Swings of Modules with Low Temperature Joining Technique*, 2006, Naples, Italy

Berdinsky, A.S., Shaporin, A.V. ,Yoo, J.-B., Park, J.-H., Alegaonkar, P.S., Han, J.-H., Son, G.-H.: *Field enhancement factor for an array of MWNTs in CNT paste*. Applied Physics A: Materials Science & Processing, Springer Berlin/Heidelberg, Volume 83, Number 3, pp: 377 - 383

Dötzel, W.: *Mikrosystemtechnik - Wachstum ins Kleine*, Sitzungsberichte der Sächsischen Akademie der Wissenschaften zu Leipzig, Technikwiss. Klasse, Band 2, Heft 1

Ecke,R.; Rennau,M.; Zimmermann,S.; Schulz,S.E.; Gessner,T.: *Influence of barrier crystallization on CV characteristics of MIS structures (poster)*. Advanced Metallization Conference (AMC), San Diego (USA), 2006 Oct 17-19

Forke, R., Scheibner, D., Mehner, J., Geßner, T., Dötzel, W.: *Electrostatic Force Coupling of MEMS Oscillators for Spectral Vibration Measurements*. Proc. of the 20th Eurosensors (digital), Göteborg 2006 Sep 17-20

Forke, R.; Scheibner, D.; Mehner, J.; Geßner, T.; Dötzel, W.: *Micromachined Force Coupled Sensor–Actuator System for Frequency Selective Vibration Monitoring*. Proc. of the 10th International Conference on New Actuators, Bremen 2006, pp 928-931

Frömel,J.; Billep,D.; Geßner,T.; Wiemer,M.: *Application of micromechanical resonant structures for measuring the sealing of bonded sensor systems*. Microsystem Technologies, 12 (2006) pp 481-483

Frömel,J.; Geßner,T.: *Advanced packaging is the breakthrough technology of MEMS commercialisation*, 12th International Micromachine / Nanotech Symposium, Tokyo, 08.11.2006

Frühauf,S.; Schulz,S.E.; Gessner,T.: *Mesoporous SiO2 as low-k dielectric for integration in Cu/low-k interconnect systems*. Vacuums Best, (2006) pp 31-36

Gärtner, E.; Frühauf, J.: *Silicon Standards for the Dimensional and Roughness Metrology*. Metrology for the Micro and Nano Engineering, Proceedings of the VDI/VDE Society, No. 1950, p. 25-34

Gavillet,J.; Getin,S.; Quesnel,E.; Martin,S.; Gelapierre,G.; Hiller,K.; Nestler,J.; Gessner,T.; Soechtig,J.; Voirin,G.; Buergi,L.; Auerswald,J.; Knapp,H.F.; Ross,S.; Bigot,S.; Ehrat,M.; Lieb,A.; Beckers,M.-C.; Dresse,D.: *Nanostructured polymer thin films : Application to biosensors*. Nanomat 2006, Rio de Janeiro (Brazil), 2006 Jun 5-8 ; Proceedings

Gerlach, G.; Dötzel, W.: *Einführung in die Mikrosystemtechnik – ein Kursbuch für Studierende*. Fachbuchverlag Leipzig im Carl Hanser Verlag,

Gessner,T.; Baum,M.; Hiller,K.; Mehner,J.; Wiemer,M.; Otto,T.; Saupe,R.; Nestler,J.: *Smart Systems Integration - Eine Herausforderung für zukünftige Mikro- und Nanotechnologien*. VDE Kongress 2006, Aachen (Germany), 2006 Oct 23-25; Proceedings, Band 1 (2006) pp 495-500

Gessner, T., Bonitz, J., Kaufmann, C., Kurth, S., Specht H.: *MEMS Based Micro Scanners: Components, Technologies and Applications*
Konferenz: Actuator 2006 (14-16 June 2006), Bremen, Germany

Gessner,T.; Wiemer,M.; Froemel, J.; Vogel, M.: *Advanced packaging of smart systems*, SEMICON 2006, Makuhari Messe, Chiba, Japan, 2006 Dec 6-8

Gessner, T.: *Smart Systems Integration – Future challenges for Micro and Nano Technologies*, MINAPIM 2006, Manaus, Brazil, August 31 – September 2, 2006

Gessner, T.: Fraunhofer IZM – MEMS Cooperations with China. 12th World Micromachine Summit, Beijing, China, April 27-29, 2006

Gottfried,K.; Schubert,I.: *Ultra low-k integration - a challenge for CMP*. CMP Nutzertreffen (CMP user meeting), Chemnitz, 2006 , Oct 27

Gottfried,K.; Schubert,I.; Schulz,S.E.; Geßner,T.: *Cu/barrier CMP on porous low-k based interconnect schemes*. MAM, Grenoble (France), 2006 Mar 6-8; Microelectronic Engineering, 83 (2006) p 2218-2224

Gottfried,K.; Schubert,I.: *Ultra low-k integration - a challenge for CMP*. Cabot Microelectronics CMP Meeting, Dresden, 2006 Jun 21

Gottfried,K.; Schubert,I.: *CMP processes for copper / porous low-k based damascene architectures*. CMP User Meeting, München, 2006 Apr 7

Hanf, M.; Schaporin, A; Hahn, R.; Dötzel, W.; Gessner, T.: *Micro mirror array as novel encoding mask in a Hadamard transform spectrometer*. ACTUATOR 2006, 10th International Conference on New Actuators, Bremen, 2006, p. 732-735

Knechtel,R.; Wiemer,M.; Frömel,J.: *Wafer level encapsulation of microsystems using glas frit bonding,* Microsystem Technologies, 12 (2006) pp 468-472

Kolchuzhin, V., Mehner, J., Gessner, T., Doetzel, W.: *Parametric Finite Element Analysis for Reduced Order Modeling of MEMS*. Proc. 7th International conference on thermal, mechanical and multiphysics simulation and experiments in micro-electronics and micro-systems "EuroSimE 2006", Como, Italy, Apr. 23-26, 2006, pp 220-225

Kolchuzhin, V., Mehner, J., Gessner, T., Doetzel, W.: *Parametric Simulation of MEMS Based on Automatic Differentiation of Finite Element Codes*. Technical Proceedings of the 2006 NSTI Nanotechnology Conference and Trade Show "Nanotech 2006", Boston, USA, May 7-11, 2006, Vol. 3. pp 507-510

Leidich,S.; Voigt,S.; Kurth,S.; Geßner,T.: *Microwave Phase Shifter with Electromagnetic Signal Coupling in Silicon Bulk Technology*. Int. J. Microwave and Optical Techn., 1 (2006) pp 1-9

Leidich,S.; Geßner,T.: *Using Circuit and Electromagnetic Simulation Software in RF-MEMS Design Process*, 3. AWR User Group Meeting, Munich, 2006 Oct 4-5

Lutz, J.: *Halbleiter-Leistungsbauelemente*, Springer-Verlag 2006

Markert, E.; Zeun, H.; Herrmann, G.; Müller, D.; Heinkel, U.: *SystemC-AMS-Modell eines DeltaC-U-Wandlers für ein Inertialnavigationssystem.* 9. ITG/GMM-Fachtagung Analog'06 "Entwicklung von Analogschaltungen mit CAE-Methoden", Dresden, 27.-29. September 2006, pp. 243-248

Markert, E.; Dienel, M.; Herrmann, G.; Müller, D.; Heinkel, U: *Modeling of a new 2D Acceleration Sensor Array using SystemC-AMS*; International MEMS Conference 2006 (iMEMS 2006), May 9-12, Biopolis, Singapore; Journal of Physics: Conference Series, 34 (2006) pp 228-234

Martinez-Limia, A.; Plänitz, P.; Radehaus, **C.:** *Ab initio structural and electronic properties of dangling-bond-free SiO_xN_y*, Phys. Rev. B 73, 165213 (2006)

Mehlich, H.; M. Bodach, B. Veit, J. Lutz: *Investigations of Reliability of Supercaps*, PCIM Europe 2006, Nuremberg, Germany

Mehner, J., Forke, R., Scheibner, D., Dötzel, W., Gessner, T.: *A Tunable Resonant Vibration Measurement Unit Based on a Micromachined Force Coupled Sensor-Actuator System.* Proc. of IEEE Sensors Daegu, Korea 2006 Oct 22-25, B3L-C-3

Mrwa, A.; Ebest, G.; Erler, K.; Rindelhardt, U.: *Experimental Investigations Towards Implementation of RIE and RTP Into the Multicrystalline Solar Cell Process. 21th European Photovoltaic Solar Energy Conference., p. 815, 04.-08.09.2006 Dresden*

Nadimi, E.; Radehaus, C; Nakhmedow, E.P.;Wieczorek, K.:*Calculation of the direct tunneling current in a metal-oxide-semiconductor structure with one-side open boundary*, Journal of Applied Physics 99, 104501 (2006)

Nestler,J.; Hiller,K.; Gessner,T.; Buergi,L; Soechtig,J.; Ross,S.; Voirin,G.; Bigot,S.; Gavillet,J.; Getin,S.; Fillon,B.; Ehrat,M.; Lieb,A.; Beckers,M.-C.; Dresse,D.: *A new technology platform for fully integrated polymer based micro optical fluidic systems* . 4M2006 - Second International Conference on Multi-Material Micro Manufacture, Grenoble (France), 2006 Sep 20-22; Proceedings, pp 35-38

Nestler,J.; Hiller,K.; Otto,T.; Geßner,T.: *Microfluidic bubble actuators based on hydrogels.* uTAS2006 - 10th International Conference on Miniaturized Systems for Chemistry and Life Sciences, Tokyo, 2006 Nov 05-09

Otto, T.; Saupe, R.; Weiß, A. ; Stock, V.; Bruch, R.; Gessner, T.: *Principle and Applications of a new MOEMS-Spectrometer*, San Jose, 2006, Proceedings of SPIE, Volume 6114, pp. 77-86 (2006)

Otto, T.; Saupe, R.; Weiß, A.; Stock, V.; Gessner, T.: *Temperature Scanner Based on MEMS-Technology*, Actuator 2006, Bremen, Conference Proceedings, pp. 231-234

Reithmeier, E.; Frühauf, J.; Rahlves, M.; Kraft, A.; Seifert, M.: *Hot Pressing of Multifunctional Standards for the Optical 3D Microscopy,* Metrology for the Micro and Nano Engineering, Proceedings of the VDI/VDE Society, No. 1950, p. 35-44

Reuter,D.; Bertz,A.; Billep,D.; Scheibner,D.; Doetzel,W.; Geßner,T.: *In-process gap reduction of capacitive transducers.* Sensors and Actuators A, 126 (2006) pp 211-217

Schroer, C. G.; O. Kurapova, J. Patommel, P. Boye, J. Feldkamp, B. Lengeler, M. Burghammer, C. Riekel, L. Vincze, A. van der Hart, M. Küchler, *Hard x-ray nanoprobe with refractive x-ray lenses*, in Y. Kagoshima, ed., Proceedings of the 8th International Conference on X-ray Microscopy, vol. 7 of IPAP Conference Series, pp. 94-96 (IPAP, Tokyo, 2006)

Schulz,S.E.; Gessner,T.: *Achieving ultra low dielectric constant for nanoelectronics interconnect systems, Invited talk* . FORNEL Workshop, Wuerzburg, 2006 Mar 15

Schulz,S.E.; Schulze,K.: *Achieving ultra low k dielectric constant for nanoelectronics interconnect systems, Invited talk*. 2006 8th International Conference on Solid-State and Integrated Circuit Technology, ICSICT-2006, Shanghai (China), 2006 Oct 23-26; pp 298-301

Schulze,K.; Schulz,S.E.; Gessner,T.: *Impact of Dielectric Material and Metal Arrangement on Thermal Behaviour of Interconnect Systems.* Advanced Metallization Conference (AMC), San Diego (USA), 2006 Oct 17-19

Schulze,K.; Schulz,S.E.; Gessner,T.: *Evaluation of air gap structures produced by wet etch of sacrificial dielectrics: Extraction of keff for different technology nodes and film permittivity*. Materials for Advanced Metallization (MAM), Grenoble (France), 2006 Mar 4-6; Microelectronic Engineering, Volume 83, Issues 11-12 (2006) pp 2324-2328

Schulze, K.; Schulz, S.E.; Rennau, M.; Gessner,T.: *Formation of Air Gap structures via wet etch removal of sacrificial dielectrics*. Advanced Metallization Conference 2005, Colorado Springs CO, U.S.A., 2005 Sept 27-29; MRS Conf. Proc. AMC XXI, Material Research Society, Warrendale PA (2006), pp 309-316

Schulze,K.; Schulz,S.E.; Rennau,M.; Gessner,T.: *Evaluation of Air Gap structures produced by wet etch of sacrificial dielectrics (talk)*. IEEE EDS Workshop on Advanced Electron Devices, Duisburg (Germany), 2006 June 13-14

Seifert, M., Hiller, K., Frühauf, S., Hanf, M., Pohl, R., Shaporin A.: *Arrays of Sensors with Variable Stiffness;* The VI scientific conference "Solid state chemistry and modern micro and nano- technologies", 18./23.09. 2006, Kislovodsk, Russia, pp. 319-321

Siemieniec, R.; F.-J. Niedernostheide, H.-J. Schulze, W. Südkamp, U. Kellner-Werdehausen, J. Lutz: *Irradiation-Induced Deep Levels in Silicon for Power Device Tailoring*, Journal of the Electrochemical Society, 153 (2) G108-G118 (2006)

Siemieniec, R.; H.-J. Schulze, F.-J. Niedernostheide, W. Südkamp, J. Lutz: *Compensation and doping effects in heavily helium-radiatedsilicon for power device applications*, Microelectronics Journal 37, 204-212, (2006)

Siemieniec, R.; Paul Mourick, Mario Netzel, Josef Lutz: *The Plasma Extraction Transit-Time Oscillation in Bipolar Power Devices – Mechanism, EMC Effects and Prevention*, IEEE Trans El.Dev., Vol 53 No 2, 369-379 (2006)

Voigt, S.; Leidich, S.; Kurth, S.; Geßner, T.; Doetzel, W.: *24 GHz RF-MEMS Phase Shifter with Non-Galvanic Electromagnetic Coupling Fabricated in Silicon-Bulk Technology*. Journal of Physics: Conference Series, 34 (2006) pp 228-234

Waechtler,T.; Gruska,B.; Zimmermann,S.; Schulz,S.E.; Gessner,T.: *Optical Properties of Sputtered Tantalum Nitride Films Determined by Spectroscopic Ellipsometry*. Talk given at the 4th Workshop on Ellipsometry, Berlin (Germany), 2006 Feb 20-22

Waechtler,T.; Gruska,B.; Zimmermann,S.; Schulz,S.E.; Gessner,T.: *Characterization of Sputtered Ta and TaN Films by Spectroscopic Ellipsometry*. Talk given at the 8th International Conference on Solid-State and Integrated Circuit Technology, ICSICT-2006, Shanghai (China), 2006 Oct 23-26; Proceedings, pp 2184-2186

Waechtler,T.; Shen,Y.Z.; Jakob,A.; Ecke,R.; Schulz,S.E.; Wittenbecher,L.; Sterzel,H.-J.; Tiefensee,K.; Oswald,S.; Schulze,S.; Lang,H.; Hietschold,M.; Gessner,T.: *Evaluation of Phosphite and Phosphane Stabilized Copper(I) Trifluoroacetates as Precursors for the Metal-Organic Chemical Vapor Deposition of Copper*. Poster presented at the Materials for Advanced Metallization Conference - MAM 2006, Grenoble (France), 2006 Mar 6-8

Zimmermann,S.; Zhao,Q.T.; Hoehnemann,H.; Wiemer,M.; Kaufmann,C.; Mantl,S.; Dudek,V.; Geßner,T.: *Different approaches to integrate patterned buried CoSi2 layers in SOI substrates*. Material for Advanced Metallization MAM, Grenoble (France), 2006 March 4-6

10 International guests

Visiting scientists:

January 9	Prof. T. Esashi, Tohoku University, Sendai, Japan
March 8	Anthony Chu, Richard H. Brown, Measurement Specialities, Aliso Viejo, CA, USA
June	Prof. Dr.-Ing. Jan Mühlbacher, Dozentenaustausch, TU Pilsen, Tschechien
June	Prof. Dr.-Ing. Vaclav Kus, Dozentenaustausch, TU Pilsen Tschechien
June	Doz. Dr.-Ing. Vlastimil Skocil: Dozentenaustausch, TU Pilsen, Tschechien
June 17	Dr. Martin Domeij, Royal Institute of Technology (Kungliga Tekniska Högskolan), KTH, Stockholm, Sweden
June 29	Prof. Reinhard Bruch, University of Nevada, Reno, USA
July 4-7	Prof. Ran Liu, Fudan University, Shanghai, China. Prof. Di Chen, Shanghai Jiao Tong University, China
July 27	Mr. Takuya Nakamura, Mr. Akiyoshi Aoyagi, SONY Corp., Semiconductor Business Unit, Japan
September 25	Ralf Hofmann, Applied Materials, Advanced Technologies Group, Santa Clara CA, USA
September 27	B.J. Templeton (Director Worldwide Sales and Marketing), Stuart Herbert (European Sales and Marketing Manager), Dr. Shuji Ikeda (Director Technology), atdf, Austin TX, USA
September 28	Thomas Gaspar (Director of Sales), Thomas West Inc., Sunnyvale CA, USA Brigitte Ohlenschlager, TELTEC, semiconductor technic GmbH, Germany
November 13	Eric van Grunsven, Philips Applied Technologies; Fred Roozeboom, NXP Corporate Research, Eindhoven, The Netherlands
November 16	Jean-Luc Delcarri (President), Otto Laistner, ALTATECH Semiconductor, Saint Ismier, France
November 18-25	Delegations of professors and students from Fudan University & Shanghai Jiao Tong University, China for the IRTG "Materials and Concepts for Advanced Interconnects" Autumn School
November 21-22	Dr. Lucile Arnaud, CEA-LETI, France
November 20-22	Prof. Mikhail Baklanov, IMEC, Belgium
November 20 – December 10	associate Prof. Alexander Gusev, North Caucasus State Technical University, Stavropol, Russia
December 1 - December 31,	associate Prof. Vitaly Tarala, North Caucasus State Technical University, Stavropol, Russia

Students:

Seat, Filip	University of Ljubljana, Slovenia
	October 2005 – March 2006 SOCRATES
Zhang, Xiao Chuan	MEMS Res. Ctr., Xiamen Univ., China PhD
	Since September 2005
Kopuri, Vikram Gupta	Portland State University, Portland OR, USA
	June 22 - September 19, 2006
Young Cher Chris Kim	Portland State University, USA
	June 22 - September 19, 2006
Popazu, Cristina	Universität "Politehnica" Bukarest, Romania
	October 2006 – March 2007 SOCRATES

Scientific coworkers / PhD:

Alexej Shaporin	Novosibirsk Technical University, Russia
	November 2002 – December 2006
Wladimir Kolchuzhin	Novosibirsk Technical University, Russia
	November 2002 – December 2006
Dr. Chenping Jia	University of Xian, China,
	January 2003 – December 2006
Xinming Zhao	China
	June 2006 – December 2006
Tatjana Prohoda	North Caucasus State Technical University, Stavropol, Russia
	Oct 2006 - March 2007

International Research Training Group „Materials and Concepts for Advanced Interconnects"

Olena Chukhrai	Ukraine
Teodor Toader	Romania
Sukumar Rudra	India
Anastasia Moskvinova	Russia